Title
Hybrid Organic–Inorganic Photomechanical Actuators Based on Organized Molecular Crystals

Permalink
https://escholarship.org/uc/item/3cd9h6d0

Author
Dong, Xinning

Publication Date
2021

Peer reviewed|Thesis/dissertation

UNIVERSITY OF CALIFORNIA
RIVERSIDE

Hybrid Organic–Inorganic Photomechanical Actuators Based on Organized
Molecular Crystals

A Dissertation submitted in partial satisfaction
of the requirements for the degree of

Doctor of Philosophy

in

Chemistry

by

Xinning Dong

December 2021

Dissertation Committee:

    Dr. Christopher J. Bardeen, Chairperson
    Dr. Haofei Zhang
    Dr. Quan Jason Cheng

The Dissertation of Xinning Dong is approved:

_____

_____

_____
Committee Chairperson

University of California, Riverside

Acknowledgments

First and foremost, I would like to express my sincere gratitude to my advisor Prof. Christopher J. Bardeen, who is always supportive, patient and encouraging during my PhD study. Prof. Bardeen is the role model of me. I learnt a lot from him such as how to think like a doctor, how to communicate with people, how to tell a good story and how to stay positive in life. I feel really lucky to be his student as he always cares about my development in academic research and career path.

I would like to thank Prof. Haofei Zhang, Prof. Jason Cheng, Prof. Francisco Zaera, Prof. Ming Lee Tang and Prof. Ruoxue Yan for serving as the committee members in my SYRE or ORAL exams. They gave me lots of advice and even critical comments which are all valuable and pushed me to be an eligible PhD student.

I would like to thank my collaborators Dr. Daichi Kitagawa, Kohei Morimoto, Prof. Peter Palffy-Muhoray, Dr. Tianyi Guo, Prof. Ryan Hayward, Dr. Wenwen Xu and Dr. Jason Myers who offered me tons of help on studying organic compound properties and synthesis, crystal growth, measurements of physical properties, crystal analysis and optical fiber. I would also like to thank Dr. Illkuen Lee for teaching me operating SEM and taking care of it.

I would like to thank my group members Dr. Kerry Hanson who is always kind to me and keeps me staying positive, Dr. Hossein Mostafavi, Dr. Fei Tong, Dr. Robert Dillon, Nathan Tierce, Wangxiang Li, Adam Berges, Brandon Lui, Taylor Lewis, Thomas Gately, Touhid Bin Anwar, Pranaya Ghate, Kevin Lam and Marielle Sewell for being awesome teammates with me.

iv

I would like to thank my friends: Dr. Yige Li, Dr. Tianyi Yu, Xiao Hong, Dr. Yanxiang Wang, Dr. Yangyang Wang, Dr. Yuzheng Wang for their help and support in my daily life.

Lastly, I would like to offer my special thanks to my parents and fiance Wei-Ting for being there with me through all of hard times. This thesis can not be done without them.

Acknowledgement of Previously Published Material

ABSTRACT OF THE DISSERTATION

Hybrid Organic–Inorganic Photomechanical Actuators Based on Organized Molecular
Crystals

by

Xinning Dong

Doctor of Philosophy, Graduate Program in Chemistry
University of California, Riverside, December 2021
Dr. Christopher J. Bardeen, Chairperson

Photomechanical actuators are smart materials that transform photon energy into mechanical energy without any wired connections. Photonmechanical molecular crystals have shown superior performance on nanoscopic and microscopic scales due to their high elastic moduli, high-energy density and fast response time compared with polymer actuators. However, the development of macroscopic crystal actuators that can be used in the real world has yet to be demonstrated.

The work in this dissertation solves the problem by organizing photomechanical nanocrystals in porous inorganic templates (Al_2O_3). It combines the best of both worlds where it is processable like polymers but it also attains high performance of organic crystals. 1,2-bis(2-methyl-5-phenyl-3-thienyl)perfluorocyclopentene, a diarylethene (DAE) derivative that undergoes a unimolecular photoisomerization between its ring-open and ring-closed isomers was used as the active organic element. The isomers are thermally stable but can be switched back and forth using UV and visible light for hundreds of cycles. Very small (sub-mg) amounts of material can move masses that are 10^5 times larger without being

physically connected to an external power source. A light-to-work conversion efficiency for a molecular crystal photomechanical actuator has been for the first time quantitatively estimated, providing a starting point for future optimization.

Additional studies investigated how both the organic and inorganic components could affect the photomechancial response. Two alumina templates with different morphology and elastic modulus were compared. The template with a lower average elastic modulus generate about one order of magnitude more photomechanical work. Two diarylethene derivatives with different crystal deformations were studied to determine the dependence of photomechanical response on chemical and crystal structure.

The hybrid approach was then extended to porous SiO_2 membranes with variable thicknesses in order to improve optical penetration and reproducibility. The photon-induced bending could be repeated for 150 cycles without loss of performance which suggests good fatigue resistance. The thickness dependence of the performance was studied, revealing thinner templates gave larger displacements. This work demonstrates that the hybrid method for making photomechanical actuators on macroscopic scales can be extended to other host materials and template geometries without sacrificing performance.

Contents

List of Figures

xiii

List of Tables

Chapter 1

Introduction

1.1 Background of Photomechanical Materials and Motivation

In 2016, the Nobel Prize in Chemistry was awarded jointly to Jean-Pierre Sauvage [22], Sir J. Fraser Stoddart [23] and Bernard L. Feringa [24] for their design and synthesis of molecular machines. This is a milestone marked the fundamental and practical significance of the motion of natural and artificial objects that scientists have been working on for decades. Molecular machines are one type of actuator that transforms chemical energy into mechanical motions.

Actuators, or "smart" actuators, are devices which perform mechanical movements with response to external stimuli, such as magnetic [25, 26], thermal [27, 28], chemical [29, 30], humid [31], and light energy [32]. Among these stimuli, photons are ideal tools as they travel fast with energy and information and allow remote control without

1
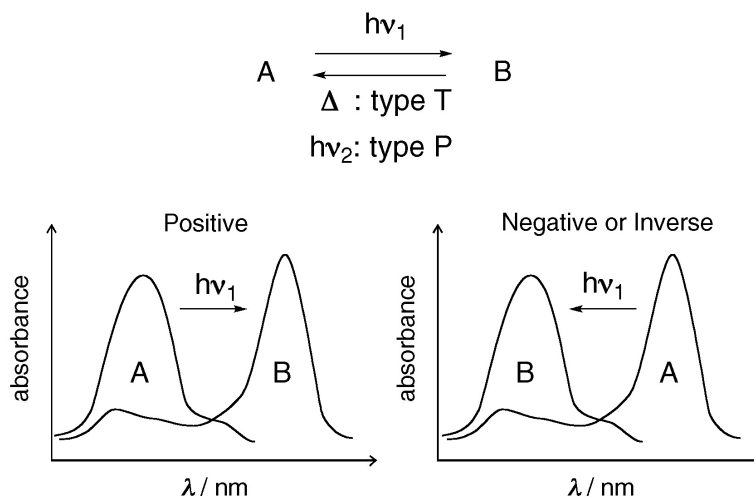
Figure 1.1: Definition of photochromism between A and B. (Reproduced with the permission of Elsevier) [1]

any wired connections [33]. Light sources can be manipulated by changing the wavelength, direction, power and duration to cause actuators to perform different actions. Based on these advantages, the term "photomechanical" is defined for chemicals designed to undergo mechanical motion upon photoirradiation. With optical manipulation, photomechenical materials have potential for applications like photolithography [34], photomemory [35, 36], optical sensors [37], nano tweezers [38], nano sweepers [39], smart switches [40] and photo adhesives [41–44]. These smart photomechanical actuators are made to mimic movements in nature like bending [45], twisting [14], crawling [46], rolling [47], jumping [48], peeling [49]. In addition to external factors like light properties, photomechanical motions can also be influenced by internal materials factors like shape [50] and thickness [15]. This allows photomechanical materials to maintain high flexibility and serve as intelligent materials.
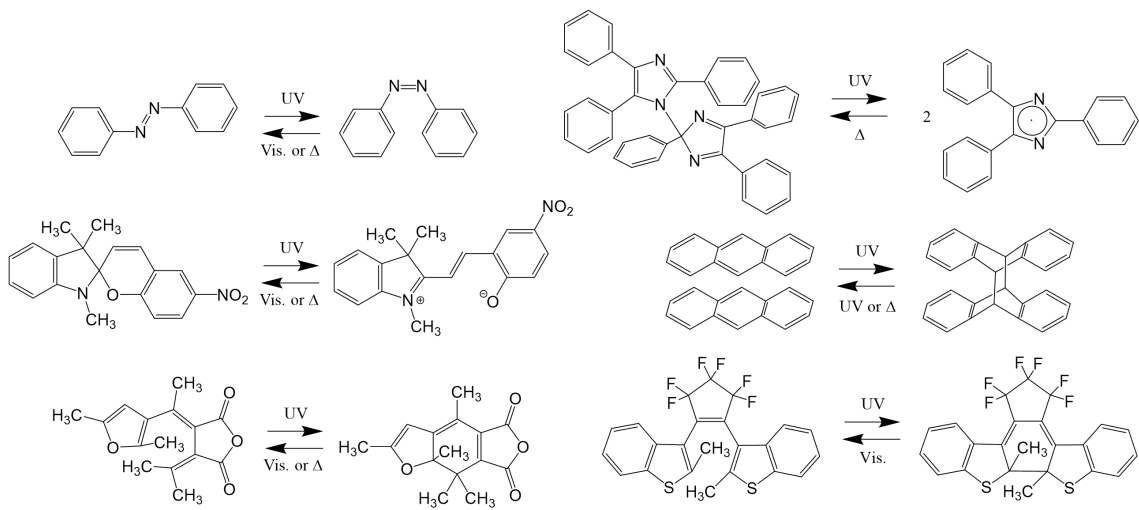
Figure 1.2: Typical photochromic reactions.

1.2   Photochromes

To transform light into motion, people use molecules that isomerize to do the work. The active units in photomechanical materials are the photochromes. A photochrome, or a photochromic compound, is a photoresponsive molecule which changes color reversibly upon light irradiation due to the transformation between two chemical states having different absorption spectra. The concept of photochromism was first brought out by the discovery of the reversible photodimerization of anthracene by Fritzsche in 1866 [51]. Based on different stability of the colored states and colorless states, photochromes can be divided to positive and negative types. Based on thermally stability of the reverse reactions, photochromes can be also divided to T- and P-types (Figure 1.1) [1, 52].
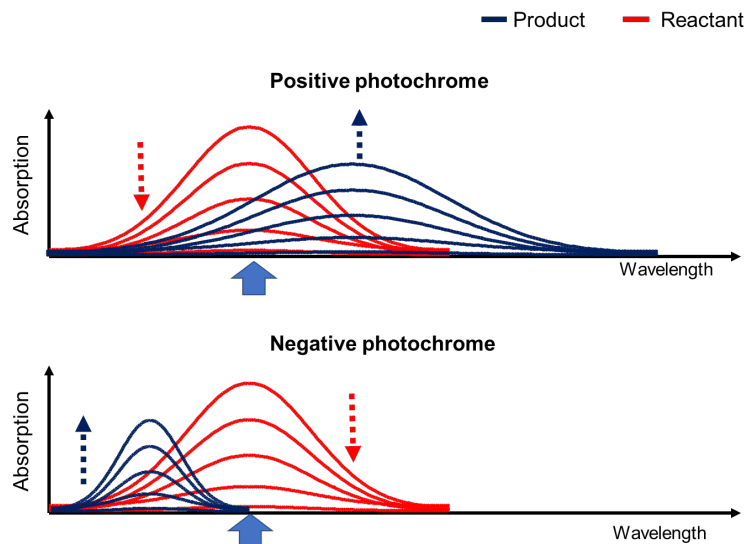
Figure 1.3: Schematic illustration of typical UV-Vis absorption spectra of positive photochromes vs. negative photochromes.

1.2.1 Typical Photochromic Reactions

Typical photochromic reactions are shown in Figure 1.2. They can be classified according to their reaction modes. One is E/Z isomerization, the other is bond-cleavage and bond-forming. These include *trans-*, *cis*-isomerization of azobenzene, the structural change between spiropyran and zwitterionic merocyanine forms, ring closing and opening photoisomerization of fulgides, dissociation of hexaarylbiimidazole(HABI) into a geminate radical pair, [4+4] photodimerization of anthracene derivatives, and ring closing and opening photoisomerization of diarylethenes.

1.2.2 Positive and Negative Photochromism

The phenomenon of color changing in photochromes have two types: color deepening and color fading. Photochromism in which an intense color appears upon UV irradiation
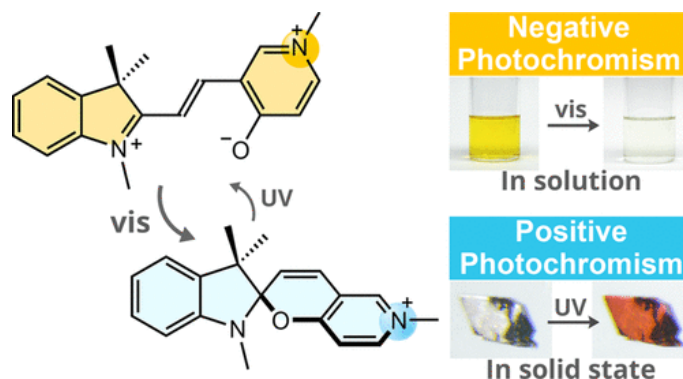
Figure 1.4: Switching positive and negative photochromism of spiropyran. (Reproduced with the permission of American Chemical Society) [2]

and reverts back to a colorless state is called positive photochromism, where the colorless state is more stable than the colored state. On the other hand, negative photochromic compounds have a more stable colored state than colorless state and show color fading upon radiation with visible light, and the intense color recovers in the absence of light. In other words, positive photochrome shows a red shift and negative photochrome shows a blue shift of the absorption spectra upon light irradiation (Figure 1.3).

Spiropyran is a typical photochromic molecule which usually exhibits positive photochromism in solution because its colorless state in a neutral spiropyran (SP) form is more stable than its colored zwitterionic merocyanine (MC) form. However, by stabilizing the MC form with environmental factors such as hydron bonds [53] or metal ions [54], spiropyran can be switched to exhibit negative photochromism. Funasako and coworkers reported salts composed of a pyridinium-fused spiropyran that exhibits positive and negative photochromism in solid and solution state respectively (Figure 1.4) [2]. Some other photochromes with interesting negative photochromism properties have been reported such as (E)-4-Fluoro-cinnamaldehyde malononitrile ((E)-4FCM) [55], 9-methylanthracene

5
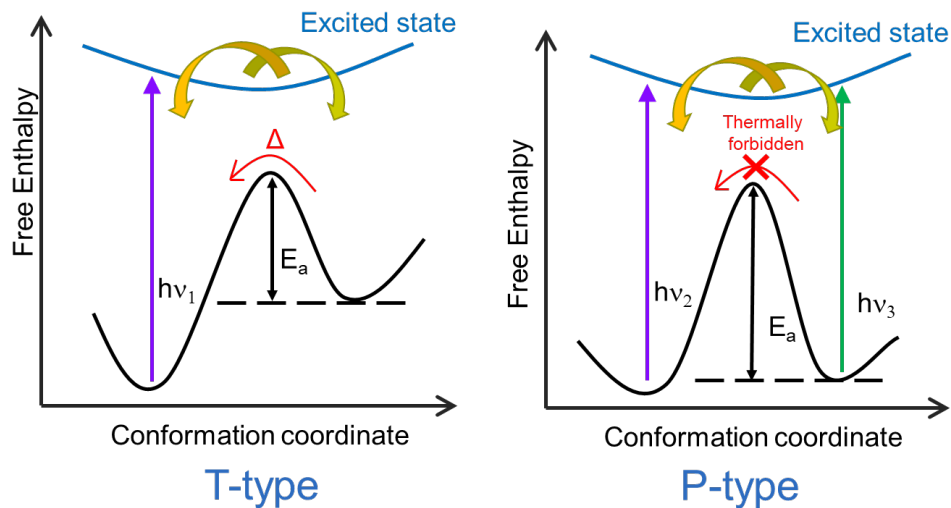
Figure 1.5: Comparison of potential energy surfaces of T-type and P-type photochromes.

(9MA) [16,56] and donor-acceptor Stenhouse adducts (DASA) [57,58]. They attract attention due to their 100% of light penetration and potential applications in bioimaging.

1.2.3 T-type and P-type Photochromism

Photochromes can be also divided to T-type and P-type based on their thermal stability. If the isomers are thermally stable and convert back to their original state via photons, they are classified as "P-type" photochromes. On the other hand, if the activation energy of their back reaction is small enough so they can revert back to their original state thermally, they are classified as "T-type" photochromes [59] (Figure 1.5).

Most fulgides and diarylethenes are categorized as "P-type" photochromic compounds [52, 60], while the others are usually "T-type" photochromes. For example, the back reaction's activation energy of a typical "T-type" photochrome azobenzene is around
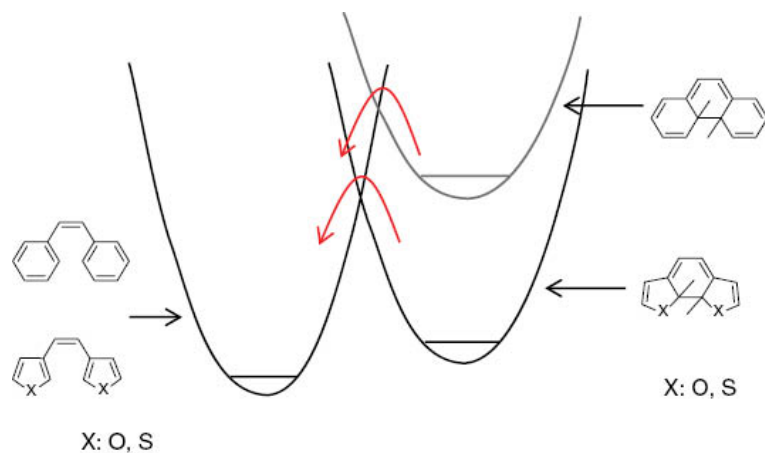
Figure 1.6: Replacing phenyl rings of stilbene by thiophene or furan rings decreases the ground state energy difference between two isomers, therefore increases the energy barrier of cycloreversion reactions. [3]

80 kJ/mol [61]. However, P-type photochromic compounds like diarylethene have much larger activation energies of about 150 kJ/mol which prohibits the thermal back cyclization. The enthalpy difference (ΔH) between the two isomers determines thermal reactivities. For diarylethenes, the closed-ring isomer is thermally stable when ΔH is less than 60 kJ/mol [62–68].

1.2.4 Diarylethene Derivatives

Diarylethene was first developed by Irie in the late 1980s as a P-type photochrome with high thermal stability for both isomers. By replacing the phenyl rings of stilbene by five-membered heterocyclic rings like thienyl or furyl rings with low aromatic stabilization energy, the difference of ground state energy between open-ring and close-ring isomers was decreased. By the Horiuti-Polanyi rule, the energy barrier of cycloreversion has been increased which forbids thermal back reaction (Figure 1.6) [3]. Diarylethenes are ideal
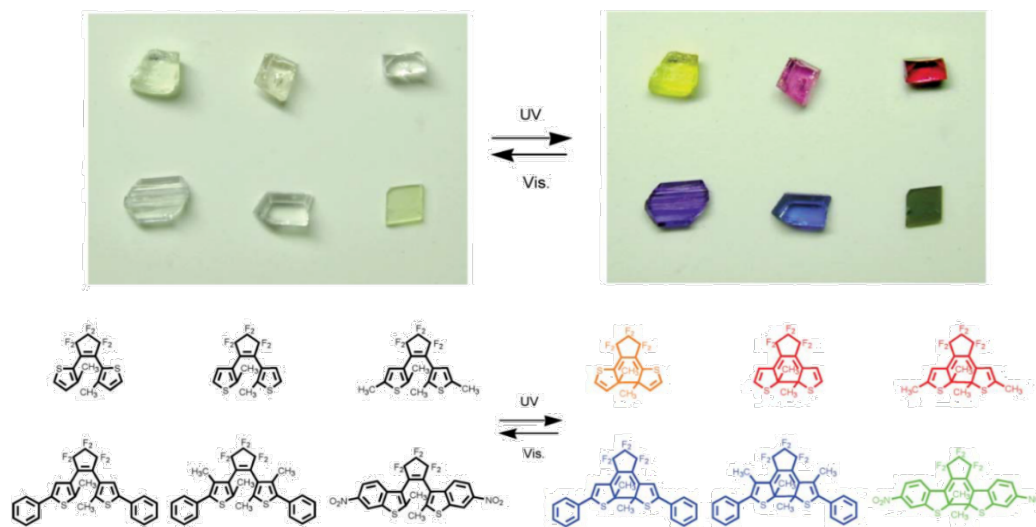
Figure 1.7: Photoinduced colors of different diarylethene single crystals. (Reproduced with the permission of Royal Society of Chemistry) [4]

photochromes for light-driven actuators due to their internal advantages: thermal stability of both isomers, fatigue-resistance, high absorption, rapid response and reactivity in solid state [69].

A family of diarylethene derivatives showing different photoinduced color change in the solid state has been synthesized (Figure 1.7) [4]. The color change can be controlled by the length of π-conjugation. Diarylethenes with longer π-conjugation have a red shift of absorption resulting in violet and blue colors.

P-type diarylethenes are known by their high thermal stability of the ring-closed isomers, whereas the thermal cycloreversion reaction is determined by three factors: (1) aromatic stabilization energy of the heterocyclic aryl groups: phenyl groups have higher aromatic stabilization than thiophene groups resulting in higher thermal cycloreversion reaction; (2) electron-withdrawing substituents: electron-withdrawing groups weakening

8
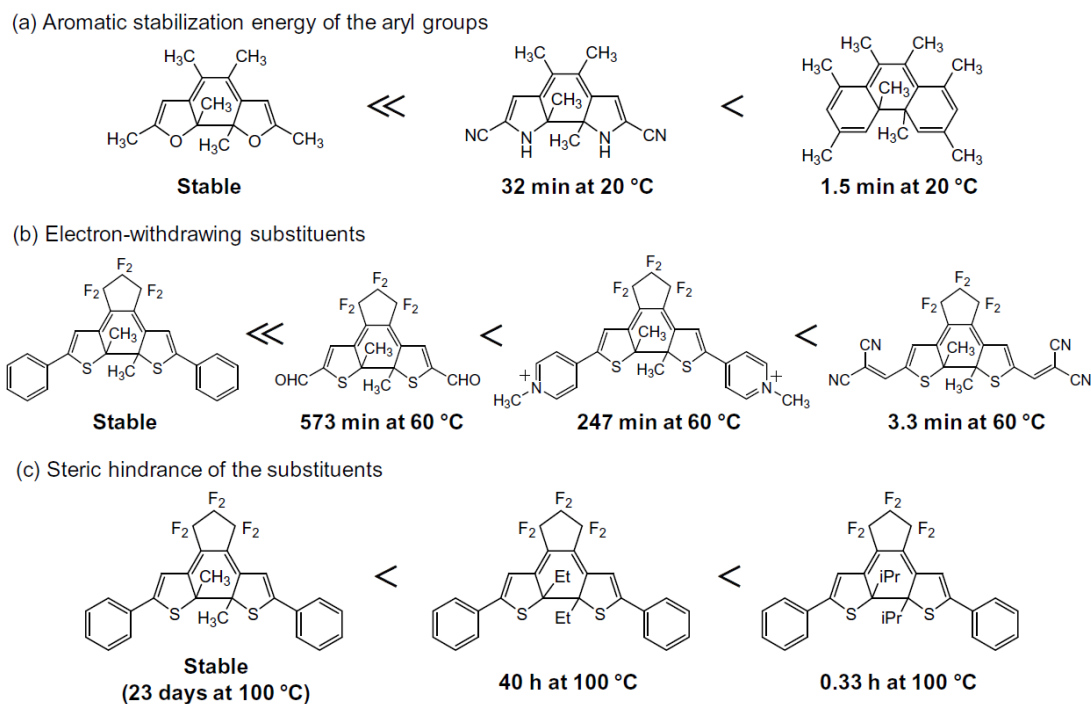
Figure 1.8: Thermal cycloreversion reactivity of diarylethenes is determined by three factors. [5]

the central carbon-carbon bond to give a high thermal cycloreversion reaction; (3) steric hindrance of the substituents at the reactive carbons: bulky groups weaken central carbon-carbon bond (Figure 1.8) [5].

1.3 Organize Photochromes at Nanoscopic Level

The photochromes in polymers or crystals can be organized at the nanoscopic level so their photoisomerization motion can be amplified.
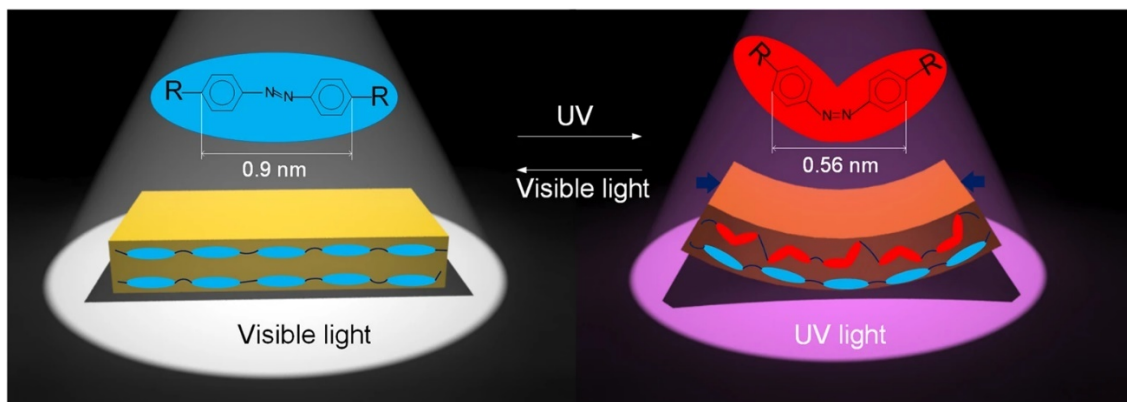
Figure 1.9: *Trans-cis* photoisomerization of azobenzene in an LCP film. [6]

1.3.1   Photomechanical Liquid Crystalline Polymers

Polymers are long-chain large molecules composed of repeating moieties of small molecules. Their advantages are well-known, such as low production costs, high processability and high flexibility. Light-actuating shape-changing polymer systems can be engineered by introducing light-responsive groups into polymer networks. Different classes of photomechanical polymers include liquid crystalline polymers, hydrogels, and shape-memory polymers.

Studies on photomechanical materials began with polymers in the 1960s. Merian reported a 0.1% photoinduced shrinking of polymer fibers that incorporated azobenzene in 1966 [70]. Subsequent research have lifted the veil on photomechanical polymer systems. Horie and coworkers induced macroscopic deformations of azobenzene polymer networks by improving the homogeneity [71]. A hydrogel with supramolecular bonds between azobenzene and α-cyclodextrin (αCD) at cross-linking points was made by Harada and coworkers [72]. An obvious photomechanical effect was achieved as the hydrogel showed a large deformation

10

such as swelling and shrinkage upon photon irradiation.

Photomechanical deformations of dry polymers were limited to less than 1% for a long time until the discovery of photoresponsive liquid-crystalline materials [73, 74]. Liquid crystal polymers (LCPs), liquid crystal polymer networks (LCNs), and liquid crystal elastomers (LCEs) are liquid crystalline materials that possess photoactuating motions. In general LCPs are made by introducing liquid crystal (LC) moieties, or mesogens, to the polymer backbones. LC mesogens allow homogeneous molecular alignment across large scales due to their self-assembling properties, while polymer chains support the conformation. The deformation of this actuating system is triggered by the photoisomerization of the mesogens, together with the confirmation change of polymer backbones. The co-existence of the characteristics of LC materials and polymers in a single system makes LCPs functional soft materials that can be controlled by light. The most popular photochromic moiety used in LCPs is Azobenzene. The *trans-cis* isomerization of this photochrome was found to induce reversible bending-unbending behavior upon light irradiation (Figure 1.9) [6]. The length of *trans*-isomeric azobenzene is 0.9 nm and it will convert to *cis*-isomeric azobenzene with length 0.56 nm when irradiated by UV light. It will recover to its original state when irradiated by white light. As the top surface of the LCP will mostly absorb UV light due to its strong absorption, a partially reacted bimorph structure leads to bending of the LCP instead of shrinking.

The concept of LCPs was pioneered theoretically by de Gennes in 1975 [75] and experimentally confirmed using a polysiloxane backbone by Finkelmann and coworkers in 1981 [76]. In 2003, following up with Finkelmann's research, Ikeda and coworkers prepared
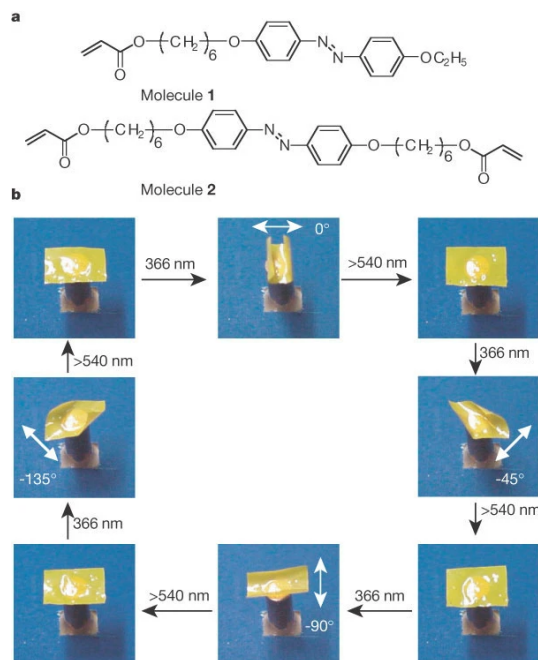
Figure 1.10: Controlling bending direction of an azobenzene LCP with linearly polarized light. (Reproduced with the permission of Springer Nature) [7]

a glassy liquid crystalline polymer network with azobenzene mesogens as active units [7].

Figure 1.10a shows the chemical structures of the liquid-crystal monomer (molecule 1) and crosslinker (molecule 2) used for preparation of the film. Figure 1.10b shows a LCP film (4.5 mm × 3 mm × 7 μm) bending in different directions in response to irradiation by linearly polarized light of different angles of polarization (white arrows) at 366 nm, and being flattened again by visible light longer than 540 nm. This work showed for the first time that the direction of deformation of photomechanical azobenzene material could be controlled by irradiation with linearly polarized UV light (Figure 1.10b). With *trans-cis* isomerization induced by a polarized UV absorption of azobenzene mesogens at surface, the prepared LCP showed axis-selective bending. The results of Ikeda and coworkers significantly motivated scientists to explore the field of managing photomechanical response with light wavelength,
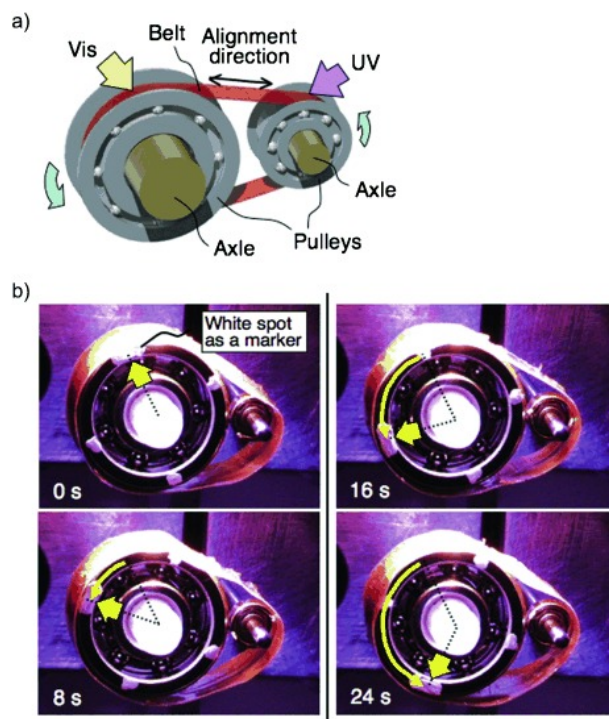
Figure 1.11: A light-driven plastic motor with a PE-LCE flexible film. [8]

intensity and polarization.

As light is only absorbed by the photoreactive moieties from the surface, the photochromes deep down are inactive in this system and they tend to be brittle as well. To solve this problem, Ikeda and coworkers further investigated flexible substrates such as polyethylene to improve the mechanical properties. Large stress generated by UV absorption on the surface of LCP material could be protected from fracture due to the incorporation of soft polyethylene (PE) as a substrate to the azobenzene contained LCP system. Such flexibility allowed this material to be used to rotate pulleys [8] and imitate walking as an inchworm [9]. A light-driven plastic motor system is shown in Figure 1.11. A PE-LCE

13
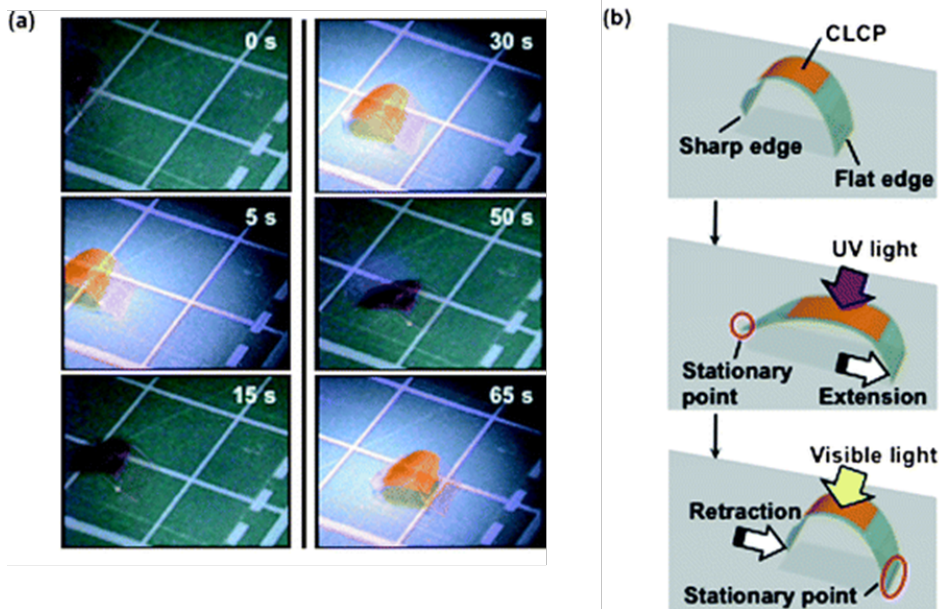
Figure 1.12: A photoinduced inchworm walk of a PE-LCE soft polymer by alternate irradiation with UV and visible light at room temperature. (Reproduced with the permission of Royal Society of Chemistry) [9]

bilayer (thickness: 50 μm, 18 μm) was made to rotate a 10 mm (left)–3 mm (right) diameter pulley under irradiation with UV and visible light. The same bilayer material demonstrating inchworm walking is shown in Figure 1.12. Upon exposure to UV light, the film extends forward because the sharp edge acts as a stationary point, and the film retracts from the rear side by irradiation with visible light because the flat edge acts as a stationary point.

1.3.2 Photomechanical Molecular Crystals

The general idea of photomechanical molecular crystals is to use crystal order to organize and amplify the mechanical effectes of photomechanical reactions. (Figure 1.13) Compared with photomechanical polymers, photomechanical crystals directly relate molecular motion to macroscopic motion because they are composed of pure active molecules.

14
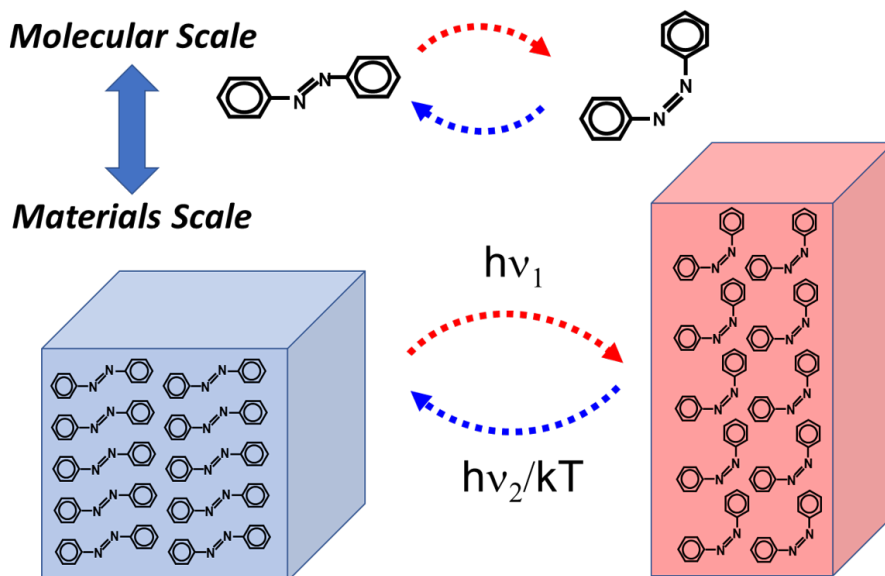
Figure 1.13: Schematic illustration of the mechanism of photomechanical molecular crystals composed of azobenzene molecules

Crystals have a faster response time because they are able to rapidly transfer energy through the well-ordered and densely packed lattices [77], where the crystal structure details such as crystal packing and interactions can be precisely determined by X-ray analysis [78].

The first photomechanical effects of molecular crystals was reported by Abakumov and Nevodchikov in 1982 showing a free-radical complex crystal bending. [79]. In the next 20 years, little attention has been paid on this field until a breakout by a diarylethene crystal. Irie, Kobatake and coworker reported a reversible surface morphology change on a diarylethene crystal in 2001 [10]. A 1 nm high step was found on the crystal surface upon UV irradiation and the step was flattened back to the original level after irradiation with visible light. Figure 1.14 shows AFM images of photoirradiation on two crystal surfaces (100) (A to C) and (010) (D to F): (A) and (D) are before photoirradiation; after irradiation with 366-nm light for (B) 10 s and (E) 15 s; and after irradiation with visible light, (C) and (F).
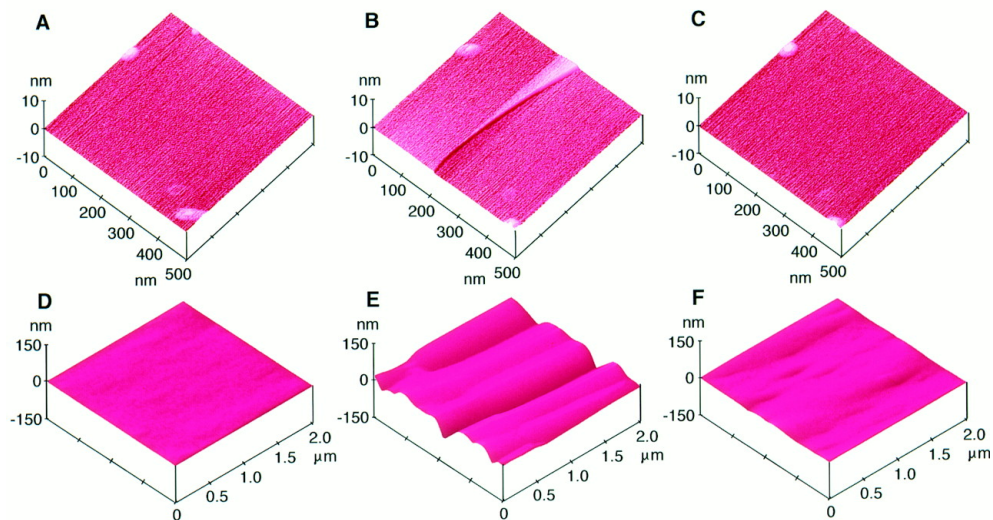
Figure 1.14: AFM images photoirradiation on two diarylethene single crystal surfaces (100) (A to C) and (010) (D to F). (Reproduced with the permission of The American Association for the Advancement of Science) [10]

The surface morphology change is due to a molecular structural change of regularly packed diarylethene molecules inside the single crystal. Microscopic changes for diarylethene single crystals when exposed to light was found in the continuing research by Irie, Kobatake and coworkers in 2007 [11]. Molecular crystals composed of diarylethene photochromes with sizes ranging from 10 to 100 micrometers have reversible macroscopic changes in shape and size upon UV and visible light (Figure 1.15).

At the same time, Bardeen, Al-Kaysi and coworker reported a 15% of microscopic extension on a bundle crystal microrods in 2006 [12]. The nanorods, 200 nm in diameter and 60 micrometers in length and grown in an anodized alumina oxide (AAO) template, were composed of 9-*tert*-butylanthroate (9-TBAE), which undergoes a rapid [4+4] pho-todimerization which leads to a 15% expansion in length without fragmentation (Figure
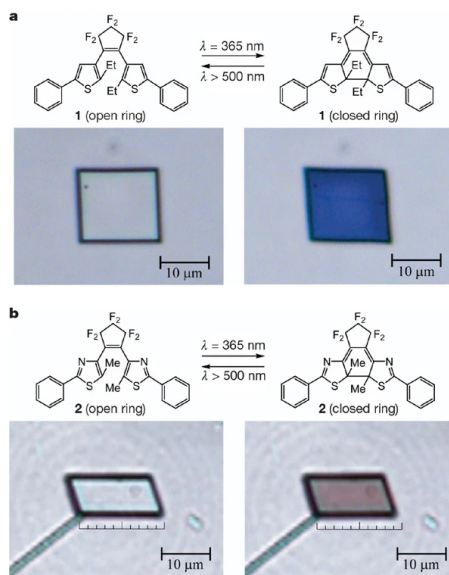
Figure 1.15: Two diarylethene single crystals illustrates their deformation of an angle change (a) and a contraction (b) on irradiation with ultraviolet and visible light. (Reproduced with the permission of Springer Nature) [11]

1.16). Following research by Bardeen and coworkers discovered a new class of motion, a photoinduced reversible twist in crystalline microribbons of 9-Anthracenecarboxylic acid (9AC)(Figure 1.17) [13]. The presence of two incommensurate chemical species of photoreacted dimers and the unreacted monomers induced stress which triggered the twisting.

The twisting motion of photomechanical microribbon crystals could be controlled by the direction of light as shown by research of Kobatake, Kitagawa, Bardeen and coworkers [14]. Controlling twisting modes from helicoid to cylindrical of a photomechanical crystal ribbon composed of diarylethene could be achieved by changing the UV illumination direction (Figure 1.18). Photomechanical motion of crystals can be controlled by other external characteristics of light such as wavelength [80], power [81], polarization [82] as well as internal characteristics such as thickness and molecular reorientation. Kobatake and Kitagawa
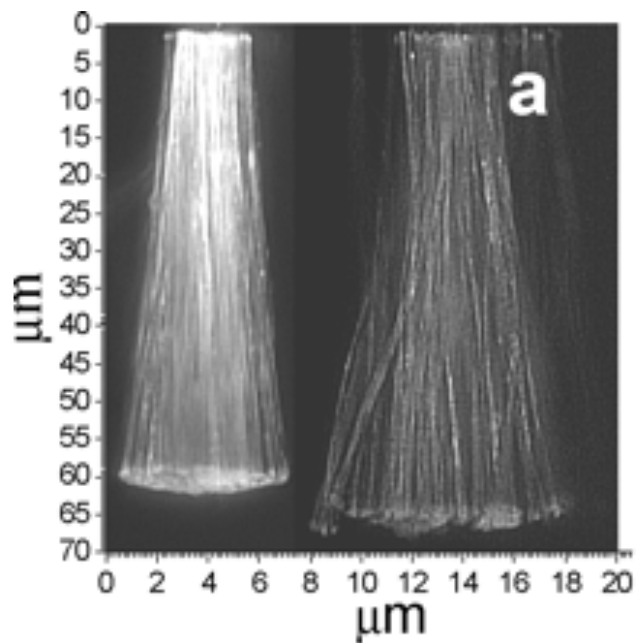
Figure 1.16: Fluorescence image of a bundle of 9-TBAE nanorods, before and after irradiation with 365 nm. (Reproduced with the permission of American Chemical Society) [12]
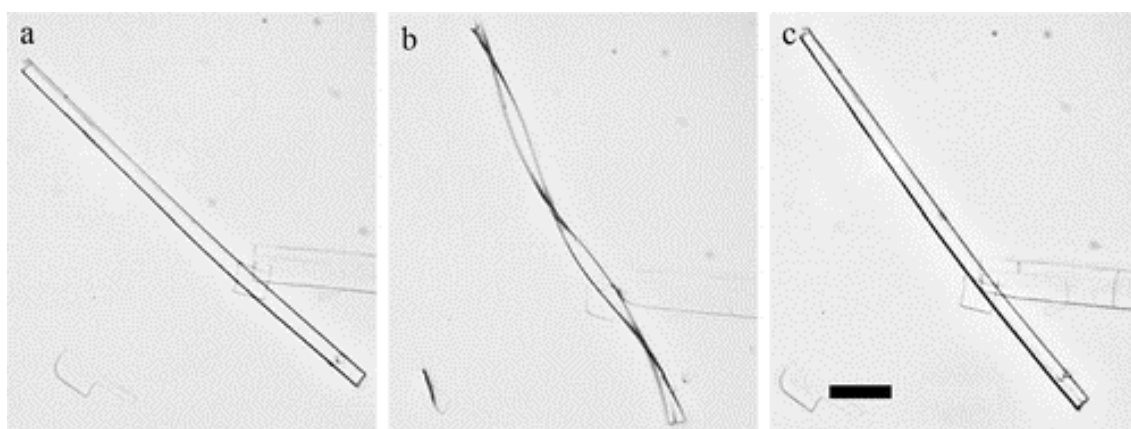
Figure 1.17: Optical microscopy images of a 9AC ribbon's reversible twisting behavior. (Reproduced with the permission of American Chemical Society) [13]
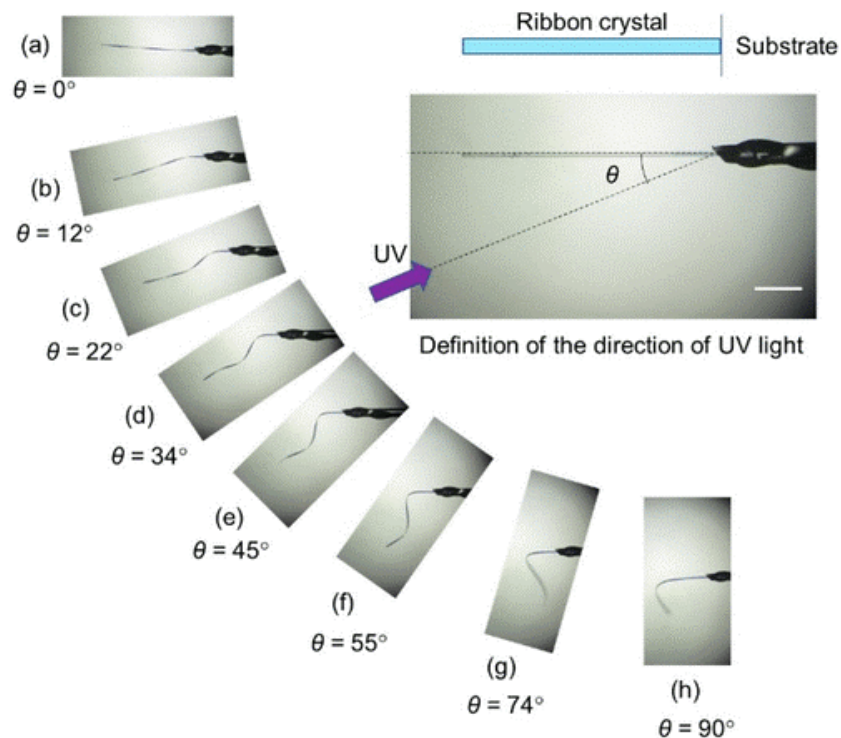
Figure 1.18: Diarylethene single crystals shows different twisting motions, ranging from a helicoid to a cylindrical helix, depending on the angle of the incident light. [14]

reported the bending speed of a diarylethene rod crystal depended on the crystal thickness (Figure 1.19) [15]. Bardeen and coworkers developed a method of crystal growth to generate different internal molecular orientations of 9-Methylanthracene (9MA) [16]. Two different shapes of the ribbon microcrystals were obtained by this method. The hexagonal shape showed a rolling motion whereas the rectangle shape showed a twisting motion upon UV irradiation (Figure 1.20).
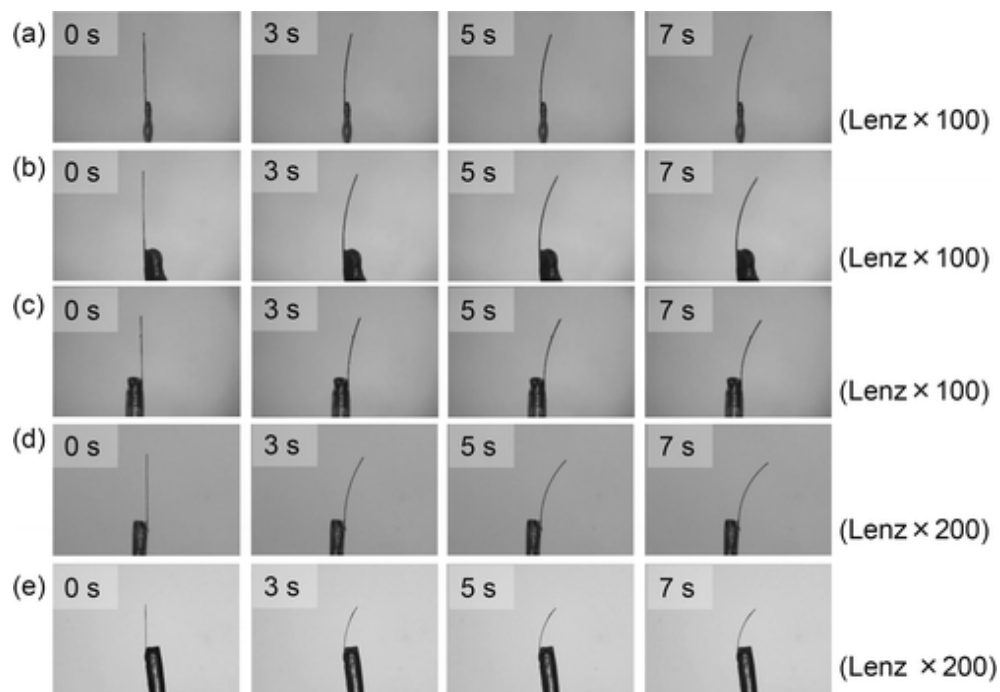
Figure 1.19: Photoinduced diarylethene single crystal bending upon irradiation with UV light to the (0 1 0) face in different thickness samples: (a) 16.70, (b) 12.58, (c) 9.97, (d) 5.34, and (e) 3.82 μm. (Reproduced with the permission of American Chemical Society) [15]
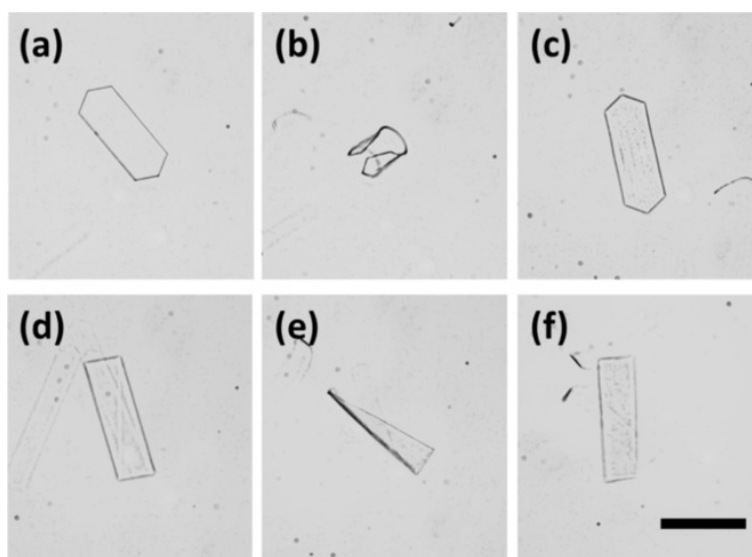
Figure 1.20: Reversible rolling of a 9MA hexagonal micro crystal and reversible twisting of a 9MA rectangle micro crystal upon UV. [16]

1.4 Organize Crystals at Micro-level (This Work)

Photomechanical crystals have shown superior performance on microscopic scales thanks to their high elastic moduli, high-energy density and fast response time compared with polymers. However, the development of macroscopic crystal actuators that can be widely used in real world is limited by their size. On the one hand, growing large crystals is difficult since crystals growth is sensitive to environment and can be easily disturbed. On the other hand, large crystals tend to fracture because of internal stress, and thick crystals suffer from low light penetration which prohibits light to mechanical work conversion.

The work in this thesis solves the problem by organizing photomechanical nanocrystals in templates. It combines the best of both worlds where it is processable like polymers but it also attains high performance of organic crystals. In Chapter 3, a hybrid organic-inorganic actuator with diarylethene nanocrystals ordered in an anodic aluminum oxide (AAO) template has been made. The actuator shares the concept of bimorph structure observed for single crystals which leads to photomechanical motion in macroscopic scale. An amount of 0.1 mg of active materials in this actuator generates enough force to tilt a 1.28 g mirror. Chapter 4 discusses the effects of both the inorganic and organic parts on the performance of this actuator. Another inorganic template with a higher elastic modulus is used to compare with the AAO template. Two diarylethene derivatives with opposite crystal deformation directions are used to investigate the curvature and performance of this hybrid bending actuator. Chapter 5 extends the hybrid approach to a glass array template with different thicknesses and much larger channels. It demonstrates that the hybrid approach provides a general way to make macroscopic light-powered actuators.

Chapter 2

Experimental Methods

2.1   Inorganic-Organic Hybrid Materials

2.1.1   AAO Template Filling

This method describes the preparation of AAO templates with crystalline nanowires of diarylethene (DAE) derivatives. An empty AAO template (Whatman Anodisc fron Sigma Aldrich, nominal pore diameter 200 nm, template diameter 13 mm) was immersed in deionized water and sonicated for 25 s. 5 mg of DAE was dissolved in 100 μL CH$_2$Cl$_2$. A Kimwipe soaked with 2 mL CH$_2$Cl$_2$ was placed on a frosted glass. A Teflon cylinder was placed on the Kimwipe, and the sonicated template was then put on the cylinder. The homogeneous prepared solution was then deposited on the empty AAO template. Based on experience, the template had better performance when the solution was deposited on the side with smaller size pores (shiny side) which is usually the side facing up from the container box. The template was then covered with a bell jar, a 2-inch diameter semi-sphere
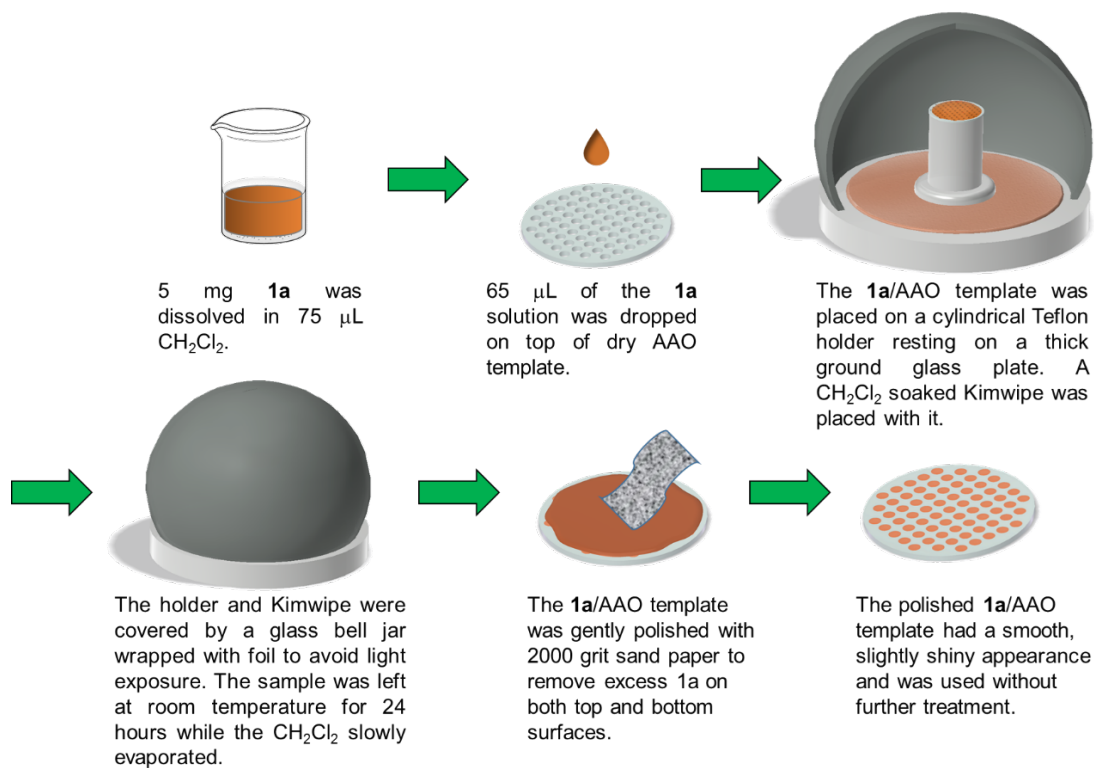
Figure 2.1: Procedure for preparation of DAE/AAO template.

glass made at UCR. The kimwipe should be just smaller than the bell jar. After 24 hours

at room temperature, the solvent should evaporate completely and the DAE will crystallize

inside the pores nicely. The dry AAO template was then polished with a 1500 grit sand

paper gently for 10 min on each side. The templates should look smooth and reflective after

polishing. (Figure 2.1)

2.1.2 Glass Capillaries Template Filling

The method of DAE filling in glass capillaries is similar to that for the AAO

templates except for sonicating and the DAE amount. AAO DAE nanowires were grown

in the glass templates by a solvent-annealing method. A solution with DAE dissolved in CH_2Cl_2 (5 mg in 100 μL for the 0.05 mm thick template; 10 mg in 150 μL for the 0.1 mm thick template; 20 mg in 200 μL for the 0.2 mm thickness template; 25 mg in 250 μL for the 0.5 mm thick template; 30 mg in 250 μL for the 1.0 mm thick template) was deposited on one side of the glass template. The template was supported on a homemade Teflon cylinder standing on a CH_2Cl_2-soaked (2 mL) Kimwipe tissue. The assembly was then covered with a bell jar, inside which the CH_2Cl_2 slowly evaporated while the DAE molecules crystallized inside the channels. After 24h of solvent annealing under the bell jar at room temperature, the DAE-glass template was removed and gently polished with 1500 grit sandpaper on the DAE deposited side to remove residual DAE from the top. From experience, the bottom side of glass didn't have DAE residual. Since the glass templates are shiny and reflective by itself, one can easily identify DAE residue on it when it looks dull.

2.1.3   Scattering Fiber Filling

DAE Solvent Filling

Pipet tips in different sizes were stacked together in a syringe as a micro-syringe. A 250 μm diameter, 1 inch long fiber was in the end of the micro-syringe (Figure 2.2). 10 mg DAE was dissolved in 200 μL CH_2Cl_2. The end of fiber was immersed into the solution. The solution was then pulled slowly to the inside of fiber with the micro-syringe. The solution filled fiber was then stored in the dark at room temperature for 72 hours for the solvent to fully evaporate.

Figure 2.2: A "micro-syringe" used for fiber filling.

Azobenzene Melt Filling

An azobenzene derivative (AB) yellow powder (10 mg) in *Trans* form was irradiated with a 365nm flashlight (from 5 mm away) for 10 min and then turned into the *cis*-AB orange liquid. The AB orange liquid was pulled into the hole-only fiber with the micro-syringe, filling 4-5 mm of the hollow fiber. After 24 hours, the *cis* liquid returns to solid *trans* form, which no longer has an orange color. Irradiation by external 365 nm light causes *trans* to isomerize to *cis* and melt, again changing color.

2.2 UV-Vis Absorption Spectroscopy for the Measurement of DAE Amount in the Templates

For diarylethene molecules, UV-vis absorption spectra were collected in hexanes as a solvent and a Varian Cary 50 UV/vis spectrophotometer. To measure the amount of

reacted DAE crystals, a UV irradiated DAE-AAO template was dissolved in 2 mL hexanes overnight. 40 μL of the DAE solution was diluted in 2 mL hexanes to get a 50 times dilution. To measure the amount of DAE crystals in a DAE-AAO template, the template was first irradiated by visible light for 10 min to make sure it was in the open form. The template was then submerged in 2 mL of hexanes overnight. The DAE solution was then diluted by 500 times. The measurement of the amount of loading DAE in a DAE-glass template is similar as above, the amount of hexanes solvent should be increased based on the thickness ratio of two templates.

2.3   Powder X-ray Diffraction

PXRD data were collected using a Bruker D8 Advance X-ray powder diffractometer (CuK$_\alpha$ radiation, λ=1.5418 Å, 45 kV/40 mA power) at room temperature.

2.4   Scanning Electron Microscopy (SEM) Measurement

2.4.1   Sputter Coating

The sample was stuck to a piece of conducting copper tape which was then fixed on a SEM stub. It was coated with Pt/Pd using a sputter coater (Cressington 108 Auto) for 40 seconds. The screw underneath the stage was adjusted so that the distance between the sample and sputter source is about 1-2 cm. The lid of the sputter coater should be covered well and sealed to avoid a long vacuuming time.

2.4.2 Scanning Electron Microscope

The SEM images were collected using a FEI NNS450 microscope with a 5 kV electron beam under high vacuum (10^{-7} torr). An Everhart-Thornley Detector (ETD) and a Through Lens Detector (TLD) were used to produce high resolution images. A higher voltage around 20 kv gives better images for highly conductive materials.

2.5 Photomechanical Displacement Measurement

2.5.1 Beam Displacement

Light from a 0.95 mW Helium-Neon laser (633 nm wavelength) was used in an interferometer set-up to measure the displacement of the actuator load. The beam was incident on a beamsplitter which reflected a portion of the beam downward onto a mirror (1 inch diameter) supported by the photomechanical DAE/AAO template. The remainder of the beam was reflected by a fixed mirror to be used as the reference. The two beams were projected onto a wall 4.8 m away and the displacement of the template beam was measured. The photomechanical DAE/AAO template was put on a transparent microscope slide with one half covered by an opaque tape. The light that converted open-ring DAE to close-ring DAE was obtained from a light-emitting diode (1 watt at 394 nm from Super Bright LEDs Inc.) placed 2.5 cm below the template. The intensity at the sample was 3.5 mW/cm^2. To convert close-ring DAE back to open-ring DAE, a 532 nm laser beam was passed through a diffuser and directed onto the template, resulting in an intensity of 56 mW/cm^2. (Figure 2.3)
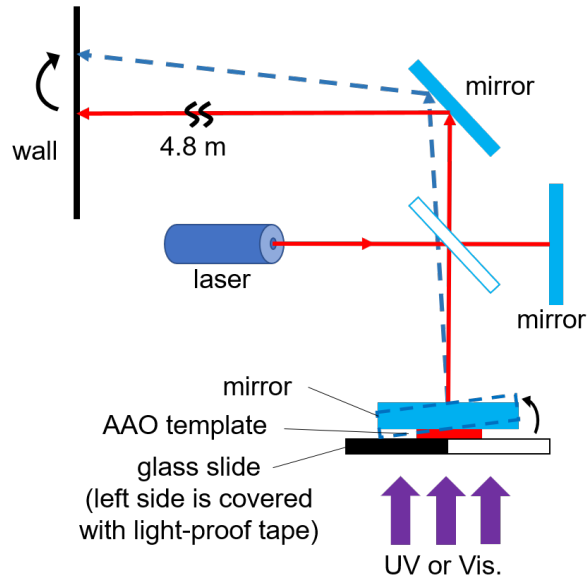
Figure 2.3: Illustrative diagram of beam displacement set-up.

2.5.2 Piezo-electronic Pressure Measurement

The elastic modulus of the templates as well as their optomechanical response was measured using a setup consisting of a sample holder, an Entran force sensor PS-30A with a specially constructed tip and a manual translation stage. The Entran force sensor was attached to the translation stage. The tip was an aluminum machined part assembled with a steel ball bearing by press fit (diameter=2.3mm) at the end. The horizontal sample, supported at the edges, was positioned under the tip. As the stage was translated downward, the tip pressed downward on the sample causing it to bend; the force sensor output gave the force the sample was exerting on the tip.

Chapter 3

Hybrid Organic–Inorganic Photon-Powered Actuators Based on Aligned Diarylethene Nanocrystals

3.1 Abstract

When photochromic molecules are organized in a crystal, the small-scale forces generated by molecular photoisomerization events can add together to generate work on micro- or macroscopic length-scales. In this chapter, photomechanical nanocrystals themselves are organized on macroscopic length-scales using a porous inorganic template. The organic diarylethene component provides the reversible photoresponse, while the porous alumina

29

component provides structural support and directionality. This hybrid organic-inorganic photomechanical material acts as a bending actuator. Using ultraviolet and visible photons as power inputs, as little as 0.1 mg of reacted material generates enough force to tilt a 1.28 g mirror and steer a laser beam. The motion can be cycled multiple times in air and under water. Actuator figures-of-merit like energy-to-work conversion efficiency and stiffness are probably limited by the high elastic modulus of the inorganic template, providing an obvious pathway for optimization.

3.2 Introduction

Organic photomechanical materials can transform molecular-scale photoisomerization events into a wide variety of mechanical behaviors, including bending, twisting, and coiling. [33, 83, 84] Polymer-based materials provide a way to fabricate and pattern photomechanical structures [85, 86] but suffer from low elastic moduli, low energy density and slow response times due to the presence of the host polymer. Assembling photochromes into neat molecular crystals avoids the need for a host, and this class of materials can in principle lead to higher energy densities, hardness and response speed. [77]

When photochromic molecules are assembled into a crystal, their photoisomerization can generate an anisotropic expansion of the crystal lattice (Figure 3.1a). This lattice expansion, when confined to one side of the crystal, can induce bending as strain builds up between the reactant and product crystal phases [15, 56, 87] This mechanism has led to impressive demonstrations of photomechanical molecular crystals that undergo light-induced bending [56, 87–94], twisting [13–15], and expansion [12] on microscopic lengthscales. But

the use of photomechanical molecular crystals in macroscopic actuator structures has been limited for several practical reasons. The growth of large crystals is difficult and time consuming. Furthermore, large crystals tend to shatter due to internal stress and also suffer from limited light penetration that lowers the total isomerization yield and prevents mechanical motion. [12, 95]

To make molecular crystals more processable, several groups have explored embedding organic nanocrystals in a polymer matrix to make a composite photomechanical material. [96–99] Using several different photochromes, they found that polymer films with embedded photoactive molecular crystals could exhibit bending, but the work generation was not quantified and the mechanical motion was not photoreversible. In these previous attempts, the molecular crystal component typically consisted of random sizes and orientations. Work in the inorganic nanoparticle field has shown that assembly of functional monodisperse nanoparticles into ordered arrays is vital for generating useful collective properties. [100, 101] Thus a current challenge is to prepare an ordered, monodisperse array of photomechanical organic nanocrystals that can harness the collective motion of the assembly.

The approach taken here is to make a "crystal" of nanocrystals, in which expansion of individual nanocrystals in an ordered array generates internal stress that causes the macroscopic structure to deform. The same bimorph mechanism that leads to mechanical motion in a single crystal (Figure 3.1a) can be realized on a larger scale through ordered growth of nanocrystals in an inorganic template (Figure 3.1b), with the template also contributing to the mechanical integrity of the composite. To realize this concept, we chose 1,2-
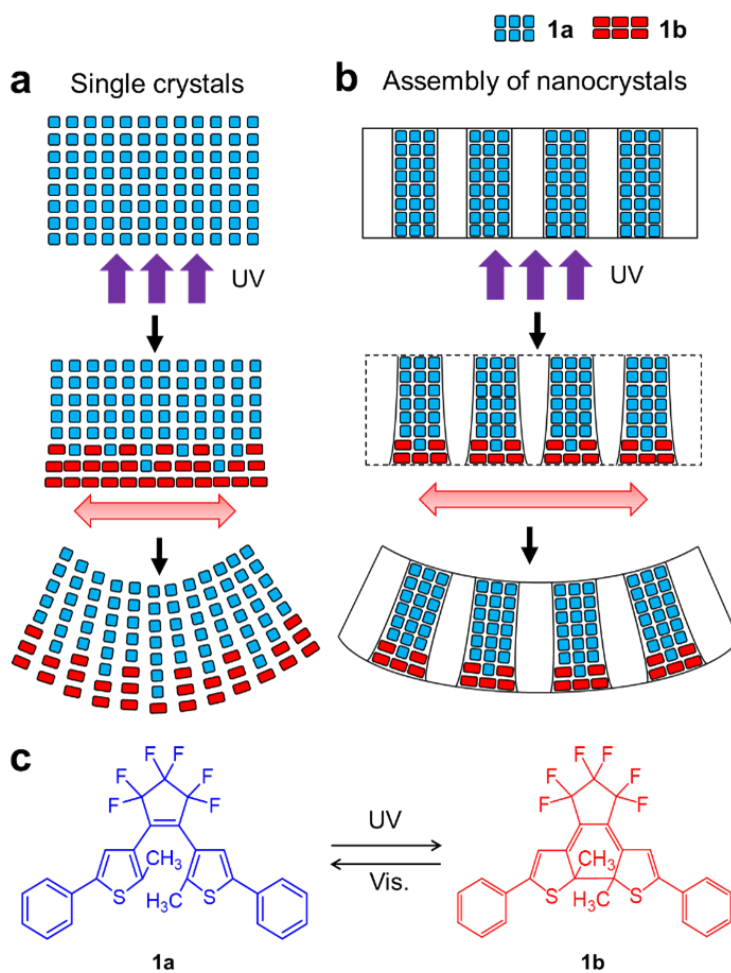
Figure 3.1: (a) Schematic illustration of how preferential formation of photoproduct on one side of a crystal leads to asymmet-ric expansion and crystal bending. (b) A porous template allows the creation of an ordered array of crystalline nanowires that can drive bending of the composite struc-ture. (c) Photochemical interconversion between ring-open (**1a**) and ring-closed (**1b**) diarylethene isomers.

bis(2-methyl-5-phenyl-3-thienyl)perfluorocyclopentene (**1a**), a diarylethene (DAE) derivative that undergoes a unimolecular photoisomerization between its ring-open and ring-closed isomers (Figure 3.1c) to be the active element. The isomers are thermally stable but can be switched back and forth using UV and visible light for hundreds of cycles. [11, 69, 102] The photomechanical behavior of individual DAE microcrystals has been extensively characterized [10, 11, 14, 15, 40, 102–106], and single DAE microneedles are capable of lifting objects $100\times$ more massive than the crystal itself. [103] But so far, no one has devised a path that leads from individual microcrystals to macroscopic actuator structures.

3.3 Crystal Orientation

In this Article, we take advantage of the ordering provided by anodic aluminum oxide (AAO) templates, a porous ceramic whose pore diameters and wall thicknesses can be tuned by electrochemical etching conditions. [107] To create ordered arrays of **1a** nanocrystals, we utilized commercially available Whatman Anodisc templates with a 60 μm thickness, a nominal pore diameter of 200 nm, and an overall diameter of 12.7 mm were used as received. A solvent annealing method (Figure S3.1) was used to facilitate growth of crystalline nanowires of **1a** in the AAO channels. [108] After crystal growth, the template is mechanically polished to remove excess **1a**. When the template was dissolved using concentrated acid, nanowires were obtained (Figure 3.2a). When exposed to 405 nm light, liberated nanowires can reversibly bend and expand, showing that the photomechanical response is preserved in the nanowire form (Figure S3.2). Polarized light microscopy confirmed that the nanowire bundles consist of oriented crystal domains (Figure S3.3). Powder

X-ray diffraction (PXRD) measurements on intact templates containing vertical nanowires (Figure 3.2b) show a dominant peak at $2\theta=15°$, corresponding to the (020) Miller plane. This plane runs perpendicular to the crystal b-axis shown in Figure 3.3. Since the PXRD pattern of the intact templates also includes contributions from residual crystallites on the surface, we dissolved the template in H_3PO_4 and collected the nanowires lying flat on an AAO filter surface. The horizontal nanowires showed only peaks corresponding to Miller planes that make right angles to the (020) plane, as expected Figure 3.2c). Together, these data confirm that **1a** preserves its crystal packing and density in the nanowires, which are oriented along the b-axis.

3.4   Hybrid Template Showed Photoinduced Bending

Photoconversion between the two DAE photoisomers can be accomplished using 405 nm and 532 nm light, wavelengths that correspond to inexpensive, solid-state laser sources. Figure 3.3 shows that partial conversion of **1a** to **1b** changes the crystal packing and causes a contraction along the b-axis and an expansion along the a-axis, both on the order of 0.1%. [109] There have been no reports of a photomechanical response for macroscopic crystals of **1a**, but we recently found that crystal microribbons composed of **1a** can undergo photoinduced twisting. [14] When one half of a DAE-infused template was illuminated with 405 nm light, it quickly turned blue (Figure 3.4a), and diffuse reflectance absorption confirmed creation of the**1b** photoisomer (Figure S3.4). Viewed from the side, the template was also observed to bend as shown in Figure 3.4b. Both the color change and bending could be completely reversed after exposure to 532 nm light. The template always
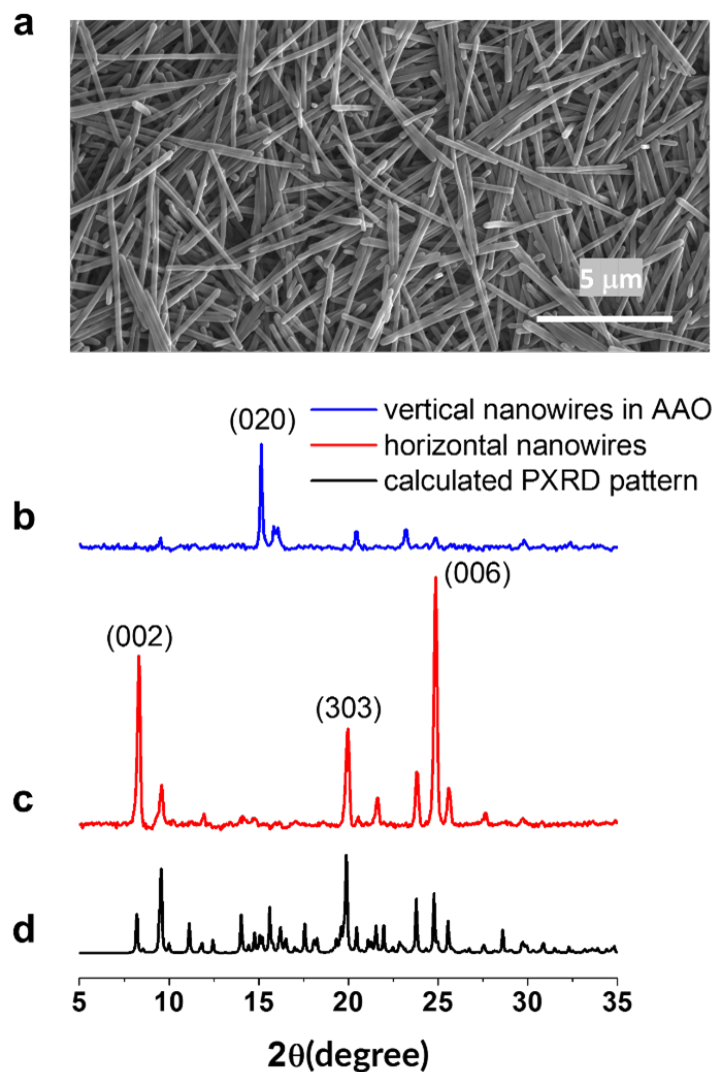
Figure 3.2: (a) Scanning electron microscopy images of obtained nan-owires. (b) PXRD data for vertical DAE nanowires aligned in the AAO template. The dominant (020) peak seen for the vertical nanowires belongs to a Miller plane that is perpendicular to the crystal b-axis, so the b-axis must lie parallel to the nanowire long axis. (c) PXRD data for horizontal nanowires lying on top of an Anodisc filter. The horizontal nanowires exhibit strong (002), (303) and (006) peaks, all corresponding to planes perpendicular to (020) plane. (d) PXRD pattern calculated from the **1a** crystal structure.
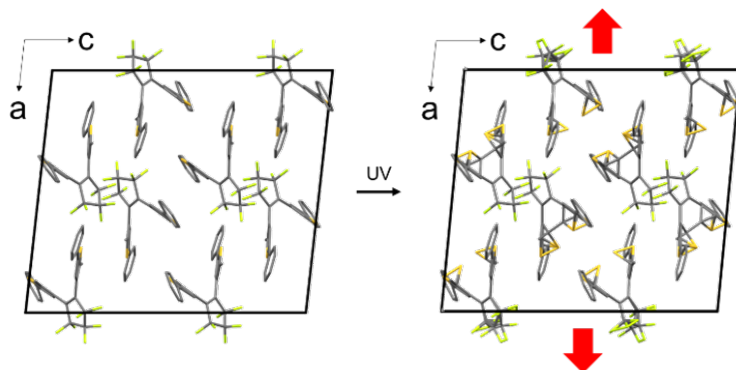
Figure 3.3: Crystal structure (view along b-axis) of **1a** before UV irradiation(left) and crystal structure of a partially convert-ed crystal containing mixture of **1a** and**1b** after UV irra-diation(right). After irradiation, the crystal expands along the a-axis and contracts along the b-axis.

bends away from the UV light, and a bend due to bottom irradiation could be canceled out by irradiation of the top to create a balanced bimorph strain (Figure S3.5). It is interesting that a macroscopic assembly of nanocrystals exhibits photomechanical bending, while macroscopic crystals do not.

3.5   Beam Steering Quantification

Because the photoinduced bending of the template results from the simultaneous deformation of many nanowires, this motion can produce significant amounts of mechanical work. To quantify the work generation as a bending actuator, a two-beam set-up (Figure 3.5a) was used to monitor the ability of the template to tilt a standard 1 inch diameter mirror and steer a laser beam. Illuminating different quadrants of a single template can tilt a standard 1 inch diameter mirror in any direction and move a laser beam from its reference position (Figure 3.5b). A laser beam deviation of 0.008 radians allows us to calculate that

36
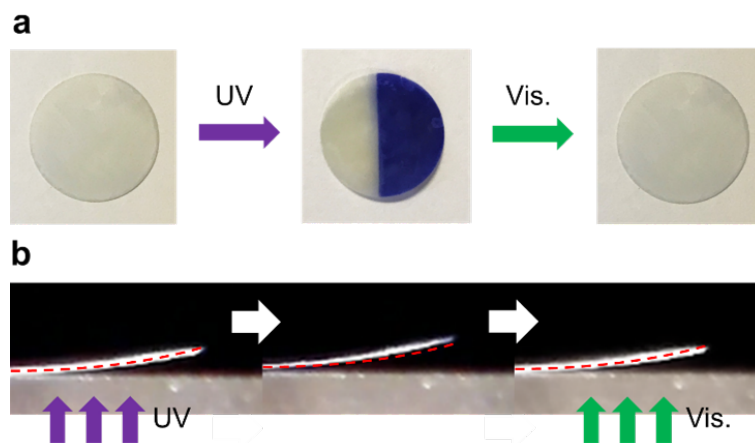
Figure 3.4: (a) Color change of AAO template after right half is irradiated with UV and then visible light. (b) Reversible template bending after exposure to UV and then visible light. The template is viewed from the side.

the mirror edge undergoes a vertical displacement on the order of 100 microns (Figures S3.8-S3.9). Movies of the light-induced mirror motion and laser beam displacement can be viewed as Supporting Information Videos 1 and 2 from ACS publications Chemistry of Materials online.

The displacement of the beam allows us to calculate an induced template curvature of 2.5×10^{-3} mm^{-1} and an effective expansion of 1.5×10^{-4} for the irradiated side of the template (Figures S3.8-S3.9). This is about $7\times$ less than the molecular expansion along the crystal a-axis as deduced from x-ray crystallographic data on a partially reacted **1a** crystal. [109] This small expansion implies less than a 0.1 nm change in a 200 nm diameter pore and likely results from competition from the expansion/contraction along the a/b-axes, as well as confinement by the AAO template, which will resist the motion of the softer organic component. The molecular interaction with the channel walls is not known, but this will ultimately determine how the organic motion is curtailed by the template.
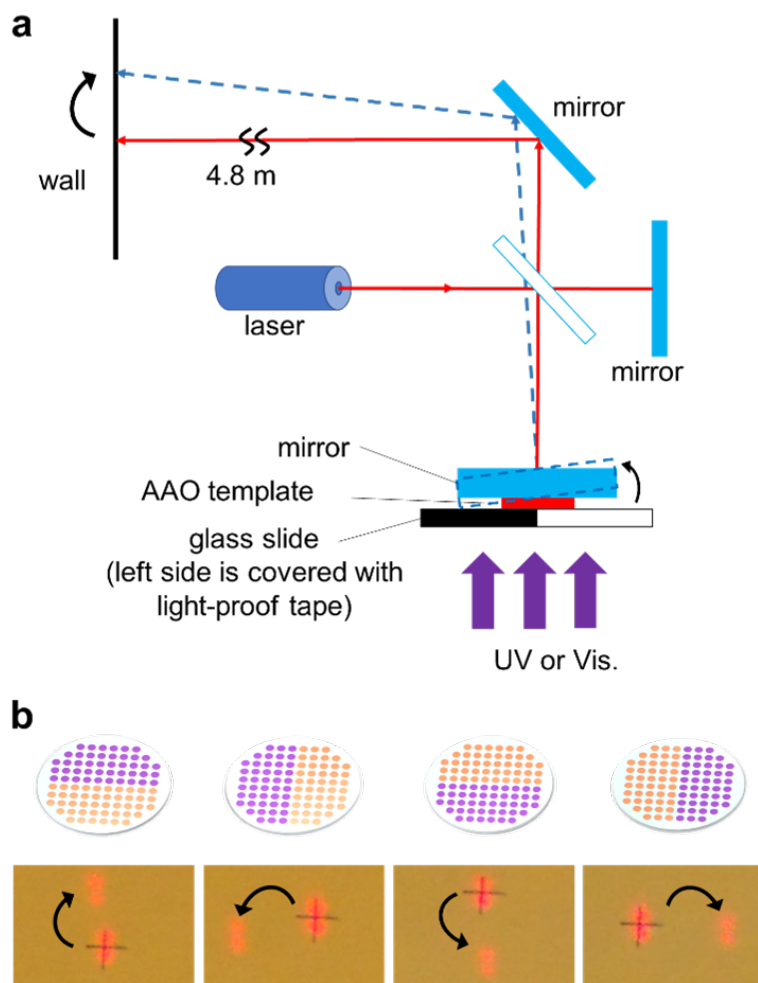
Figure 3.5: (a) Schematic outline of laser deflection set-up. (b) When different regions of the template are irradiated (shown in purple), the mirror tilts in different directions and displaces the beam (blue line) from the reference (red line). The spatial displacement of the spot from the reference spot (marked with a cross) can be used to calculate the vertical displacement of the mirror (Figures S3.8-S3.9).

3.6   Reproducibility in Air and in Water

DAE photochromes are generally resistant to fatigue but can undergo side-reactions that generate unreactive byproducts. [110] We found that the DAE-filled templates could undergo multiple displacement cycles in air, as shown in Figure 3.6a. The actuation also worked when the template was submerged under water, with only a 25% decrease in displacement and no loss of reversibility (Figure 3.6b). After about 50 cycles in air, a steady decrease in the photoinduced displacement was observed, accompanied by the appearance of a yellow color in the regenerated **1a** form. In bulk crystals, **1a** can be cycled more than 10^4 times [69], so it appears that the hybrid material undergoes accelerated degradation, possibly due to molecular interactions with the AAO walls.

3.7   Precise Control of Bending

The mechanical displacement closely tracks the photoisomerization reaction progress (Figure 3.7a). The linear dependence of the displacement ΔL on the production of **1b** allows precise control of the actuator position by controlling the duration of the light exposure. Figure 3.7b illustrates this control for sequential light exposures. When the light is turned off, the displacement undergoes a slight relaxation by about 5-10% but holds its position afterward. Note that any thermally induced expansion would be expected to completely relax during the off-period, so this observation places an upper limit on the thermal component of the actuation. When the light is turned on again, the displacement starts up where it left off. Under load, the displacement is stable in the absence of light, unlike piezoelectric
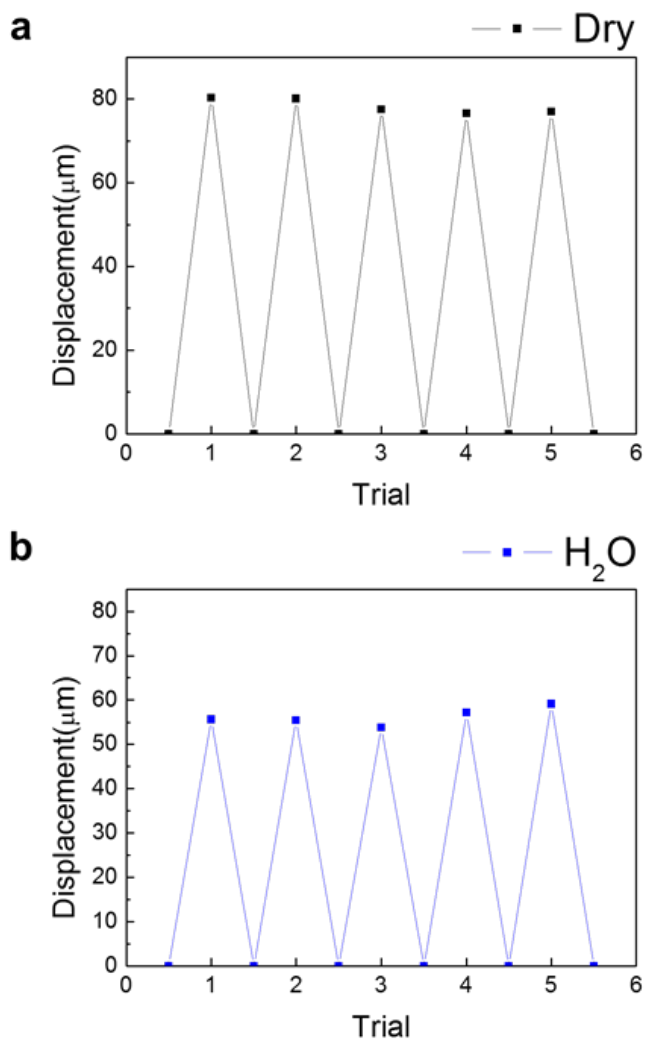
Figure 3.6: (a) Reproducibility of vertical mirror displacement for 5 2-minute UV irradiation cycles in air. (b) Reproducibility of vertical mirror displacement for 5 cycles in water of the same template.
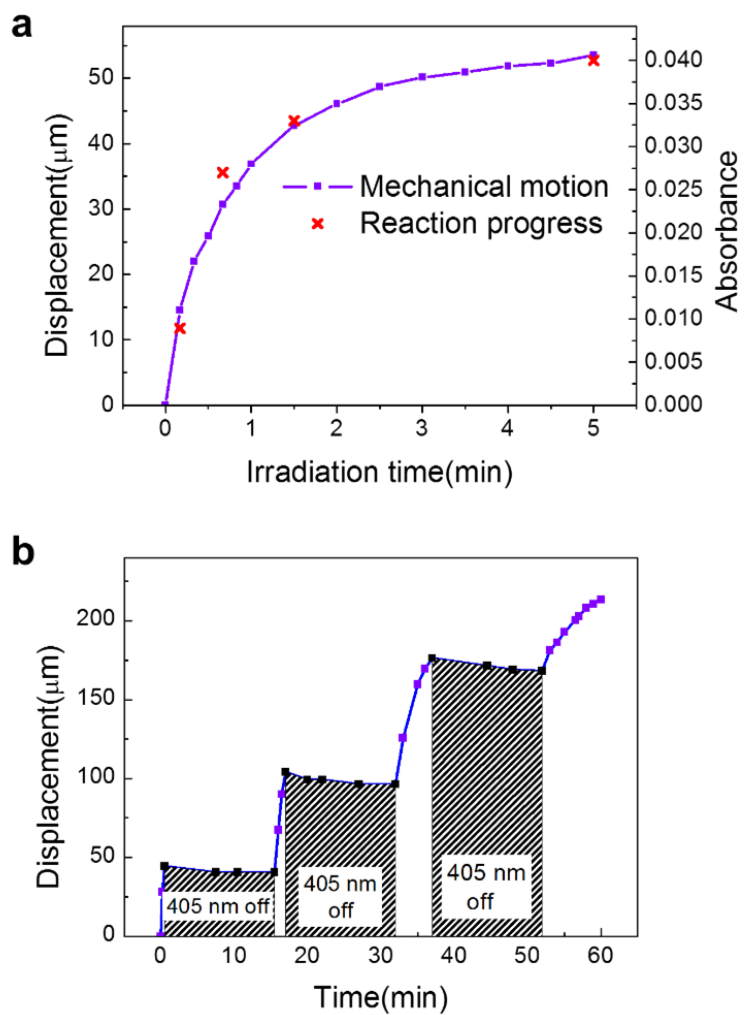
Figure 3.7: (a) Vertical beam displacement (squares) as a function of 405 nm irradiation time, and absorbance of ring-closed isomer**1b** (×). (b) Displacement versus time with 405 nm light turned on and off. The displacement is stable when the illumination is removed.

actuators which require an applied electric field to hold their position.

3.8 Photon-to-Work Conversion Efficiency

The photon-to-work conversion efficiency is an important figure-of-merit for photomechanical actuators, but the detailed mechanical analysis of bending actuator structures can be complicated. [111–113] The macroscopic samples used here allow this conversion efficiency to be measured simply in terms of a mass moved against gravity. Starting with a total mass of 1.6 mg of DAE in the template, a maximum conversion yield of 6.7% was measured by solvent extraction (Experimental Section). This means that 1×10^{-4} g of reacted DAE could generate enough force to lift a 1.28 g mirror, a mass ratio comparable to the best photothermal elastomer system. [114] From a typical beam displacement, we can calculate that the center of mass of a 1.28 g mirror was lifted by 5.5×10^{-5} m, for a total of 6.9×10^{-7} J of mechanical work. Given that 6.7% of the **1a** molecules are converted into **1b**, we calculate that 1.22×10^{17} 405 nm photons were absorbed (assuming an isomerization quantum yield of 1.039), with a total energy of 5.98×10^{-2} J. The (absorbed photon)-to-work efficiency is calculated to be 1.15×10^{-5}. This efficiency is comparable to what has been observed for photothermal bending actuators [115,116] but less than that deduced for liquid crystal elastomer bending systems. [111,117] If we consider the input energy to be the total number of incident photons, rather than just the absorbed photons, after 2 min under 7.05 mW/cm^2, we obtain an (incident photon)-to-work efficiency of 6.15×10^{-7}. These efficiencies represent the first quantitative estimate of the light-to-work conversion efficiency for a molecular crystal photomechanical actuator and provide a well-defined starting point

for future optimization.

In most cases, the efficiencies of photomechanical polymer systems have been evaluated in terms of unloaded bending or contraction. Our actuator structure generates an expansion that lifts a load. In this sense, it acts like a bending piezoelectric actuator, and it is instructive to evaluate it in terms of parameters commonly used for commercial piezoelectric actuators. This class of actuators is characterized by the maximum load they can move, known as the blocking force F_{block}, and their maximum displacement ΔL_0 in the absence of a load. The ratio of these two parameters gives the actuator stiffness $k_A = \frac{F_{block}}{\Delta L_0}$. The stiffness defines the linear relation between displacement and force generation, $\Delta L = \Delta L_0 - \frac{F}{k_A}$. By varying the load on top of the bending AAO template, we can measure the displacement (ΔL) versus force (F) curves shown in Figure 3.8. The ΔL versus loading force F curves are fit using an exponential function

$$\Delta L = \Delta L_0 e^{F/F_{block}} + y_0 \tag{3.1}$$

These fits yield R^2 values of 0.96 or greater for all templates measured, which all yielded exponential force decays (Figure S3.6). If we linearize these curves, $\Delta L \approx \Delta L_0(1 - \frac{F}{F_{block}})$, we can extract values for $\Delta L_0 = 0.16\pm0.08$ mm, $F_{block} = 0.035\pm0.006$ N and $k_A = 0.25\pm0.10$ N/mm. For comparison, commercially available piezoelectric bending actuators have $\Delta L_0 = 0.1\text{-}0.5$ mm and $F_{block} = 1\text{-}5$ N [118–120], leading to k_A values ranging from 2-100 N/mm. Our photomechanical actuators have comparable ΔL_0 values but F_{block} values that are approximately 100× lower, leading to stiffness values that are also about 100× lower.

Our composite photomechanical actuators cannot generate as much force as piezoelectric actuators, but there is substantial room for improvement. First, the F_{block} values
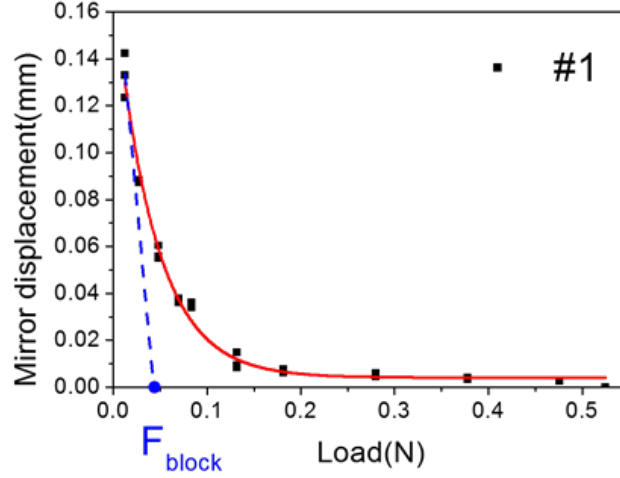
Figure 3.8: Plot of vertical displacement versus load for a typical DAE/AAO bending actuator (denoted #1, black squares), along with exponential fit (red line). A linear fit to the initial decay is shown in blue, along with the value of F_{block} extracted from this fit.

are extrapolated from the linear region of the exponential curve. As Figure 3.8 shows, the DAA/AAO actuator continues to generate displacement for values larger than F_{block}. Second, it is likely that the high elastic modulus of the AAO resists the photomechanical motion of the organic and lowers the amount of useful work that can be extracted. It is likely that using a more compliant template or a photochemical reaction that generates more force can boost both ΔL_0 and F_{block}. Third, the response time of several minutes seen in Figure 3.7b results from the low light intensities (5-10 mW/cm^2) used in our experiments and does not represent an intrinsic limitation of the material. Since the displacement tracks the photochemical reaction, increasing the light intensity to 1 W/cm^2 should lead to response times of less than a second.

The photoinduced bending requires that the photomechanical crystals are correctly oriented inside the template so that the expansion occurs in the plane of the sub-

strate. Different crystal orientations, lack of crystallinity, or incomplete filling of the channels can all suppress this effect. For example, while the majority ($\sim$80%) of our templates showed photomechanical responses that match those reported in Figures 3.4-3.8, the other 20% showed low or sometimes no photomechanical response at all. Usually the poorly performing samples suffered from poor loading, but we cannot rule out misdirected or random crystal growth. We tested two other photomechanical crystal materials, based on 1,2-bis(2,4-dimethyl-5-phenyl-3-thienyl)perfluorocyclopentene [121] and 4-fluoro-9-anthracenecarboxylic acid, [122] but neither was able to generate photoinduced bending in the AAO template. Both molecules filled the channels, but we suspect these crystals were not correctly oriented to generate stress across the horizontal plane of the template.

3.9   Conclusion

This work shows how ordering the organic active component on both the molecular scale (by oriented crystal growth in each pore) and the macroscopic scale (by growing a regular array of crystalline nanowires in a porous inorganic template) can lead to a hybrid photomechanical material capable of moving macroscopic objects solely through light power. Very small (sub-mg) amounts of material can move masses that are 10^4 times larger without being physically connected to an external power source. Lowering the template elastic modulus and varying the organic photochrome are two future pathways to improve actuator performance. These proof-of-principle experiments illustrate a way to incorporate photomechanical molecular crystals into macroscopic actuator structures, potentially opening up new applications for these interesting materials.

3.10   Supplementary Information

3.10.1   Experimental Section

Synthesis and crystal structure of 1a, partially reacted 1a/1b crystals

The synthesis of diarylethene **1a** has been described in the literature, along with the crystal structures of **1a** and partially reacted **1a/1b** crystals. [109]

Preparation of AAO templates with crystalline nanowires

A concentrated (5 mg of **1a** in 100 μL CH_2Cl_2) solution is deposited on one side of a 12.7 mm diameter AAO template (Whatman Anodisc, nominal pore diameter 200 nm). The template is suspended over a Teflon cylinder and covered with a bell jar. A Kimwipe soaked with CH_2Cl_2 is placed in the jar to slow down the evaporation rate from the template. During a period of 24 hours the CH_2Cl_2 slowly evaporates, allowing the **1a** molecules time to assemble and crystallize inside the pores. The dry AAO template is carefully polished to remove excess **1a** from the top and bottom.

Powder X-Ray Diffraction(PXRD) measurements

All PXRD data were collected using a Bruker D8 Advance X-ray powder diffractometer (CuK_α radiation, λ=1.5418 $\mathring{A}$, 45 kV/40 mA power) at room temperature. To collect PXRD data on nanowires that lie horizontally (along their long axis), the **1a** filled template was dissolved in 20% aqueous phosphoric acid to remove the alumina. The resulting **1a** nanowire suspension was deposited onto a blank AAO template, rinsed with deionized water and dried by vacuum filtration. The template was then air dried in an oven

set at 60 °C.

Scanning electron microscopy(SEM) measurements

The polished DAE/AAO template was stuck to a piece of conducting copper tape which was then fixed on a SEM stub. The sample was and coated with Pt/Pd using a sputter coater (Cressington 108 Auto) for 30 seconds. The SEM images were collected using a FEI NNS450 microscope with a 5kV electron beam under high vacuum (10^{-7} torr). An Everhart-Thornley Detector (ETD) and a Through Lens Detector (TLD) were used to produce high resolution images.

UV-Vis absorption measurements

UV-vis absorption spectra were collected in hexanes as a solvent and a Varian Cary 50 UV/vis spectrophotometer. Diffuse reflectance spectroscopy was performed using a home-built instrument. This method could not be used to quantitatively assess the degree of photoconversion due to high scattering that prevented light penetration into the template interior.

Optical microscopy measurements

An AAO template loaded with **1a** was dissolved in 20% H_3PO_4 after 24 hours. A drop of the nanowire suspension was deposited on a microscope glass slide and covered with a microscope coverslip. To monitor the photomechanical motion, an Olympus IX70 microscope was used with 100× (1.25 numerical aperture) and 40× (0.6 numerical aperture) objectives. Images and videos were taken using an AMScope MU900 digital camera. The

nanowires were irradiated using 365 nm (5.0 mW/cm^2) and 532 nm (50 mW/cm^2) light from a microscope Hg lamp filtered through a dichroic mirror. For polarized optical microscopy measurements, the sample was placed between two square (2 cm × 2 cm) polarizers aligned at a 90° angle and imaged with a 40× (0.4 numerical aperture) objective.

Laser deflection measurements

As shown in Figure 3.5a, a 0.95 mW Helium-Neon laser (633 nm wavelength) is directed into a modified interferometer set-up. The beam is incident on a glass plate which reflects one beam downward onto a mirror supported by the photomechanical template. The other beam is reflected by a fixed mirror. The two reflected beams are projected on to a wall 4.8 m away. The photomechanical template is supported on a transparent microscope slide with one part covered with light-proof tape. A 1 mm thick mirror is put on top of the AAO template, along with a variable number of metal disks to vary the load. 405 nm light to convert **1a** to**1b** is obtained from a light-emitting diode placed 2.5 cm below the template. The intensity at the sample is 7.0 mW/cm^2. To convert**1b** back to **1a**, a 532 nm laser beam was passed through a diffuser and directed onto the template, resulting in an intensity of 4.2 mW/cm^2.

5 mg **1a** was dissolved in 75 μL CH$_2$Cl$_2$.

65 μL of the **1a** solution was dropped on top of dry AAO template.

The **1a**/AAO template was placed on a cylindrical Teflon holder resting on a thick ground glass plate. A CH$_2$Cl$_2$ soaked Kimwipe was placed with it.

The holder and Kimwipe were covered by a glass bell jar wrapped with foil to avoid light exposure. The sample was left at room temperature for 24 hours while the CH$_2$Cl$_2$ slowly evaporated.

The **1a**/AAO template was gently polished with 2000 grit sand paper to remove excess 1a on both top and bottom surfaces.

The polished **1a**/AAO template had a smooth, slightly shiny appearance and was used without further treatment.

Figure S3.1: Procedure for preparation of DAE/AAO template.
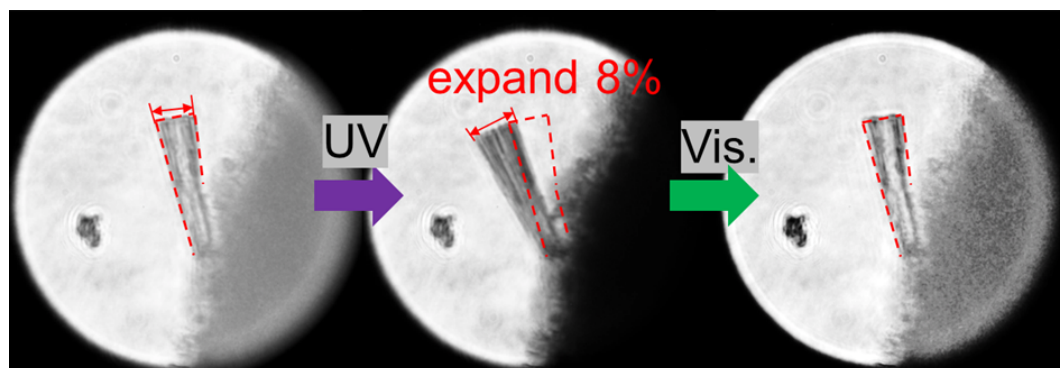
Figure S3.2: Nanowire bundles in solution expand and move after UV (405 nm) exposure and contract after visible (532 nm) light exposure. The nanowire bundle in the middle image has shifted and expanded by 8 %.
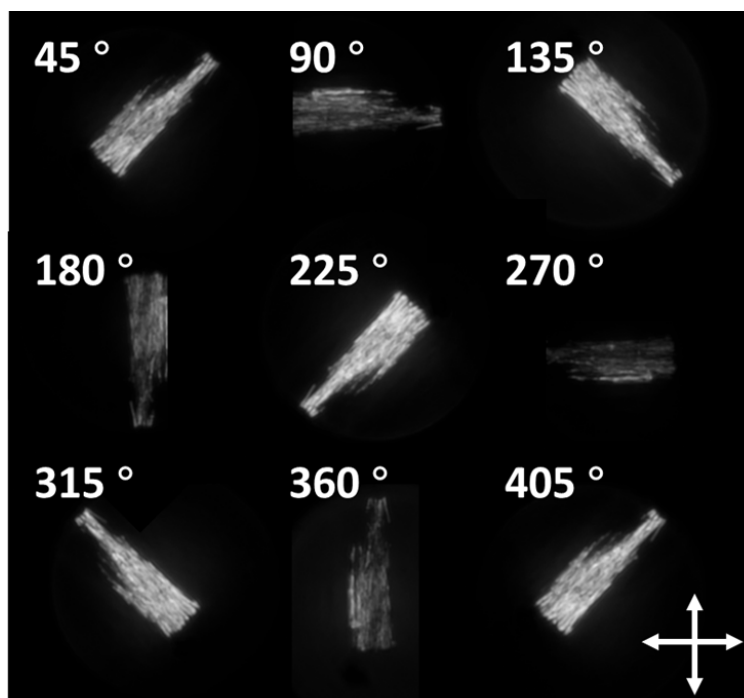
Figure S3.3: Polarized light microscopy images of a **1a** nanowire bundle. The nanowire bundle was rotated clockwise in 45 degree increments relative to the vertical polarizer. The contrast shows that the nanowires are oriented crystals, with the optic axis parallel to the long (growth) axis. The crossed arrows in the lower right corner show the direction of the crossed polarizers.
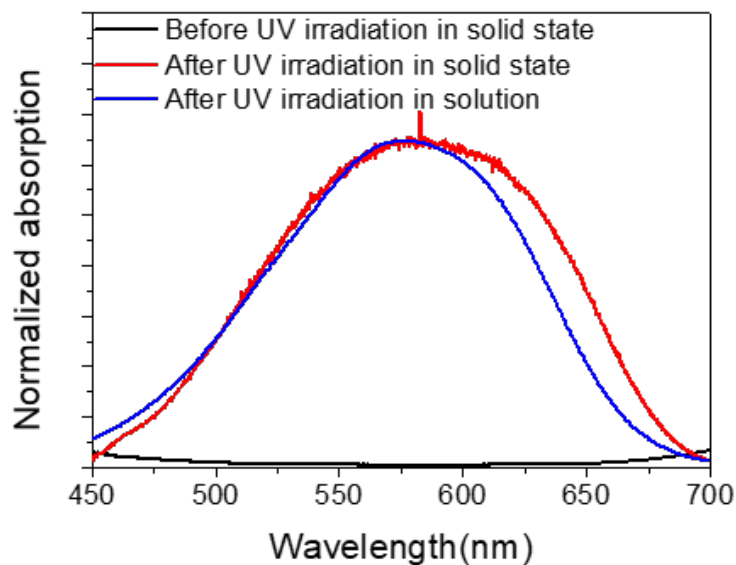
Figure S3.4: Diffuse reflectance absorption spectra of **1a**/AAO template before (black line) and after 10 s of UV (405 nm) irradiation (red line). The absorption spectrum of **1b** in hexanes is also shown for comparison (blue line).
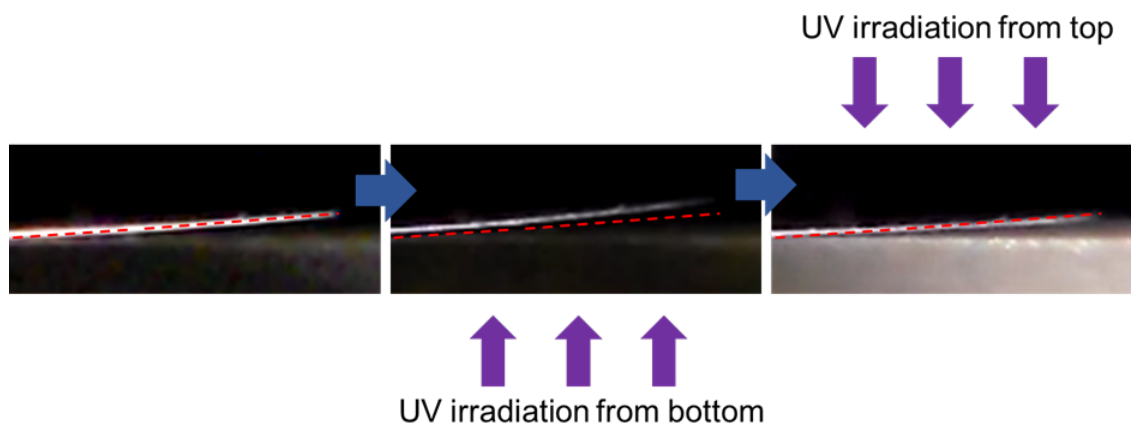
Figure S3.5: UV irradiation from the bottom causes the template to bend upward. Subsequent UV irradiation from the top causes the template to bend downward. The bottom expansion can be cancelled out by the top expansion because they form opposing bimorph structures.
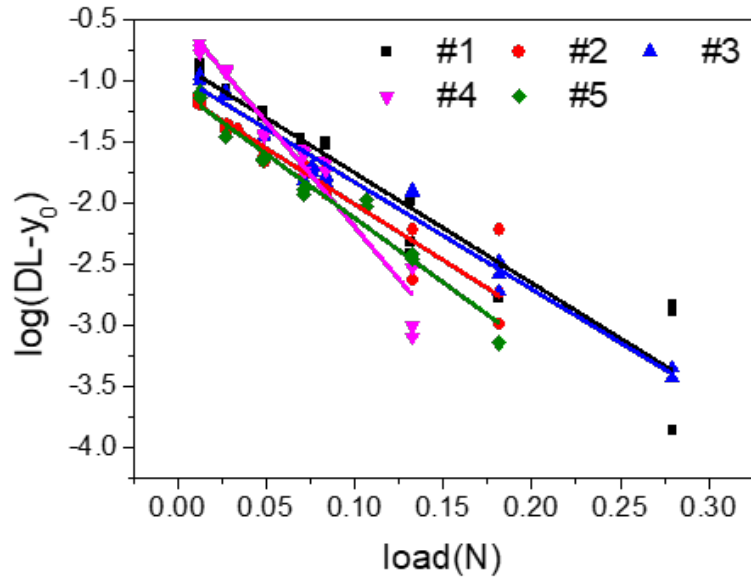
Figure S3.6: Log plots and linear fitting of $\log(\Delta L - y_0)$ versus load curves for 5 different templates.
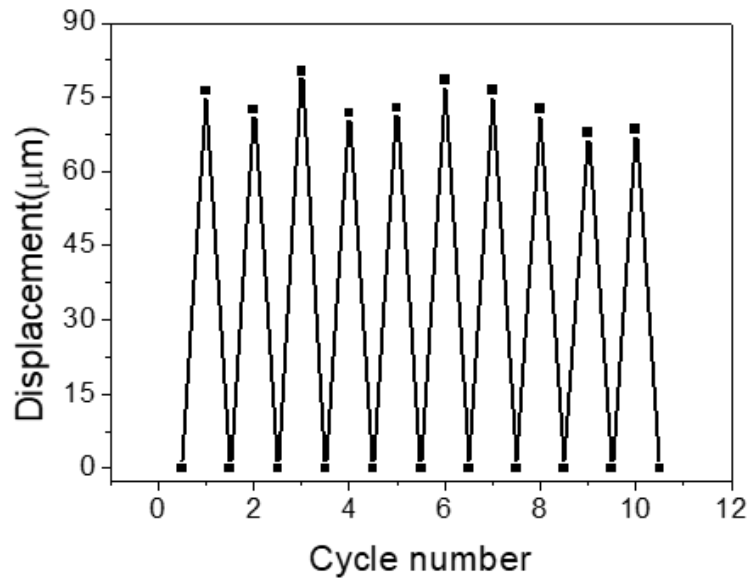
Figure S3.7: Reproducibility of vertical mirror displacement of beam displacement for a different template in air for 10 cycles.
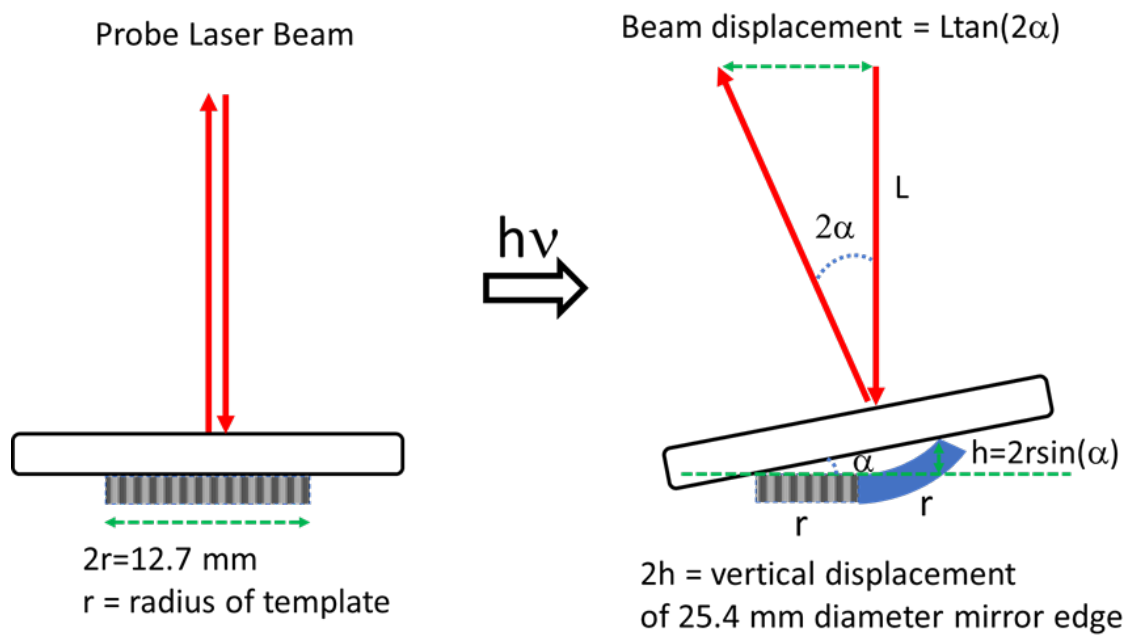
Figure S3.8: Geometry of laser beam displacement by bending template. The blue colored half of template represents the part that has been exposed to 405 nm light and undergone photoisomerization. For beam displacement measurements, distances L from the template are on the order of 5 m to detect $\alpha = 0.004$ rad.

L_1 = arc length of unreacted side of template = 6.35 mm, $2\beta R = L_1$
β = angle of isosceles triangle, $\tan(\beta)$=h/r=0.051mm/6.35mm; so β=0.008 rad
R = length of isosceles triangle that incorporates arc of bend template= 397 mm
L_2 = arc length of reacted side of template
d = template thickness = 0.06 mm
Expansion = L_2/L_1 = (R+d)/R= 1.00015
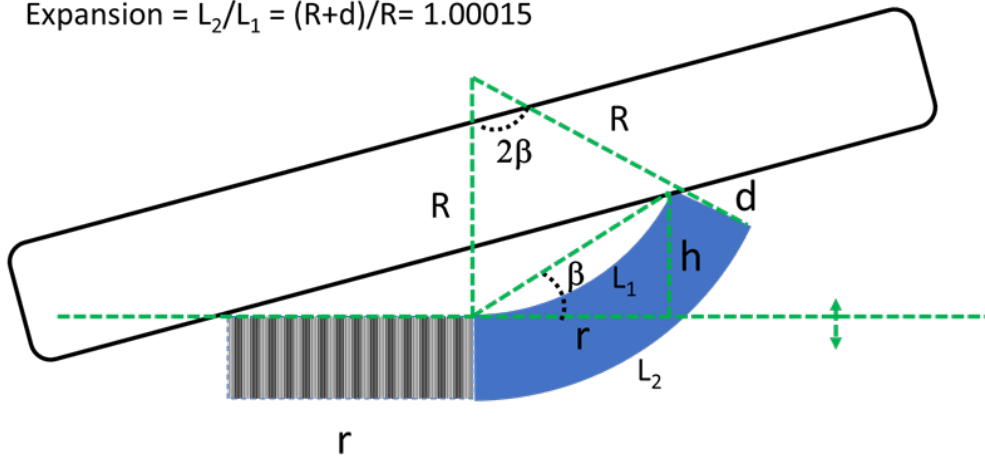
Figure S3.9: Geometry of bending template for calculating radius of curvature and expansion. Note that since the bend angle β is very small, the horizontal length of the curved template is assumed to be r = 6.35 mm.

Chapter 4

Effects of Template and Molecular Nanostructure on the Performance of Organic–Inorganic Photomechanical Actuator Membranes

4.1 Abstract

Porous anodic aluminum oxide (AAO) membranes template the growth of photochromic crystalline nanowires. The resulting organic-inorganic composite can function as a photomechanical bending actuator. In order to investigate how the nanostructural prop-

erties of both the organic and inorganic components affect the photomechanical response, the composite mechanical properties are characterized using a variety of methods. There is a significant variation in both morphology and elastic modulus for two commercially available AAO templates with nominally identical pore diameters of 200 nm. After these templates are filled with diarylethene molecules that undergo a ring-open to ring-closed photoisomerization, the light-generated curvature and mechanical work are evaluated using two different methods. The templates with a lower average elastic modulus (16 GPa versus 68 GPa) generate almost an order of magnitude more photomechanical work. The dependence of the photomechanical response on the chemical structure of the photochrome is assessed by comparing the performance of a diarylethene that undergoes a crystal expansion to that of one that undergoes a contraction, which leads to a decrease in curvature. Both the inorganic template and the organic active component play important roles in the overall photomechanical response, with substantial room to improve the performance.

4.2 Introduction

In many ways, photons are ideal energy transporters. They can travel over long distances with negligible loss and possess multiple parameters (wavelength, polarization, and even quantum state) that provide high flexibility in how they deliver energy. In most cases, photons must be converted to some other form of energy to perform useful work once they reach their destination. For example, photovoltaic materials convert light into voltage and current, which can then power electric motors and actuators. Photomechanical materials eliminate the need for electronic intermediates by converting light directly into

mechanical motion, usually via thermal expansion or photochemical reactions. Organic photochemistry provides a versatile mechanism that can be harnessed in both polymers and crystals to drive various types of mechanical motions. [33, 77, 84, 85] The composition and morphology of polymer-based photomechanical materials can be easily varied, but they also suffer from small elastic moduli, low energy densities, and slow response times. Photomechanical materials based on neat molecular crystals can, in principle, circumvent these problems. Unfortunately, it can be challenging to grow single crystals reproducibly with well-defined shapes and sizes for testing and device applications. [123,124] Furthermore, macroscopic single crystals often fracture during light exposure as neighboring reactant and product crystal domains generate interfacial strain that cannot be dissipated at a surface. [125] Nanoscale crystals avoid the fracture problem [12, 126, 127] but can only generate small amounts of work in isolation.

Embedding nanocrystals in polymer hosts is a promising route for making photomechanical materials [96–99], but ordering the nanocrystals is probably necessary to extract large amounts of work. We recently developed a new type of photomechanical actuator by creating organized arrays of molecular crystals inside a ceramic template. [128] These hybrid organic-inorganic materials consist of diarylethene (DAE) molecular crystal nanowires grown inside channels with diameter of 200nm in anodic aluminum oxide (AAO) porous templates. They rely on the hierarchical organization of the DAE molecules on both the nanometer scale (by its crystal packing) and the micron scale (by templated growth of crystalline nanowires in a dense vertical array). When exposed to ultraviolet (UV) light, the DAE molecule undergoes a ring-open to ring-closed photoisomerization reaction (Fig-
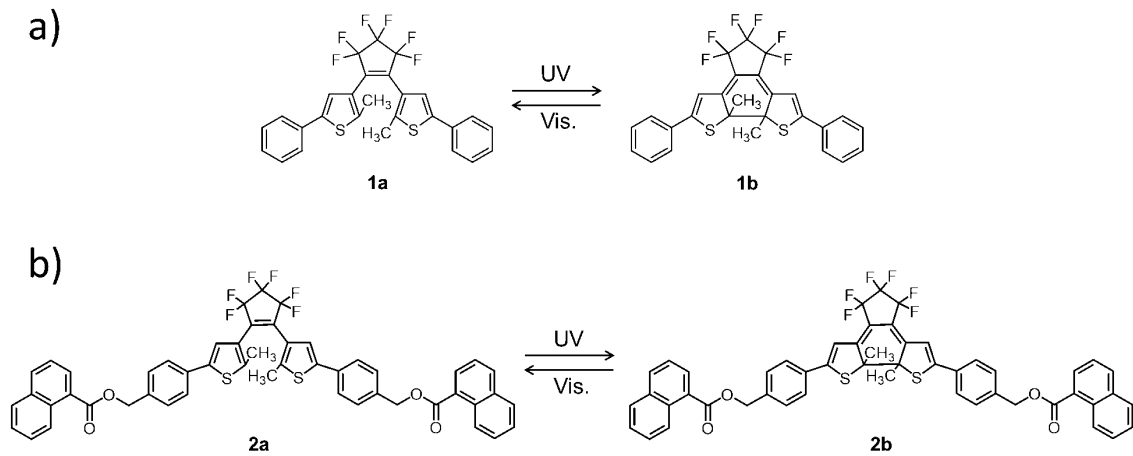
Figure 4.1: Photoisomerization reactions of (a) ring-open (**1a**) and ring-closed (**1b**) isomers; (b) ring-open (**2a**) and ring-closed (**2b**) isomers.

ure 4.1) that changes the crystal dimensions. [21] For molecule **1a**, the UV-reacted portion of the nanowire crystal expands, causing the entire composite to bend in response to the light. [129] The bending motion generated by a template weighing 0.01 g can lift objects with masses on the order of 10 g or more. The motion can be completely reversed upon exposure to visible light, which causes isomerization back to the ring-open form and could be repeated on the order of 50 cycles both in air and water.

The fabrication of a macroscopic structure based on aligned active nanocrystal elements provides a new approach to photomechanical actuators. But there remain important questions that need to be addressed before we can understand and engineer such composite materials. The first question concerns the role of the template. The porous AAO template is not just a way to grow aligned nanowires but is also a structural element of the actuating material. How do its properties affect the performance of the overall structure? A second question concerns the role of the organic component. How do different molecules and crystal

expansions/contractions affect the overall motion? In order to answer these questions, we must develop experiments that can accurately measure force-displacement curves in order to quantitatively compare different samples. The goal is to characterize the properties of these novel composite structures and assess their ultimate potential as photon-driven actuators.

In this chapter, we describe efforts to answer the above questions. Using a custom-designed force-displacement apparatus, we measure the elastic moduli of both empty and filled AAO templates. The same set-up allows us to measure force-displacement curves under illumination and calculate the light-generated curvature and mechanical work. Even before the organic component is added, we find a significant variation in both morphology and mechanical properties of two different commercially available AAO templates with nominally identical pore diameters (200 nm). These differences can change the amount of photomechanical work by up to an order of magnitude. The dependence of the photomechanical response on the chemical structure of the photochrome is assessed by comparing the previously studied DAE **1a** with a different DAE **2a**, which undergoes a crystal contraction as opposed to an expansion. We find that both the inorganic template and the organic active component play important roles in determining the overall photomechanical response. The results suggest that there is substantial room to improve the performance of these composites, especially by adjusting the elastic modulus of the porous template. The ultimate performance limits of these composites may be several orders of magnitude better than what is currently observed.

4.3   Morphology of Whatman and TOP Templates

Porous AAO templates are typically made by electrochemical etching of pristine aluminum foils followed by electropolishing. Although the basic procedure is well-established, details such as the purity of the starting Al, the applied voltages, and the composition and temperature of the etchant can all influence the final structure. [107] To examine this variability, we examined commercially available AAO templates, both with a specified pore diameter of 200 nm, from two different manufacturers,. For both templates, there was an asymmetry in the two sides. To keep track of sides, the side whose pores more closely match the specified pore diameter is denoted side A, while side B refers to the opposite side. In Figures 4.2a-b, we show SEM images of both A and B sides of the widely used Whatman Anodisc AAO template. These images can be compared to those of the TOP (Top membranes) template in Figures 4.2c-d. Both templates have 200 nm holes on the A side. However, the Whatman B side has much smaller diameter holes, on the order of 100 nm or less, and some regions where the pores are still covered by a crust of alumina that was not etched away. This thin crust with small holes actually covers up the larger diameter channels that penetrate through most of the template and are visible in some regions where the crust has broken away (Supporting Information, Figure S4.1). The B side of the Whatman template typically appears to be slightly shiny, so it is usually possible to identify each side by visual inspection. The TOP template, on the other hand, has much more uniform pore diameters. The 200 nm diameter pores on the A side broaden out to 300 nm on the B side, and there is no alumina crust as seen on the Whatman templates. For Whatman AAOs, side A has an open area ratio (OAR, defined as the empty
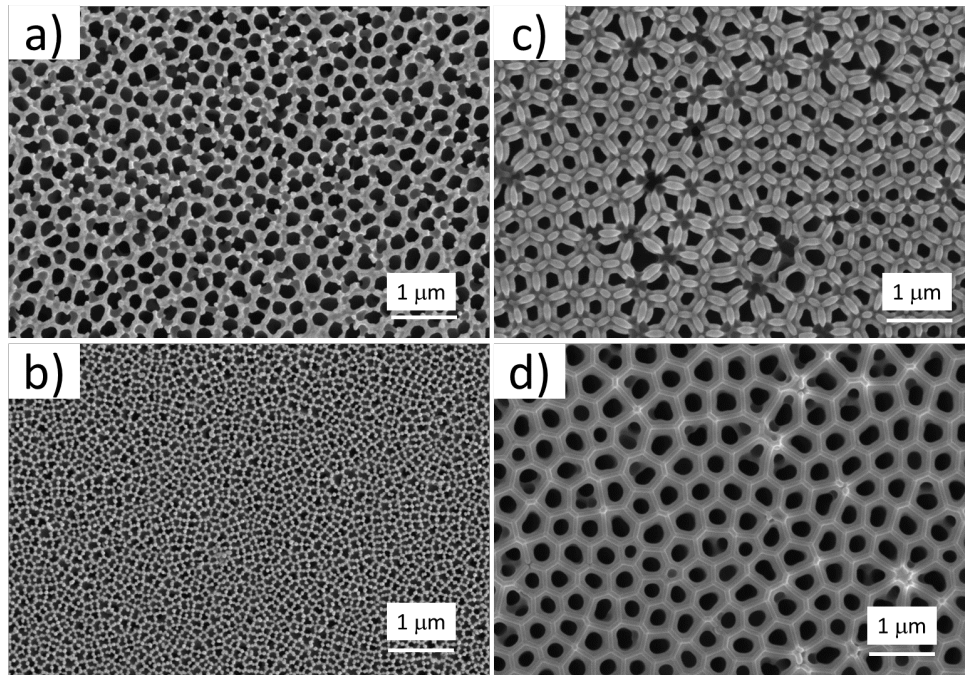
Figure 4.2: SEM images of (a) side A (average pore diameter 215 nm) and (b) side B (average pore diameter 107 nm) of Whatman AAO; Whatman AAOs were precleaned to remove surface debris; (c) A (average pore diameter 215 nm) and (d) B side (average pore diameter 268 nm) of TOP AAO. The open area ratio (OAR) was calculated to be (a) 51%, (b) 54%, (c) 21% and (d) 30% respectively.

channel area divided by the total area) of 51%, similar to the value of 54% on side B. The TOP AAOs have smaller OAR values, 21% for side A and 30% for side B.

Both Whatman and TOP templates fulfill their specifications in the sense that the A side has open pores with a 200 nm pore diameter. But the B sides are completely different: small occluded pores in the Whatman template versus larger clear openings in the TOP membrane. Both can function as filters with a 200 nm cutoff. Aside from filtration, we expect the morphology differences to give rise to different mechanical properties.

4.4   Elastic Moduli of Whatman and TOP Templates

To test the elastic modulus of the empty AAO membranes, a position-sensitive force sensor was positioned at the center of the AAO membrane whose edges were supported by a circular holder (Supporting Information, Figure S4.2). As the force sensor tip was pressed onto the membrane, the displacement was monitored as a function of applied force. The displacement x of a point that is a distance r from the disk center when a load F is applied at the center is given by [130]

$$x(r) = \frac{Fa^2}{16\pi D}\left[(1 - \frac{r^2}{a^2})(\frac{3+\nu}{1+\nu}) + \frac{2r^3}{a^2}\ln\left(\frac{r}{a}\right)\right] \tag{4.1}$$

where a is the disk radius and ν is Poisson's ratio. D is the bending stiffness of the plate given by

$$D = \frac{Eh^3}{12(1-\nu^2)} \tag{4.2}$$

where E is the elastic modulus and h is the thickness of the plate. If we set $r{=}0$, we can rearrange equation (4.1) and take the derivative, finding

$$E = \frac{3a^2}{4\pi h^3}(1-\nu)(3+\nu)\frac{\partial F}{\partial x} \tag{4.3}$$

The slope $\frac{\partial F}{\partial x}$ of the force as function of the displacement is the measured quantity (Supporting Information, Figure S4.3), and given $\nu{=}0.22$ [131], we can determine the elastic modulus E for the Whatman (TOP) templates. The measured values of E for 4 different empty AAO templates of each type are shown in Figure 4.3. There are three main observations from this data. First, the TOP E values were roughly 4× larger than those of the Whatman templates.

62
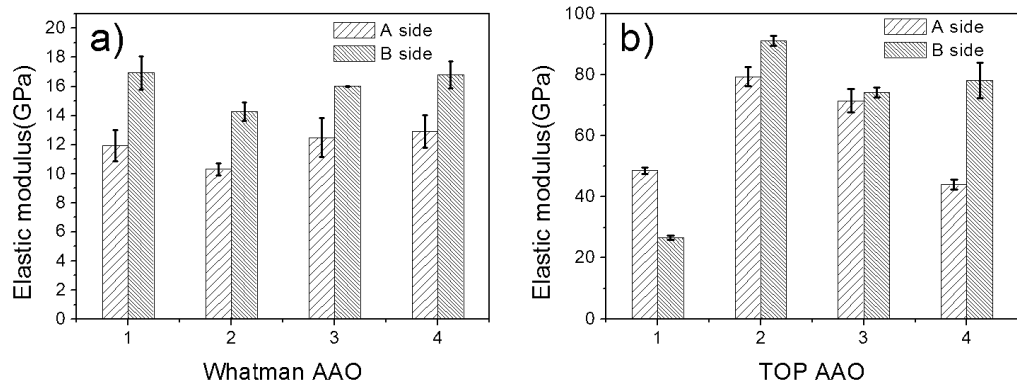
Figure 4.3: Results of elastic modulus measurements on 4 empty AAO templates pressing into side A (lower OAR) and side B (higher OAR) for (a) Whatman membranes with average E = 12±1.2 GPa (A side) and 16±1.5 GPa (B side); (b) TOP membranes with average E = 61±17 GPa (A side) and 68±28 GPa (B side).

The OAR numbers and images in Figure 4.2 indicate that about 50% of the Whatman membrane is composed of alumina, as compared to about 75% of the TOP membrane. A simple application of the rule of mixtures [132] would predict that the TOP membranes should have 0.75/0.50 = 1.5× larger E. This does not explain the factor of 4 observed, but a second consideration is that the elastic modulus of ceramics can be sensitive to the presence of chemical impurities and grain boundaries. It may be that the alumina in the Whatman template has a higher proportion of defects than that of the TOP membrane, further reducing its E value. [133, 134] A second observation is the greater variation in the E values of the TOP templates than of the Whatman templates. This was somewhat surprising, given that the TOP membranes typically had a more uniform surface appearance in the SEM images.

The most surprising observation from Figure 4.3 is that the E values depend on whether the load was applied to the A or B side. This is not completely unexpected given

the A/B side differences apparent in Figure 4.2. In both types, the B side with a larger OAR gives larger E values on average. This mechanical asymmetry is not commonly observed in bulk materials and requires some explanation. Typically, the elastic energy of a slightly bent slender beam takes the form [135]

$$U = \int EI(\frac{1}{2}\kappa^2 + \frac{1}{4}\kappa^4 + \ldots)ds \qquad (4.4)$$

where E is Young's modulus, I is the bending moment of area, $\boldsymbol{\kappa}$ is the curvature vector and is length along the beam. The energy cost of the beam is independent of the sign of the curvature; that is, the beam would bend upward as easily as downward. However, if the beam has broken up-down symmetry (as our samples do), and $\hat{\mathbf{N}}$ is the unit normal on one of the two horizontal surfaces, then a new symmetry-allowed terms of the type $(\boldsymbol{\kappa} \cdot \hat{\mathbf{N}}{=}\kappa$ can appear in the expression for the energy to give

$$U = \int EI(\frac{1}{2}\kappa^2 + \frac{1}{4}\kappa^4 + \cdots + \alpha\boldsymbol{\kappa} \cdot \hat{\mathbf{N}} + \frac{1}{2}\left(\boldsymbol{\kappa} \cdot \hat{\mathbf{N}}\right)^2 + \frac{1}{3}\left(\boldsymbol{\kappa} \cdot \hat{\mathbf{N}}\right)^3 + \ldots)ds \qquad (4.5)$$

Since the curvature is along the normal, and at equilibrium the $\alpha\boldsymbol{\kappa} \cdot \hat{\mathbf{N}}$ term can be neglected assuming there is no spontaneous curvature in the empty templates, Equation (4.5) simplifies to

$$U = \int EI(\frac{1}{2}(1 + \beta)\kappa^2 \pm \frac{1}{3}\gamma\kappa^3 + \ldots)ds \qquad (4.6)$$

Given $F{=}\frac{\partial U}{\partial x}$ and assuming that the deflection x of the center of the beam is proportional to the curvature $\boldsymbol{\kappa}$, i.e. $x{=}A\kappa$, we can show that the applied force is no longer linear in x,

$$F = mx \pm bx^2 \qquad (4.7)$$

where we have ignored higher order terms and m and b are undetermined constants. The

sign of the second term in Equation (4.7) depends in which direction the sample is being bent. The force versus displacement data from an asymmetric beam can be fit using the simple symmetric expression

$$F = m'x \tag{4.8}$$

But in the interval $(0,x_m)$, using the method of least squares, the result

$$m' = m \pm \frac{3}{4}bx_m \tag{4.9}$$

is obtained, indicating that simple linear fitting of data results in different m' and E values for the different sides.

The full force-displacement curves can be successfully fit using Equation (4.7), as illustrated in Figure 4.4. This analysis relies on symmetry arguments to explain the asymmetric E values, but it does not explain their microscopic origin. Hopefully it will provide a starting point for more sophisticated theories.

4.5   DAE Filling of Whatman and TOP Templates

From the data in Figures 4.2-4.4, it is clear that the empty TOP and Whatman AAO templates have very different mechanical properties, despite the fact that they share the same nominal pore diameter. The question is whether these differences manifest themselves in the photomechanical response after the templates are loaded with DAE. DAE crystals are grown in the template by a slow solvent annealing. After surface polishing, most of the pores of the AAO template are completely filled with DAE, as shown in the SEM images in Figures 4.5a and b. If the AAO template is dissolved in acid, the organic
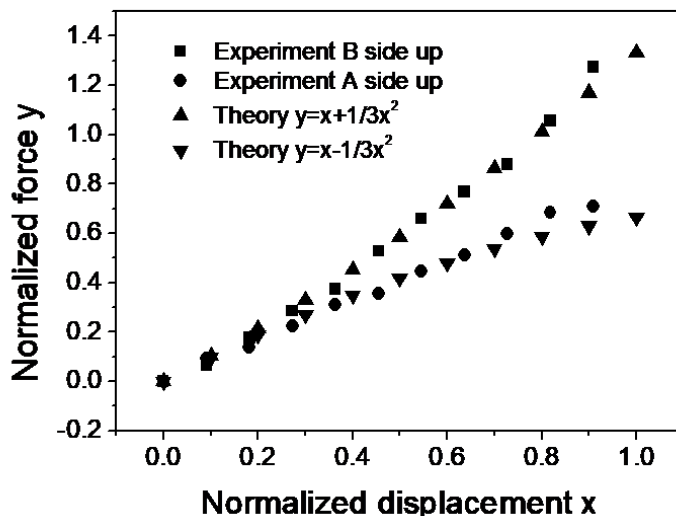
Figure 4.4: Normalized force versus displacement for an empty Whatman AAO template. The initial measurements were in the displacement range of (0-30 μm), where the straight line slope gave different E values for each side (Supporting Information, Figure S4.3). On extending the displacement range to 60 μm, the nonlinear response becomes apparent. Also shown are fits using the broken symmetry argument Equation (4.7).

nanowires can be collected and imaged (Figure 4.5c), confirming their continuous growth within the channels. Although the templates do not appear to be completely filled with DAE, we found that the amount present in both was the same to within 5% for both types of templates (2.84 mg in Whatman AAO, 2.78 mg in TOP AAO, as detailed in the Supporting Information, Figure S4.4). After polishing, the Whatman templates exhibited a pronounced curvature, even before exposure to light. This curvature was not present in the empty templates but could be induced by polishing alone. The polished templates always curved so that the side with the smaller holes (side B for the Whatman, side A for the TOP membrane) was convex. We suspect that polishing induces an asymmetric stress across the template due to DAE and AAO debris that is forced into the channels and interacts with the pore walls. After compaction due to polishing, there is more pressure on the small pore
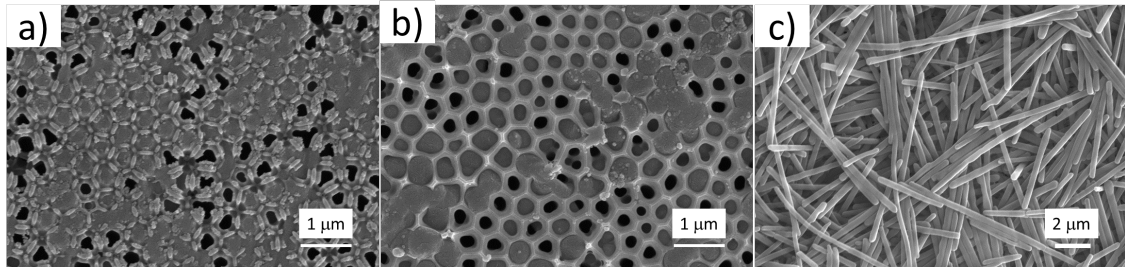
Figure 4.5: SEM images of DAE filled AAO TOP templates (a) A side (smaller pore diameter) and (b) B side (large pore diameter) (c) SEM image of DAE nanowires extracted from an AAO template by dissolving it in phosphoric acid.

side than the large pore side, causing an internal stress that slightly bends the template even before light exposure. Furthermore, the DAE-filled templates showed even more pronounced asymmetry, this time with the A side having a larger modulus. The change in asymmetry may be another consequence of the increased compaction on the side with the lower OAR due to polishing (Supporting Information, Figure S4.5).

4.6 Photomechanical Performance Measurement with Two Methods

In order to quantify the photomechanical response, we used two independent methods. For both, we mounted the DAE loaded templates so that the outer (convex) side was illuminated, which caused the curvature to become more pronounced. The first method used to measure mechanical work was monitoring the angular deflection of a laser beam that bounces off a mirror resting on top of the template. As the template bends and its edge moves away from UV illumination, it tilts the mirror and moves the laser beam (Figure 4.6a-f). The mirror displacement set-up (Figure 4.6g, Supporting Information Figure S4.6)

and resulting data (Figure 4.6h) allow us to quantify the actuation of the template. Videos of the mirror tilting and resulting laser beam displacement can be found online at Wiley Advanced Functional Materials. The Whatman sample exhibits a larger displacement of the 1.28 g mirror after irradiation than the TOP sample, and using the methods in reference 15, we find R (radius of curvature) $=0.2$ m for the Whatman template and $R=1.5$ m for the TOP membrane, along with work outputs of 1.4×10^{-6} J and 1.7×10^{-7} J, respectively. We note that the work output for the Whatman template is about a factor of 2 larger than that previously reported, which we attribute to improved filling of the template due to prewashing (Supporting Information, Figure S4.7).

The second method used the force-displacement set-up illustrated in Figures 4.7a and b to measure force-displacement curves as the template bends and its center moves towards the UV light. Figure 4.7c shows the force generated by template during UV irradiation as a function of time. It matches well with previous results using the laser displacement method, as reported in reference 15. Note that this relatively slow motion is probably limited by the low UV intensities used in these experiments. Typical force-displacement curves for both template types are shown in Figures 4.7d and e. The Whatman sample displacement is approximately $4\times$ greater than that of the TOP membrane under the same illumination conditions. The amount of force generated is $2\times$ greater than the TOP membrane. From the data in Figure 4.7, we can also calculate the total work done by both templates, which is 1.2×10^{-6} J for the Whatman template and 1.4×10^{-7} J for the TOP membrane. The center displacement can then be used to calculate the radius of photoinduced curvature, R, with $R=0.4$ m for the TOP membrane and $R=0.1$ m for the Whatman template, i.e. it has
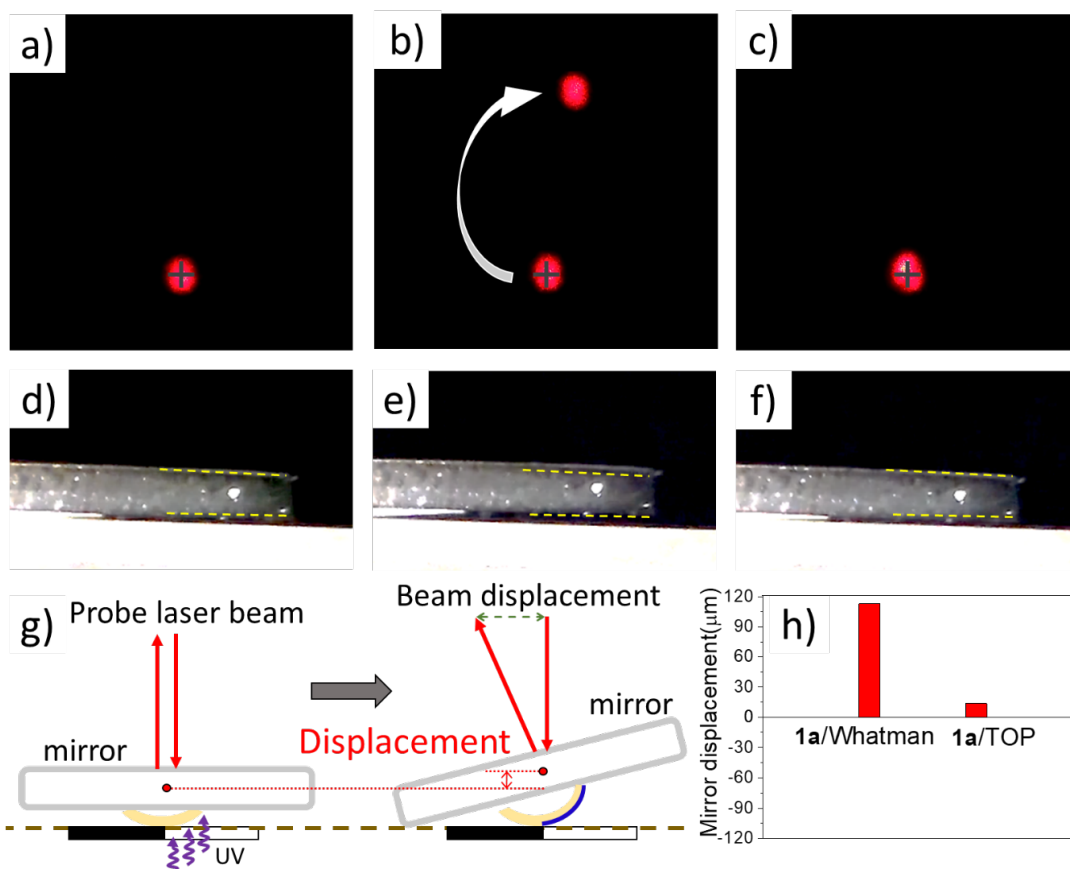
Figure 4.6: Laser displacement experiment. (a) Overlapped reference and probe beam before UV irradiation; (b) Probe beam moves upward after 2 min of UV irradiation of a **1a**/AAO template; (c) Probe beam returns back to original position after 5 min of visible light irradiation; (d) Thick mirror supported by **1a**/AAO template (thin white plate) viewed from the side; (e) Mirror tilts up after 2 min of UV irradiation on right half of **1a**/AAO template; (f) Mirror reverts to original position after 5 min of visible light irradiation; (g) Schematic of laser deflection experiment. The right side of a **1a**/AAO template is irradiated by UV light. The induced curvature lifts up one side of the mirror, and this tilt displaces the laser beam; (h) Positive displacement of the center of mass of a 1.28 g mirror by Whatman and TOP **1a**/AAO templates after UV irradiation. The calculated work was 1.4 μJ for a **1a**/Whatman template and 0.17 μJ for a **1a**/TOP template.
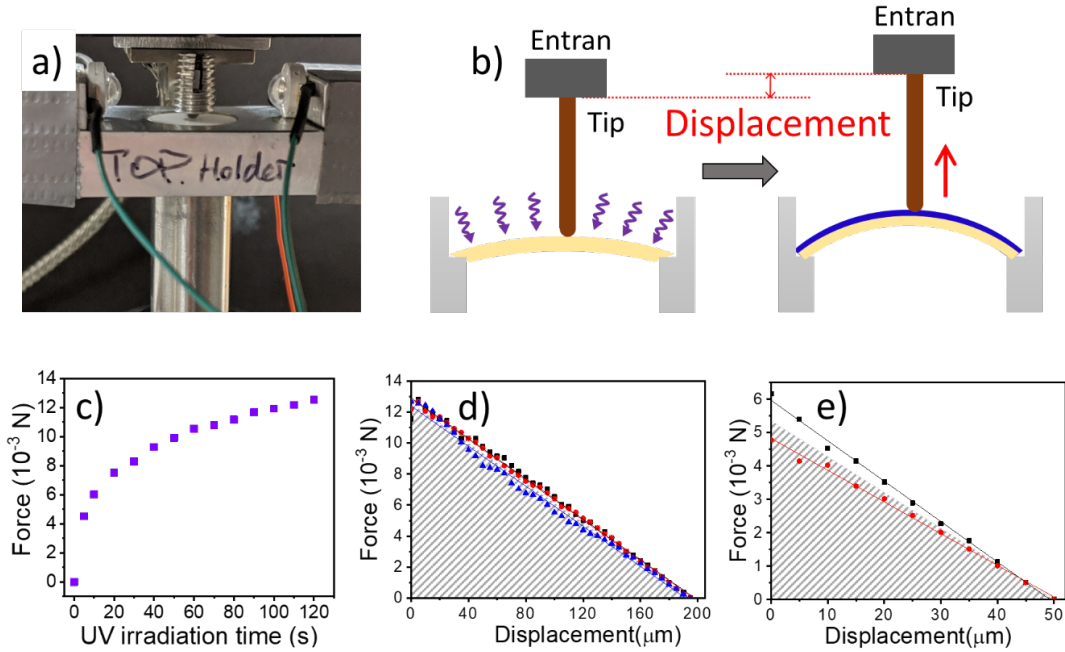
Figure 4.7: Force/displacement experiment. (a) Photograph of force-displacement set-up with white circular template held under force transducer; (b) Schematic of force-displacement experiment. The **1a**/AAO template bends toward UV light and moves the force sensing tip; (c) Force generated by UV illumination as a function of irradiation time; (d) Force-displacement curves for the same **1a**/Whatman template used to generate the data in Figure 4.6. Three trials (black, red and blue curves) are shown, and the area underneath the curves (gray) yields the calculated work of 1.24±0.05 μJ; (e) Force-displacement curves for the same **1a**/TOP template used to generate the data in Figure 4.6. Two trials (red and black curves) are shown, and the work is calculated to be 0.14±0.02 μJ.

a larger curvature $\kappa=1/R$ or greater bending.

We estimate an error range of about 10-20% in the work measurements, so the photomechanical work calculated using the mirror-deflection and force-displacement methods agree to within the error range. The overall agreement is encouraging considering that these are different experiments performed in different labs. Note that the ability to completely reverse the DAE photoisomerization using visible light makes it possible to perform multiple of measurements on a single template, circumventing the problems associated with

the template-to-template variations shown in Figure 4.3.

4.7 Performance of a Photochrome that Undergoes a Crystal Contraction

According to our model, it is the pressure of the expanding DAE nanowires in the bottom of the template that create the photomechanical curvature and generates force. The fact that the filled template already has an initial curvature suggests that the DAE is in contact with the channel walls even before light exposure. If this is the case, then a different DAE derivative whose crystal dimensions shrink after irradiation should show a qualitatively different photomechanical response. **2a** is a molecule that crystallizes into needles that grow lengthwise along the a-axis. [15] When the needles are exposed to UV light, they expand along the a-axis and contract along the orthogonal c-axis (Supporting Information, Figure S4.8). Assuming that nanowires in the AAO channels grow in a similar manner with the a-axis along the channel and the c-axis oriented in the plane of the template [136,137], then UV exposure should cause a contraction instead of an expansion on the exposed side if the nanowires adhere to the walls of the holes in the AAO templates. In this case, we would expect UV exposure to relax the initial curvature as the DAE pulls away from the channel walls and the internal pressure at the organic-inorganic interface decreases. Indeed, when these curved templates are exposed to UV light, the curvature decreases even as the applied force remains approximately constant (Figure 4.8). The photoinduced contraction of the nanowire crystals due to the **2a**→**2b** isomerization lowers the internal strain in the plane of the template and relaxes the curvature (Supporting Information, Figure S4.9). Exposure

71
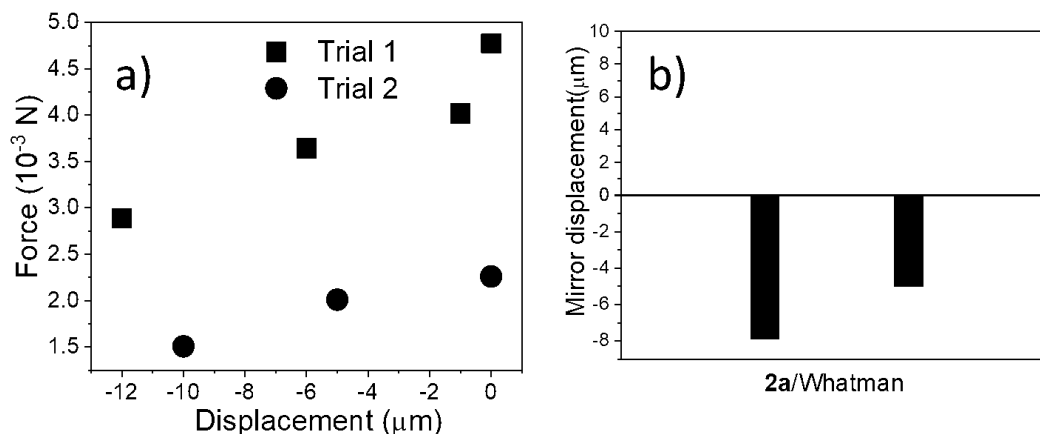
Figure 4.8: (a) Results of two force displacement experiments on a **2a**/Whatman AAO template. An initial force was applied (the force of trial 1 was larger than trial 2) to the center of a template with convex side toward tip. This side was then irradiated by UV light, and the template's curvature decreased, while the contact force also decreased as the sensor tried to follow the curvature. (b) Laser deflection data for two different **2a**/AAO templates. The negative displacement data means that the mirror edge is lowered vertically.

to visible light reverses the reaction, as judged by the loss of the blue color, but did not

restore the curvature. This observation suggests that once contact with the channel walls

is lost, it cannot be re-established in an effective way.

In Figure 4.9 we present a schematic illustration of the different photomechanical

outcomes associated with photoisomerization of **1a** and **2a**. In both cases, the loaded

template has an initial curvature due to the internal stress generated by the polishing.

Upon exposure to UV light, the **1a** crystal expands and increases the curvature, while the

2a crystal contracts and decreases the curvature. Both of these reactions are reversible

upon exposure to visible light, and the mechanical motion can be cycled multiple times.

Figure 4.9 provides some guidance for the design of the crystalline organic component of

the actuator. To observe a bending actuation of the template, the photochromic reaction

must generate motion in the horizontal plane of the template. This requires not only the identification of solid-state reactions that generate molecular displacement along at least one crystal axis, but also alignment of that axis with the template. The synthesis of new photochromic crystals must be accompanied by the development of strategies for directional crystal growth. It should also be pointed out that DAE is a "positive photochrome" in which the product ring-closed isomer still absorbs strongly at UV wavelengths. In our samples, we found it impossible to convert more than about 10% of the DAE molecules in the template, since further penetration of the UV light is blocked by the photoproduct absorption. Since we previously found that the mirror displacement closely tracked the amount of converted DAE[15], it is likely that using DAE derivatives that can undergo larger conversion in the crystal form [20, 138] might lead to improved mechanical output, assuming that the appropriately oriented crystal nanowire could be grown inside the pores.

The role of the molecular component in determining the photomechanical response is not surprising. What was more surprising was the large influence of the inorganic template on the actuator performance. The Whatman templates consistently generated significantly more work and displacement. We hypothesize that these differences can be attributed to the lower average E=14 GPa for the Whatman templates compared to the average E=65 GPa for the TOP membranes. To achieve a given radius of curvature κ, energy is required to bend the template. Equations (4.4)-(4.6) show that this energy U is proportional to E. Assuming that the mechanical energy released by the organic component is fixed, a stiffer template with larger E leads to a smaller κ and smaller displacement. In other words, the high elastic modulus of the AAO resists deformation by the softer organic component,

73
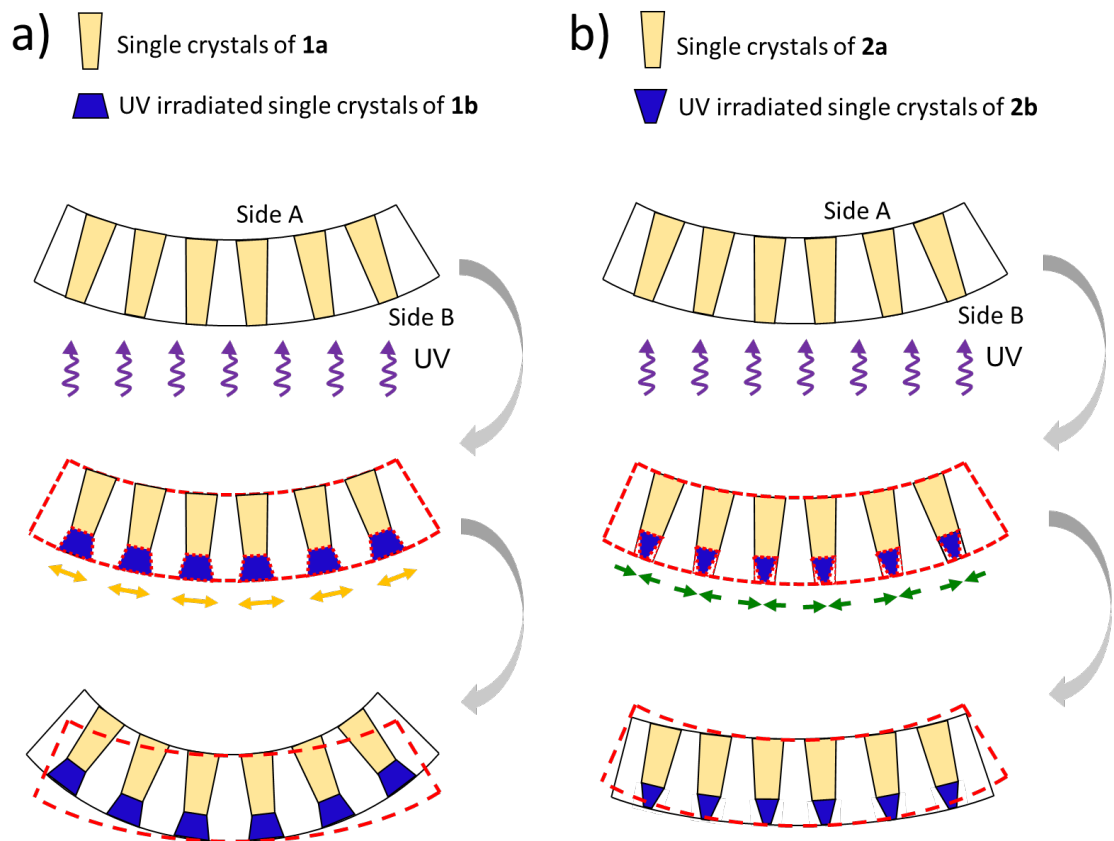
Figure 4.9: Schematic illustration of how the template curvature is affected by different molecular crystal changes. The DAE/AAO template has an initial curvature after polishing due to the pressure of the DAE and debris pushing against the channel walls. (a) The lower regions of the **1a** crystal nanowires expand after irradiation, pushing against the channel walls and increasing the template curvature. (b) The lower regions of the **2a** crystal nanowires contract after irradiation, detaching from the channel walls and relieving the internal pressure that causes the initial template curvature.

causing it to store energy in the elastic deformation of the AAO rather than working against the external load. In our samples, this resistance can be mitigated to some degree by taking advantage of the built-in asymmetry of the membrane and hence in U and causing the bending to occur in the preferred direction (away from the small pore side). Ideally, the modulus of the template should be reduced to match that of the organic component, so that the composite would act as a single mechanical unit. The **1a** crystal modulus has not been measured, but has been estimated to be ~11 GPa for a related DAE crystal [103], close to that of the Whatman template. Further lowering of the template E could be accomplished in several ways: 1) changing to a softer template material, for example a polymer; 2) tuning the AAO purity and defect density; 3) tuning the template microstructure (pore shape, size and density) and thickness.

Finally, we note that the commercial porous AAO templates used in this work possess several nonideal properties that complicate the data analysis, including template-to-template variability, surface heterogeneity, and an A→B side asymmetry in mechanical properties. Ideally, we would have more uniform templates where we could systematically vary pore diameter, shape, spacing, elastic modulus, and thickness. It may be that top-down lithographic methods are more suited for making uniform templates to organize and align the photoactive nanocrystals.

4.8   Conclusion

The results of this chapter show that the properties of the porous inorganic template play a crucial role in determining the photomechanical work generated by a hybrid

organic-inorganic membrane actuator. Detailed characterization of the AAO template morphology and mechanical properties show that they are asymmetric and there are substantial differences between commercially available templates with the same nominal pore diameter. The mechanical differences are reflected in the photomechanical force-displacement measurements, with the conclusion that the higher modulus TOP template generates significantly less work output because its higher elastic modulus leads to greater resistance to the DAE crystal expansion. We conclude that there is considerable room to improve the performance of these nanocomposite structures by engineering the nanostructure of both the inorganic framework and the active organic component.

4.9 Supplementary Information

4.9.1 Experimental Section

Materials

The syntheses of diarylethenes **1a** [109] and **2a** [15] have been published previously. CH_2Cl_2 and hexanes (HPLC Grade) were bought from Fisher Chemical. Whatman Anodisc inorganic filter membranes were purchased from Sigma-Aldrich (unsupported, 12.7 mm diameter, pore size 0.2 μm, thickness h=60 μm, autoclavable) had a measured radius a=6.35. The TOP AAO templates were purchased from Topmembranes Technology (nominal 13 mm diameter, pore size 0.2 μm, thickness h=50 μm, part number DP450-200-50000) had a measured radius a=6.75 mm.

Preparation of DAE/AAO templates

DAE nanowires were grown in the AAO templates by a solvent annealing method. [108] A Whatman AAO template was immersed in deionized water and sonicated for 25 s. A solution with DAE (5 mg) dissolved in CH_2Cl_2 (100 μl) was deposited on one side of the AAO template. The template was suspended over a homemade teflon cylinder standing on a CH_2Cl_2 soaked Kimwipe tisue. The template was then covered with a bell jar, inside which the CH_2Cl_2 slowly evaporated while the DAE molecules crystallized inside the channels at room temperature. After 24 hours of solvent annealing under the bell jar, the DAE/AAO template was removed and gently polished with a 2000 grit sand paper to remove residual DAE from the top and bottom. The exact same procedure was used for the TOP AAO templates, except for the initial sonication in deionized water.

Scanning electron microscopy (SEM) measurements

The empty AAO template was attached to a SEM stub by conducting copper tape. The sample was coated with Pt/Pd for 40 seconds with a sputter coater (Cressington 108 Auto). The SEM images were collected using a FEI NNS450 microscope with a 20 kV electron beam under high vacuum (10^{-7} torr). An Everhart-Thornley Detector (ETD) was used to produce high resolution images.

Laser deflection measurements

Light from a 0.95 mW Helium-Neon laser (633 nm wavelength) was used in an interferometer set-up to measure the displacement of the actuator load. The beam was incident on a beamsplitter which reflected a portion of the beam downward onto a mirror

(1 inch diameter) supported by the photomechanical DAE/AAO template. The remainder of the beam was reflected by a fixed mirror to be used as the reference. The two beams were projected onto a wall 4.8 m away and the displacement of the template beam was measured. The photomechanical DAE/AAO template was put on a transparent microscope slide with one half covered by an opaque tape. The light that converted **1a** to **1b** (**2a** to **2b**) was obtained from a light-emitting diode (1 watt 394 nm from Super Bright LEDs Inc.) placed 2.5 cm below the template. The intensity at the sample was 3.5 mW/cm^2. To convert **1b** back to **1a** (**2b** back to **2a**), a 532 nm laser beam was passed through a diffuser and directed onto the template, resulting in an intensity of 56 mW/cm^2.

Force-displacement measurements

The elastic modulus of the templates as well as their optomechanical response was measured using a setup consisting of a sample holder, an Entran force sensor PS-30A with a specially constructed tip and a manual translation stage. The Entran force sensor was attached to the translation stage. The tip was an aluminum machined part assembled with a steel ball bearing by press fit (diameter=2.3mm) at the end. The horizontal sample, supported at the edges, was positioned under the tip. As the stage was translated downward, the tip pressed downward on the sample causing it to bend; the force sensor output gave the force the sample was exerting on the tip.
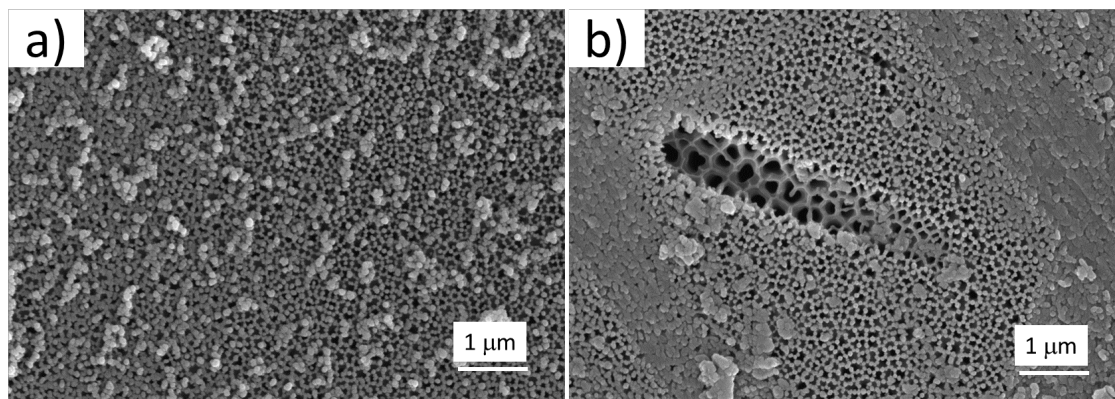
Figure S4.1: Images of the Whatman membrane B side (opposite the 200 nm pore side) without precleaning. (a) Small pore diameter "crust", with extra debris particles. (b) Some regions have larger diameter channels (average diameter of 230 nm) visible in regions where the "crust" has been partially etched away.
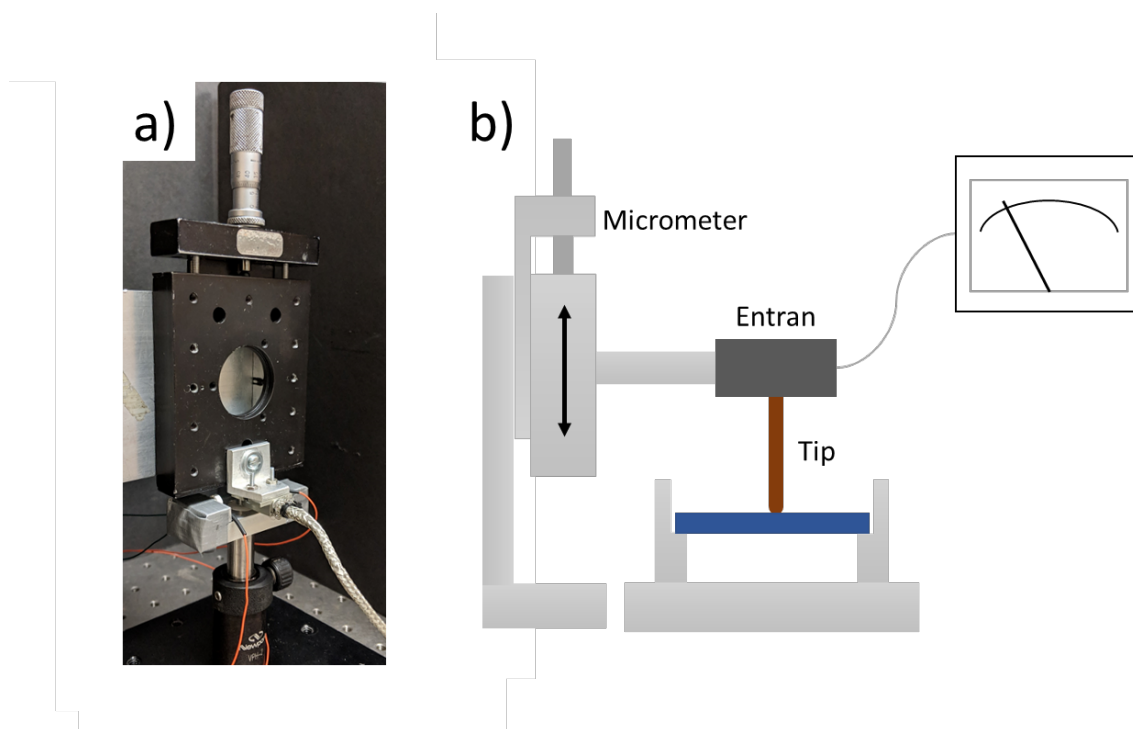
Figure S4.2: (a) Photo and (b) scheme of force-displacement measurement set-up. The blue disk is the AAO membrane supported at the edges by a custom-built holder.
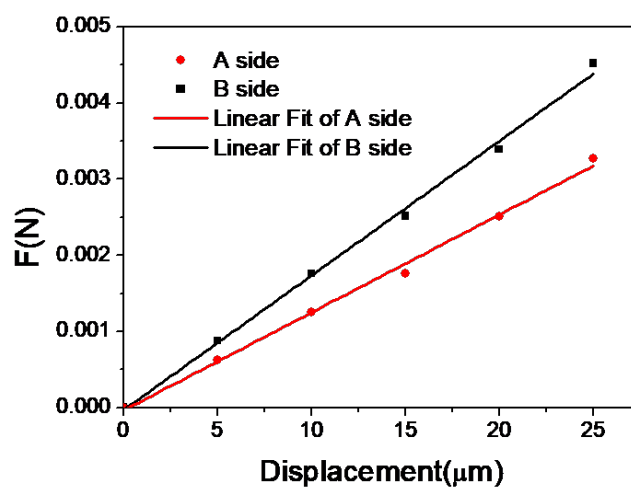
Figure S4.3: Sample data from the force-displacement measurement of the elastic modulus (E) of both sides of an empty Whatman AAO membrane. The force probe presses on either the A or B side, and the slope of the force-displacement curve is proportional to E (Equation (3) in text). A linear fit of the data yields a larger E value for the B side.
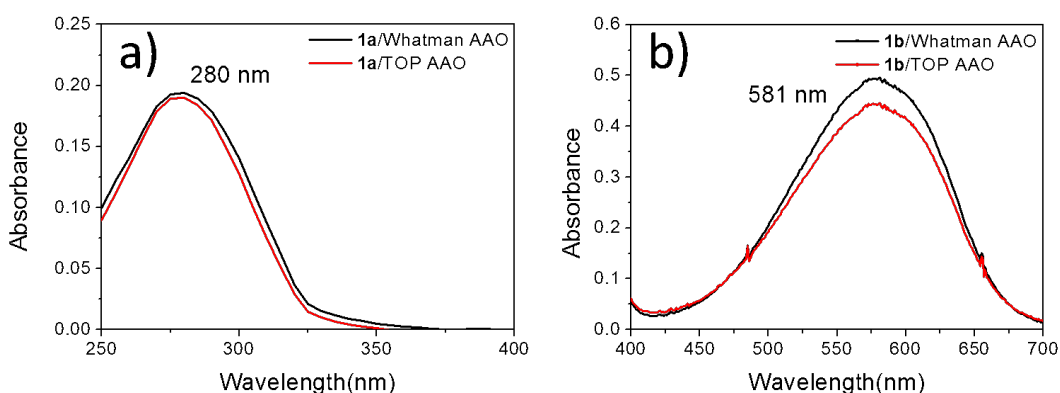
Figure S4.4: Measurement of crystal loading in Whatman and TOP AAO templates. (a) Measurement of total loading using absorbance of ring-open **1a** isomer. After measuring the mechanical properties of a **1a**/AAO template, the template is immersed in 1000 mL of hexanes. From the absorbance of the dissolved **1a**, measured at 280 nm, we calculate that there is 2.84 mg of **1a** in the Whatman template and 2.78 mg **1a** in the TOP template. (b) Measurement of conversion yield using absorbance of ring-closed **1b** isomer. After exposure to UV light on the B side for 2 minutes, the template is immersed in 100 mL of hexanes and the **1b** absorbance at 581 nm is measured. From the absorbance, we calculate the mass of 1 in the Whatman template (0.165 mg, corresponding to 5.8% conversion to **1b**) and the TOP template (0.149 mg, corresponding to 5.4% conversion to **1b**). The DAE loadings and conversion yields of the Whatman and TOP templates are within 5% of each other for this sample. This result indicates that differences in photomechanical work are not coming from differences in crystal loading or chemical reaction yield.
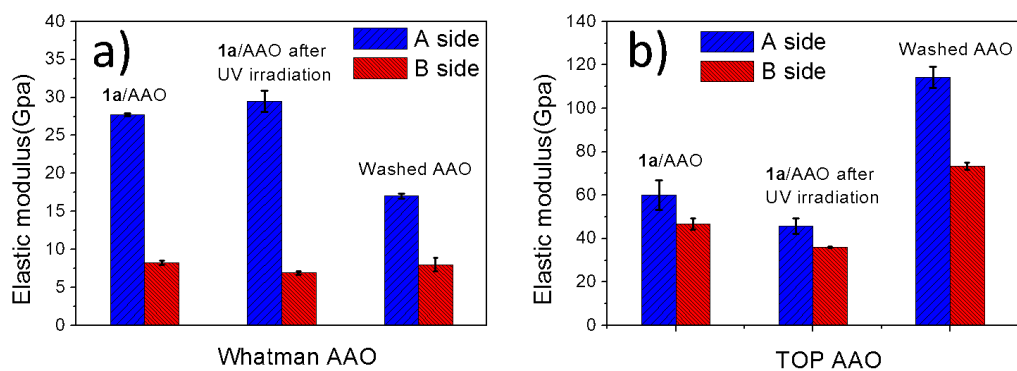
Figure S4.5: Elastic modulus data of **1a**/AAO templates. (a) The elastic modulus E measured for the same Whatman template at three points: after filling with **1a** and polishing, after UV irradiation, and after washing out the **1a** and **1b**. (b) The elastic modulus E measured for the same TOP template at three points: after filling with **1a** and polishing, after UV irradiation, and after washing out the **1a** and **1b**. For both templates, exposure to UV does not have a systematic effect on E, but removing the DAE molecules causes opposite effects for the Whatman templates (decreased E) and TOP templates (increased E). We suspect that these differences may come from the different effects of polishing and washing on the different pores in these two types of templates.
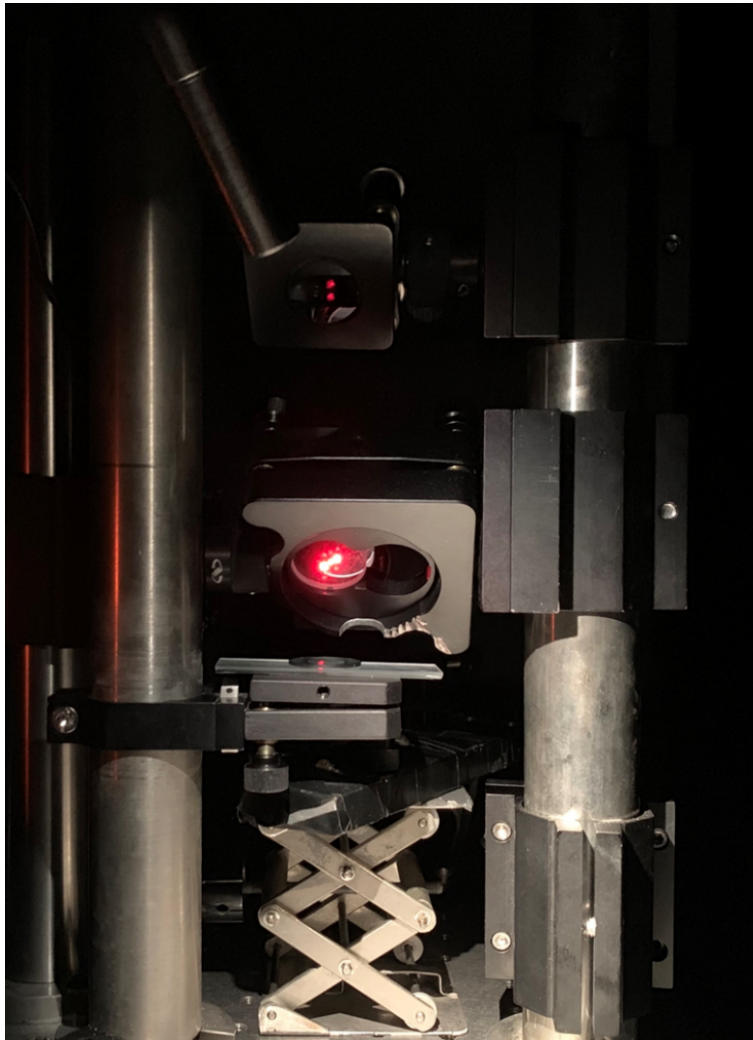
Figure S4.6: Photo of laser displacement experiment set-up.
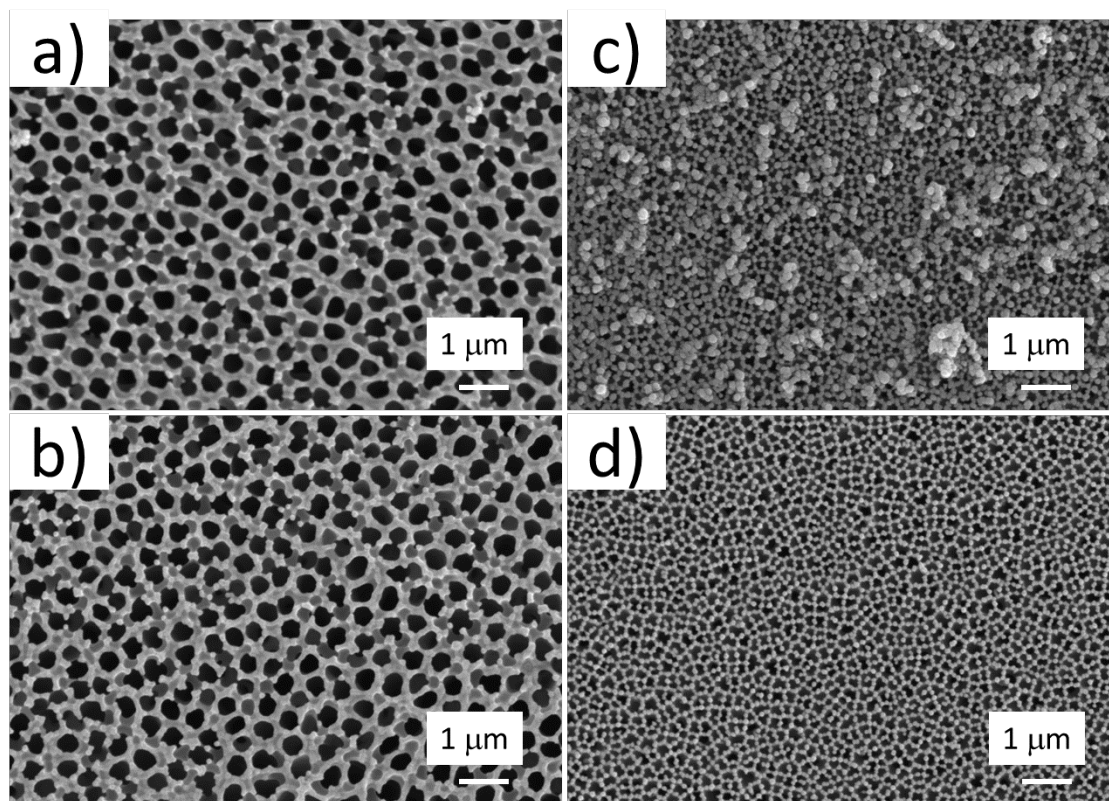
Figure S4.7: SEM images of Whatman Anodisc AAO templates before and after sonication. (a) A side before sonication;(b) A side after sonication; (c) B side before sonication; (d) B side after sonication. Sonication can remove debris from the B side and improve DAE filling.
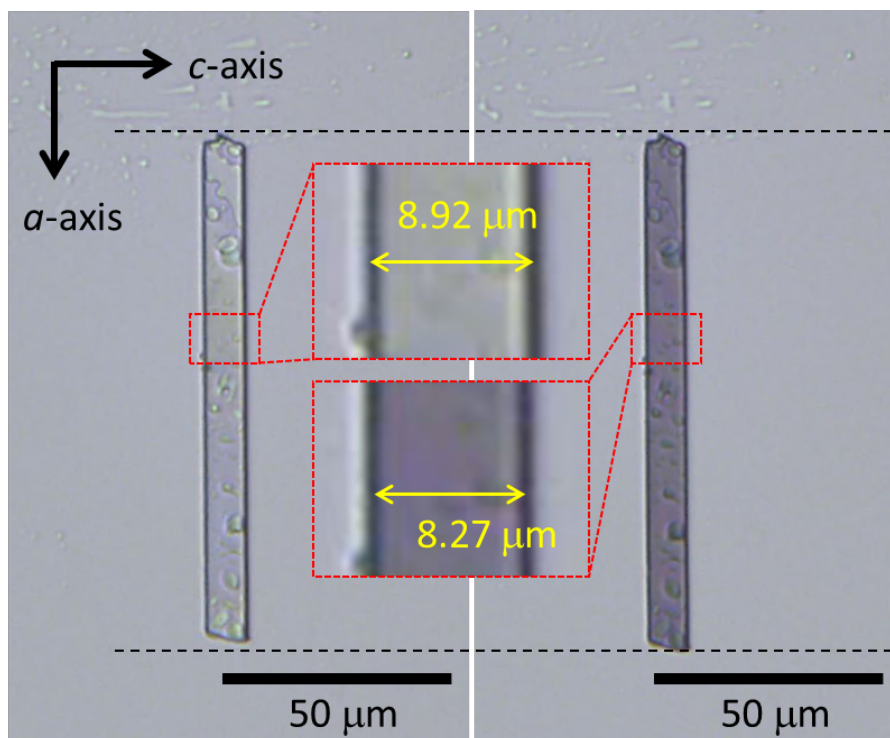
Figure S4.8: Optical microscope images of a **2a** needle-like crystal before and after UV irradiation. It expands along the a-axis by $\sim$1% and contracts by $\sim$7% along the c-axis. In the AAO template, we assume the crystal grows with the a-axis aligned along the channel, and the c-axis perpendicular to the channel.
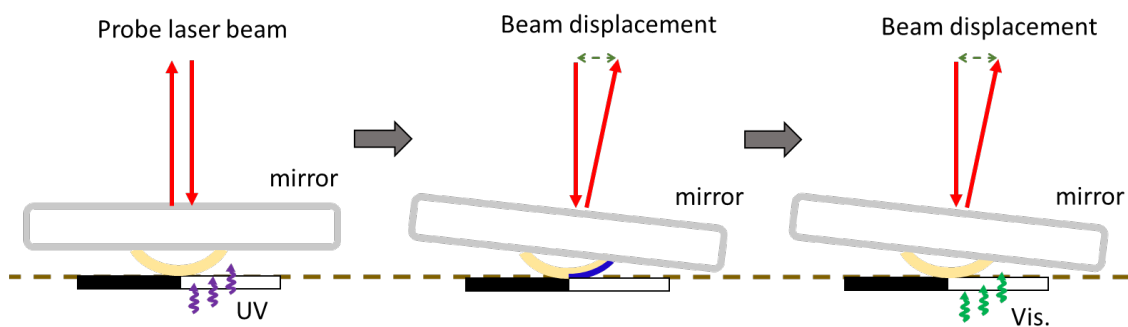
Figure S4.9: Laser deflection scheme for **2a**/AAO templates. Contraction on the right half template upon UV irradiation makes the mirror tilt to the right, causing a negative beam displacement. **2b** reverts back to **2a** upon visible light irradiation, but the curvature is not restored.

Chapter 5

Performance Characteristics of Composite Glass-Diarylethene Crystal Photomechanical Actuator Membranes

5.1 Abstract

Hybrid organic-inorganic composites based on photochromic crystals grown inside porous inorganic membranes provide a new approach to photomechanical materials. Diarylethene (DAE) nanowires grown in alumina membranes exhibit reversible photoinduced bending and lifting capabilities. In this chapter, the hybrid approach is extended to porous glass membranes with variable thicknesses in order to improve optical penetration and re-

producibility. Despite the different template material (SiO_2 instead of Al_2O_3) and much larger channels (5 micron diameter instead of 0.2 micron diameter), we find similar photomechanical behavior for this new class of templates. The ability to re-use individual glass templates across different DAE filling cycles allowed us to determine that the DAE filling step is crucial for determining the mechanical work done by the bending template. The degree of bending also depends on the template thickness, with thinner templates giving larger displacements. The light-induced bending can be repeated for up to 150 cycles without loss of performance, suggesting good fatigue resistance. While the use of glass templates does not lead to a large increase in work output or efficiency, this study demonstrates that the hybrid organic-inorganic approach can be extended to other host materials and template geometries and suggests that optimizing the filling and template thickness can improve the work output by at least one order of magnitude.

5.2 Introduction

Photons provide a highly efficient way to transport energy, but at some point that energy must be harnessed to perform mechanical, electrical or chemical work. Photomechanical materials are designed to absorb photons and directly convert the light into a mechanical response. Many physical mechanisms can be used to accomplish this transformation, including photothermal expansion [139], photostriction due to carrier generation [140], and photoisomerization of molecules in a polymer matrix [6]. Crystals composed of photochromic molecules have also attracted attention as photomechanical materials [16,122,141–144], and a wide variety of photochemical reactions have been shown to generate crystal deformations

like bending or expansion [12, 121]. In principle, this class of materials should enjoy several advantages, including high work density, high elastic modulus, and fast response [145]. In practice, they face significant challenges, including fracture induced by photogenerated stress, sensitivity to environmental factors like solvents, and the difficulty of incorporating single crystals into macroscopic actuator devices [146–148].

One approach to solve these problems is to create hybrid materials that consist of oriented arrays of photochromic organic nanocrystals embedded in an inert inorganic host material, like an oxide. We previously showed that thin ($\sim$50 micron) porous anodic aluminum oxide (AAO) disks could be infiltrated with photochromic diarylethene (DAE) molecules that grew oriented nanowire crystals inside the 200 nm diameter channels [148, 149]. When exposed to UV light, the molecules underwent a ring-open to ring-closed photoisomerization which caused the crystals to expand along their b-axis. The expansion of the nanowires caused an internal stress, forcing the template to bend away from the illumination (Figure 5.1). Both the photochemistry and the bending could be reversed by the application of visible light, making this a reversible switch-and-hold actuator. Using this composite approach, we were able to make macroscopic bending actuators containing only a few milligrams of the DAE that could lift up to 40 grams. The structured inorganic matrix served to create a "crystal" of nanocrystals, providing order, protection and scalability for the organic component.

But while the hybrid molecular crystal approach to photoactuation is promising, it also faces some difficulties. Porous AAO templates are fabricated by electrochemical etching and we found considerable structural variability among different templates, as well
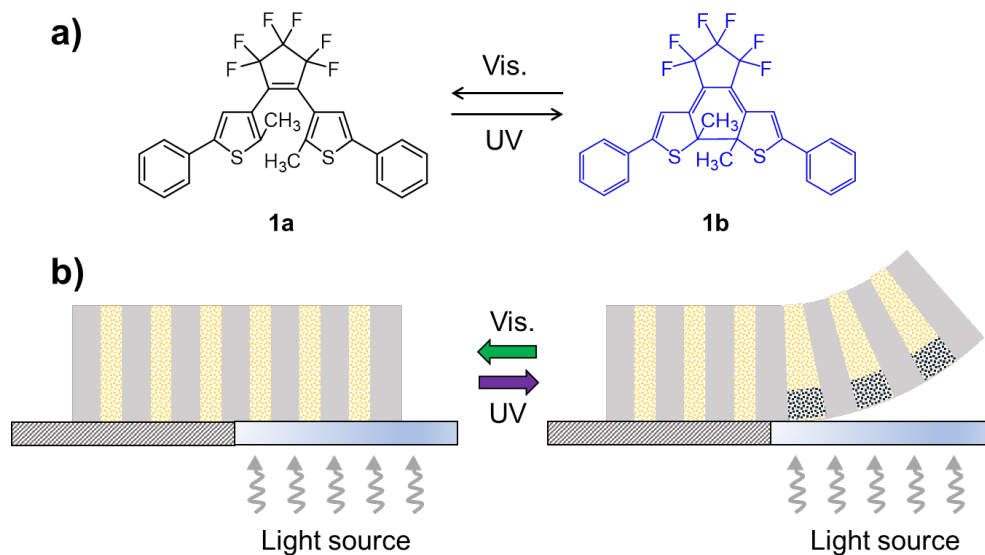
Figure 5.1: (a) Photochemical reaction between ring-open (1a) and ring-closed (1b) diarylethene isomers. (b) Photomechanical bending of the DAE-glass composite forced by created ring-close DAE crystals upon induced light.

as a non-uniform pore diameter across the template. They also have a limited set of pore diameters and thicknesses. There is some indication that the high elastic modulus of Al_2O_3 may limit the work output of the organic that is constrained within it. Finally, alumina tends to be highly scattering, severely limiting the optical penetration depth.

In order to address these limitations of the AAO templates, in this chapter we turn to a different template based on a glass microcapillary array. This type of porous solid is made by pulling an array of uniform capillary tubes that have assembled in a regular hexagonal-closed-packed (hcp) pattern. Sections can be cut out of the tube, leading to porous disks with variable channel diameters and thicknesses down to 0.05 mm. Composed of optical quality glass, these porous templates provide a completely different host matrix for our photoresponsive DAE crystals. Despite the use of a different template material (SiO_2 instead of Al_2O_3) with much larger channels (5 micron diameter instead of 0.2 micron

diameter), we find similar photomechanical behavior for this new class of templates. The use of glass membranes allows us to empty and refill individual templates and evaluate how variable filling by the DAE leads to variable photomechanical behavior. The thickness dependence and cycling behavior are studied in detail. Overall, while the use of glass templates does not lead to a large increase in work output or efficiency, it does demonstrate that the hybrid organic-inorganic approach can be extended to other host materials and template geometries. Ultimately, our goal is to develop custom templates that can be completely filled with oriented photomechanical nano- or microcrystals that can serve as the active element for macroscopic solid-state photoactuators.

5.3   Surface Morphology and Elastic Modulus of Empty Glass Templates

We first characterized the empty glass templates. In our previous study of AAO templates, we found considerable variations in the surface pore morphology, even when comparing the top and bottom of a single template. This top-bottom asymmetry also led to an asymmetric elastic modulus for these templates, complicating any analysis of how the host mechanical properties influence the performance of the composite. The porous glass templates used in this chapter provide a much more uniform matrix for DAE filling. The top and bottom of a glass template are indistinguishable, both showing a close-packed array of uniform 5 micron holes. Figure 5.2 shows microscopy images of the template before and after DAE filing and solvent annealing. The hole pattern is still visible even after DAE filling, unlike the AAO templates where polishing leaves a smooth, featureless crust on
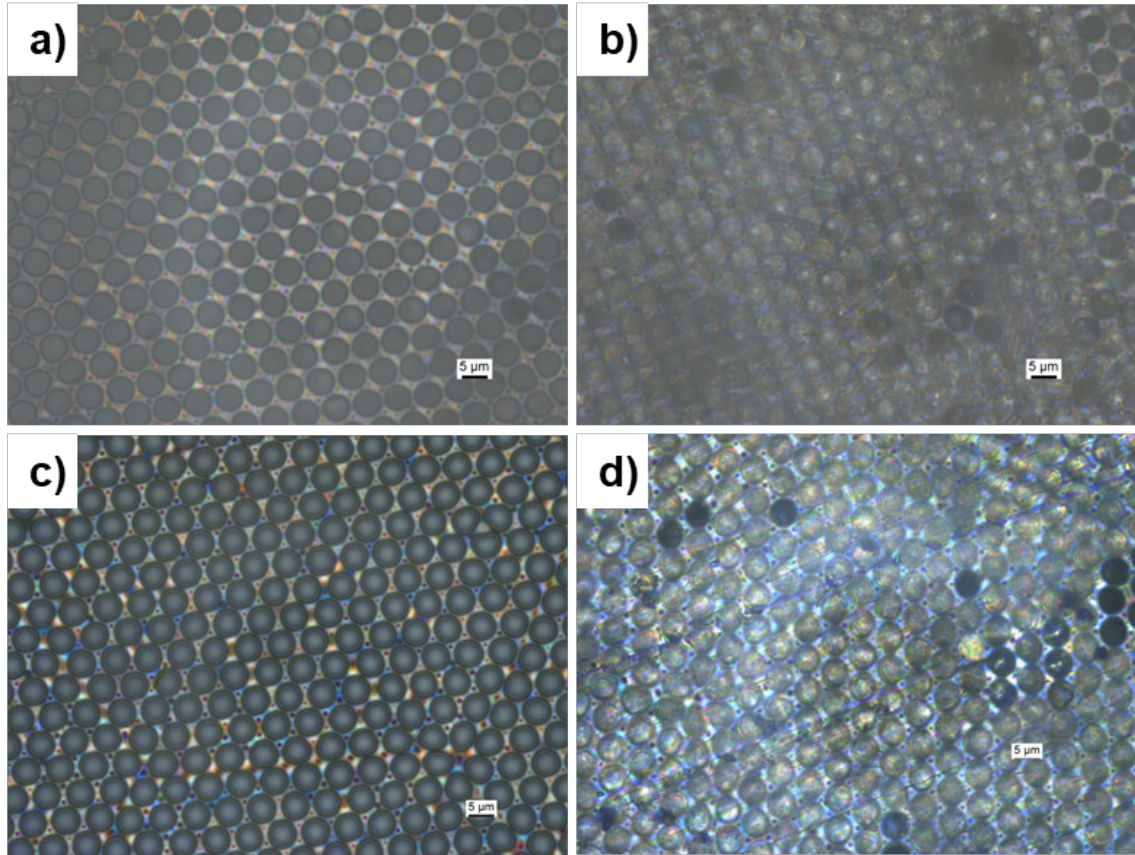
Figure 5.2: Microscopic images of glass templates before and after being filled with DAE crystals. (a) Bare 0.1mm thick glass template. (b) DAE crystals filled 0.1mm thick glass template. (c) Bare 0.5mm thick glass template. (d) DAE crystals filled 0.5mm thick glass template.

the surface. The mechanical uniformity of the glass templates is confirmed by the elastic modulus measurements shown in Figure 5.3. Templates of different thicknesses exhibit the same modulus of approximately 13±1.0 GPa, to within measurement error. Furthermore, unlike the AAO templates, this result does not depend on which side (labeled A and B in the figure) is probed.
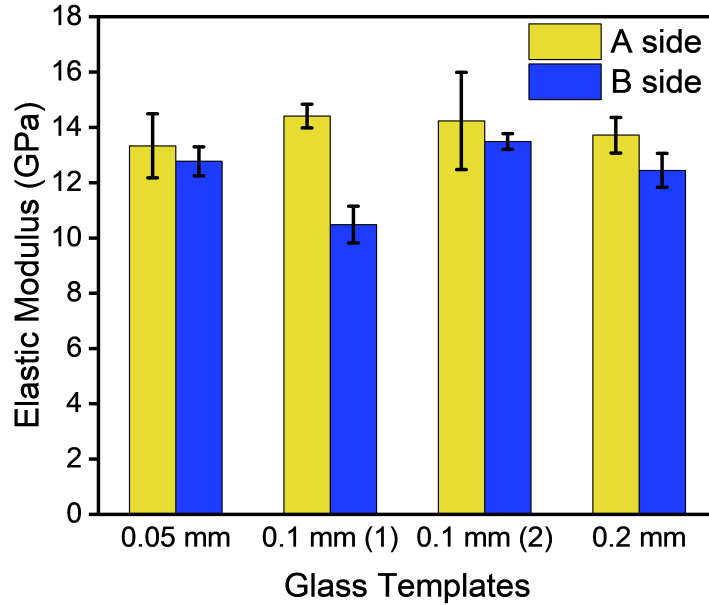
Figure 5.3: Young's moduli of top and bottom sides on bare glass templates with variable thicknesses.

5.4 Photomechanical Bending

The photomechanical bending of the DAE-glass templates was measured with the same optical lever set-up used in our previous work [148, 149]. The displacement of a laser beam reflected by a mirror resting on the template is measured and related to the light-induced bending of the template. The angular displacement of the beam can be directly related to the vertical displacement of the mirror and also the curvature of the template, as described in Figure S5.2. Figure 5.4 shows typical mirror displacement vs. time acquired during a UV irradiation cycle. The mirror only moves upward when the 394 nm light is on. After the light is turned off, there is a slight decrease in height that takes place over several minutes. The average amount of settling in the glass template was 9% , comparable to what
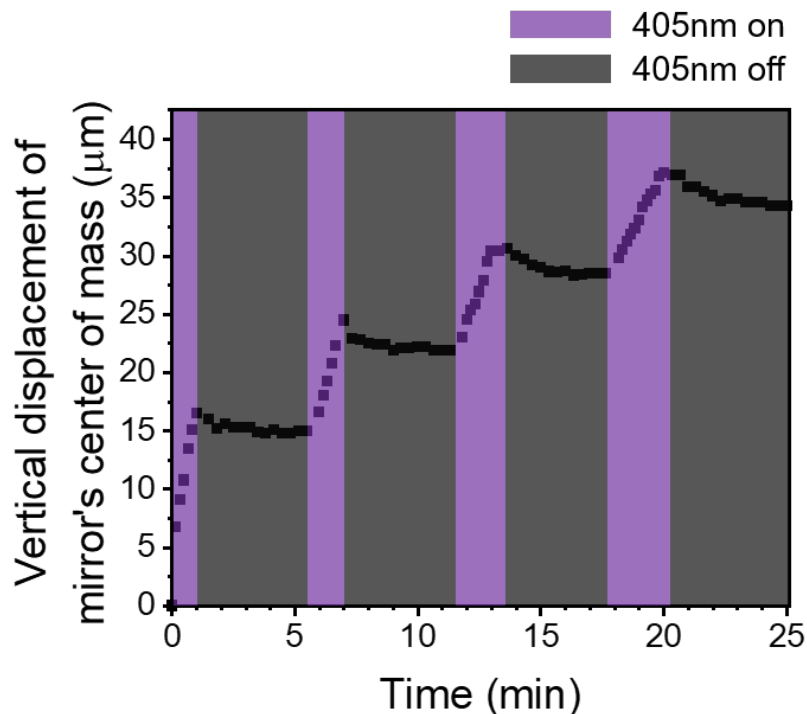
Figure 5.4: Settling experiment of a 0.1 mm thick DAE-glass template. Vertical displacement of mirror's center of mass dropped 9%, 11%, 7% and 8% during four times of 405nm off period respectively.

was observed for the AAO templates. We think this settling reflects the contribution of the thermal expansion of the glass on the irradiated side of the template. Absorption by both DAE isomers can cause a thermal gradient from the bottom to the top of the template, and the resulting thermal expansion will contribute a small amount to the total curvature. As the template cools in the dark, the thermal expansion relaxes while the strain due to the reacted organic crystal remains.

5.5 Repeated Filling Cycles for One Glass Template

During the course of the optical lever measurements, we found that the actuation results varied considerably from sample to sample. A similar variation had been observed in the DAE-AAO actuators, but in that case we could not determine if the variation was due to changing template properties or to DAE filling. The robustness of the glass templates, along with the fact that they did not require heavy polishing, enabled us to re-use the same template for multiple DAE filling cycles. This allowed us to eliminate template variability and concentrate on the DAE filling step. For a 0.2 mm thick template that was filled 5 different times, we observed bending curvature κ varying from 0.3 m^{-1} to 0.6 m^{-1}, as shown in Figure 5.5a. The total amount of DAE for each fill could be assessed by dissolving it in a fixed volume of hexane and determining the concentration from absorbance measurements. We found a rough correlation between DAE loading and the maximum bending curvature, as shown in Figure 5.5b, but DAE loading is probably not the only factor that determines the mechanical response. The maximum amount of DAE that can be loaded into a 0.2 mm thick, 12.7 mm diameter glass template with an open-area ratio (OAR) of 0.5 is estimated to be 12 mg. Our loadings of 2-8 mg are all below the theoretical limit. The amount of bending will also be affected by how the DAE is distributed within the template. We tried to account for this possibility by rotating a single template and illuminating different quadrants. We observed different amounts of bending depending on which side of the template was irradiated (Figure S5.4). Our inability to completely fill the template necessarily leads to a variable mechanical response. Even the same level of filling can be expected to generate a variable mechanical response, since the same DAE molecules
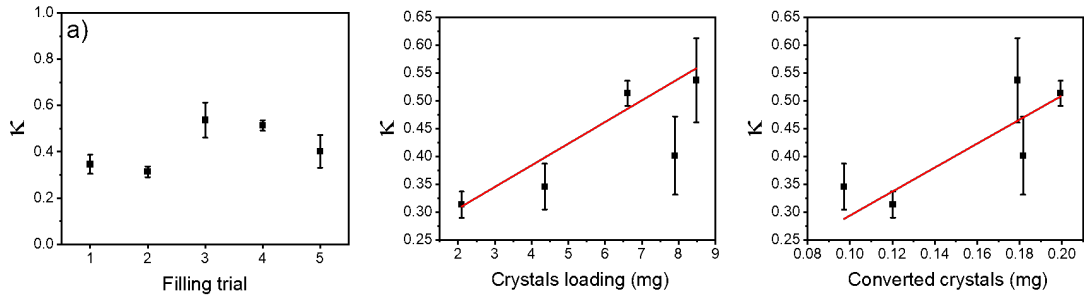
Figure 5.5: Variability in photomechanical response with repeated fillings of a 0.2mm thick glass template. (a) κ (template curvature) values in five filling trials. (b) κ (template curvature) versus the amounts of crystals loadings (right y-axis) in five filling trials. (c) κ (template curvature) versus the amounts of converted crystals (right y-axis) in five filling trials.

may crystallize in different regions for different fill cycles.

5.6 Thickness Dependence on Photomechanical Performance

Keeping in mind that there is significant sample-to-sample variability in template performance, for the remainder of this chapter we concentrate on the best-performing samples that exhibited beam deflections in the top 20% of samples prepared. Deflections from the other 80% of the samples could be as little as a few microns, however we never encountered samples that gave no deflection at all. For the best samples, using the beam deflection experiments, we were able to extract a value for the work output of the bending templates when exposed to 405 nm light. This ranges from 0.5 to 2.0 μJ for the 0.05 mm and 0.1 mm templates. The measured work outputs were similar to those obtained for DAE-AAO templates with a similar elastic modulus. Our general conclusion is that the details of chemical composition and pore geometry of the templates do not have a large impact on

95

their work output. The availability of glass templates with varying thicknesses allowed us to examine how bending depends on thickness. We confirmed that UV irradiation of a filled template only converts the molecules to a depth of 3-4 μm, so the majority of the DAE remains in the ring-open form throughout the cycling. In this limit, the expanding layer that drives bending is always much less than the template thickness. In this limit, increasing the template thickness should reduce the bending because it increases the resistance to the small actuating layer. As expected, we did observe a strong dependence of bend height on template thickness, as shown in Figure 5.6a. For a 1 mm thick glass template, no bending could be detected at all. For fixed force, the curvature κ of a beam or plate should obey a power law,

$$d \propto \kappa \propto b^\gamma \tag{5.1}$$

A log-log plot of the vertical displacement d versus template thickness b, shown in Figure 5.6b, gave a value of $\gamma=2.1\pm0.3$. Standard elasticity theory predicts $\gamma=3.0$, but this assumes a perfectly homogeneous medium and uniform force, neither of which are necessarily fulfilled in our composite system. Nevertheless, if we assume $\kappa \sim b^2$, we predict at least a 25× increase in curvature for a template with a reduced $b=10$ microns, i.e. thinner templates should generate significantly more displacement and work output. The challenge would be to make and handle such ultrathin porous structures, which have to be free-standing in order to deform under illumination.
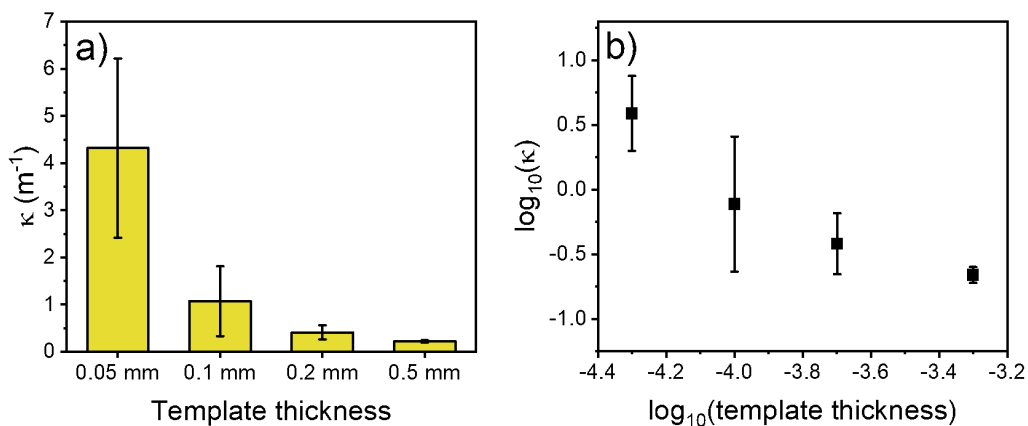
Figure 5.6: Thickness dependence of photomechanical response. (a) κ from DAE-glass templates with variable thicknesses. (b) log-log plot of relationship between κ and template thicknesses.

5.7 Fatigue Resistance

A practical actuator may undergo thousands of cycles, so fatigue resistance must be assessed. We originally expected that the fatigue resistance would be entirely determined by the photostability of the organic DAE component. To test this, we compared the cycling ability of a 0.06 mm thick AAO-DAE template with that of a 0.1 mm thick glass-DAE template. The AAO template bending decreased linearly over the first 100 cycles before stabilizing at 22 μm of vertical displacement, a 25% decrease from the initial value of 30 μm (Figure 5.7a). While macroscopic DAE crystals can typically undergo hundreds of photochromic cycles, the fact that the 200 nm nanowires retain most of their response after 150 cycles was surprising because we previously found that isolated nanowires of a closely related DAE molecule would undergo a crystal-to-amorphous transition after 5-10 illumination cycles. We suspect that confinement within the AAO template helps prevent the molecular rearrangements needed for this transition. The glass-DAE composite did not

97

exhibit the same systematic decline observed in the AAO but did show more variation in its bending. The reason for this heightened variability of the glass template is not clear. It could result from an unstable stress field inside the glass, possibly because the much larger pore diameters accommodate larger DAE crystals that can support more variable behavior. But two points should be emphasized: 1) both templates support repeatable actuation by the DAE over more than 100 UV-green irradiation cycles; and 2) the fatigue resistance of the composite depends on the host material.

5.8 Possible Optimization of Bending Performance

The experimental results above demonstrate that DAE filling of inorganic templates is a general strategy for making robust, fatigue-resistant bending actuators. They also point to several possible future directions to optimized bending performance. First, thinner templates should improve the bending displacement by an order of magnitude or more, all while using less material. The optical penetration depth of the excitation light through the ring-closed isomer will ultimately limit how thin the template can be and still support a layer of unreacted molecules to generate a bimorph structure, but this depth is on the order of 3-4 microns for our DAE at 394 nm.

A second direction to improve performance is to improve the filling of the template by the organic component. Our current method of solvent infiltration followed by annealing can successfully grow crystalline wires within the templates, and for studies on isolated wires that have been extracted from the templates, a high yield is not necessary. Similarly, the study of confinement effects in a porous solid does not require 100% filling. But if we
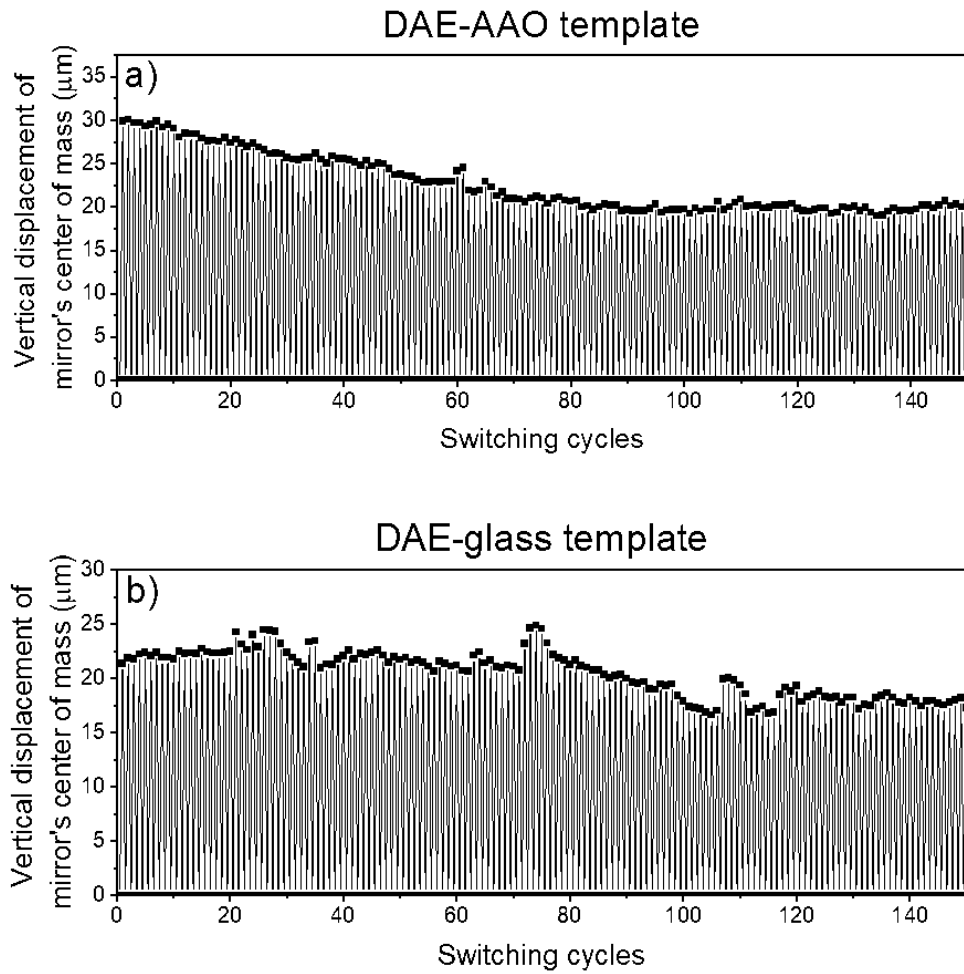
Figure 5.7: Comparison of 150 cycles of vertical displacement of mirror's center of mass ($h/2$) from photomechanical motion on (a) a 0.06 mm thick DAE-AAO template and (b) a 0.1 mm thick DAE-glass template.

leave the wires inside the template and use the composite as a single material, the filling fraction becomes important. Controlling molecular crystal growth is a difficult problem due to the intrinsically random nature of nucleation and the nonlinear kinetics of crystal growth. In order to improve filling, one potential strategy is to provide an energetic driving force, like surface functionalization to encourage the DAE molecules to enter the oxide pores. Another approach would be to dispense with the solvent and simply use melt-filling, so the molecules can completely fill the pores in liquid form. Without solvent evaporation to leave void spaces, the solidified DAE would be able to fill all the available space. Of course, there is no guarantee that the resulting solid would be composed of well-oriented crystalline wires, but it is possible that carefully controlled thermal annealing conditions could encourage their growth.

5.9 Conclusion

The hybrid organic-inorganic approach to photomechanical actuation has been extended from porous alumina to glass templates. The work output, cycling performance, and thickness dependence have been characterized. All in all, the photomechanical behavior is remarkably similar to that of the previously studied AAO templates, despite the different chemical compositions and pore diameters. Importantly, the ability to re-use the same glass template for different DAE filling cycles has allowed us to determine that DAE filling is a crucial factor in determining the mechanical output of the template bending. A second important parameter is the overall template thickness. These two observations provide the foundation for the future development of hybrid organic crystal-inorganic composites for

photomechanical materials.

5.10 Supplementary Information

5.10.1 Experimental Section

Materials

The synthesis of 1,2-bis(2-methyl-5-phenyl-3-thienyl)perfluorocyclopentene [109] was published previously. CH_2Cl_2 was purchased from Fisher Chemical. Microcapillary plates with a 14 mm diameter and pore diameter of 5 μm were purchased from Collimated Holes, Inc. The plates had an open area ratio (OAR) of approximately 50% and measured thicknesses of $h = 0.068$ mm (part number 784-0123, nominal thickness 0.05 mm), h=0.116 mm (part number 755-0001-0.1Mod, nominal thickness 0.1 mm), h=0.220 mm (part number 784-0124, nominal thickness 0.2 mm), h=0.519 mm (part number 755-0001-0.5Mod, nominal thickness 0.5 mm), and h=1.06 mm (part number 784-0125, nominal thickness 1.0 mm).

Preparation of DAE-glass Templates

DAE nanowires were grown in the glass templates by a solvent-annealing method [108]. A solution with DAE dissolved in CH_2Cl_2 (5 mg in 100 μL for the 0.05 mm thick template; 10 mg in 150 μL for the 0.1 mm thick template; 20 mg in 200 μL for the 0.2 mm thickness template; 25 mg in 250 μL for the 0.5 mm thick template; 30 mg in 250 μL for the 1.0 mm thick template) was deposited on one side of the glass template. The template was supported on a homemade Teflon cylinder standing on a CH_2Cl_2-soaked (2 mL) Kimwipe tissue. The assembly was then covered with a bell jar, inside which the CH_2Cl_2 slowly

evaporated while the DAE molecules crystallized inside the channels. After 24h of solvent annealing under the bell jar at room temperature, the DAE-glass template was removed and gently polished with 1500 grit sandpaper to remove residual DAE from the top and bottom.

Laser Deflection Measurements

The photomechanical DAE-glass template was put on a transparent microscope slide with one half blocked by lightproof tape. Light from a 0.95 mW Henium-Neon laser (633 nm wavelength) was used in an interferometer setup to measure the beam deflection. The beam was incident on a beamsplitter which reflected a portion of the beam downward onto a mirror (1 inch diameter, 1.5 g mass) resting on top of the DAE-glass template. The remainder of the beam was reflected by a fixed mirror to be used as the reference. The two beams were projected onto a wall 4.8 m away and the displacement of the template beam was measured. A light-emitting diode, rated for 1 watt at 394 nm (Super Bright LEDs Inc) was placed 1 inch below the template and used to convert the DAE from its ring-open isomer to the ring-closed isomer. The LED intensity was 3.5 mW/cm^2 at the sample, and the measured output wavelength was 400 nm. To convert the DAE from the ring-closed isomer back to the ring-open isomer, a 532 nm laser beam was passed through a diffuser and directed onto the template, resulting in an intensity of 56 mW/cm^2.

Force-Displacement Measurements

A simple custom-made apparatus was used to measure the elastic modulus of the glass array templates and their optomechanical response. The apparatus consists of a
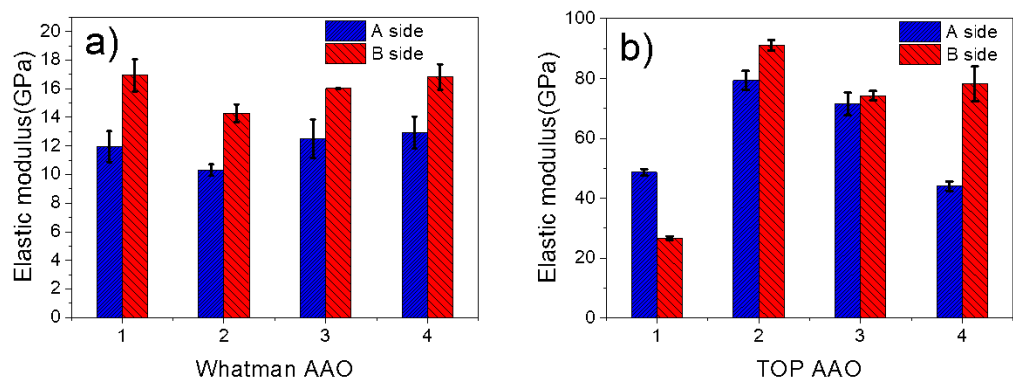
Figure S5.1: Results of elastic modulus measurements on four empty templates; a) Pressing on side A: 11.92±1.15 GPa and B side: 16.01±1.22 GPa for pure Whatman AAOs. b) A: 60.88±17.20 GPa and B side: 67.55±28.20 GPa for pure TOP AAOs.

sample holder and a specially constructed pressing tip attached to an Entran force sensor mounted on a motorized translation stage. The tip was made of an aluminum rod with a pressure fit steel ball bearing (dia. 2.3mm) at the end. During the measurements, a sample was placed in the sample holder and its edges were supported; the tip was positioned at the center of the sample. As the tip pressed downward on the sample at a constant velocity and caused it to bend, the force sensor measured the force the sample was exerting on the tip.
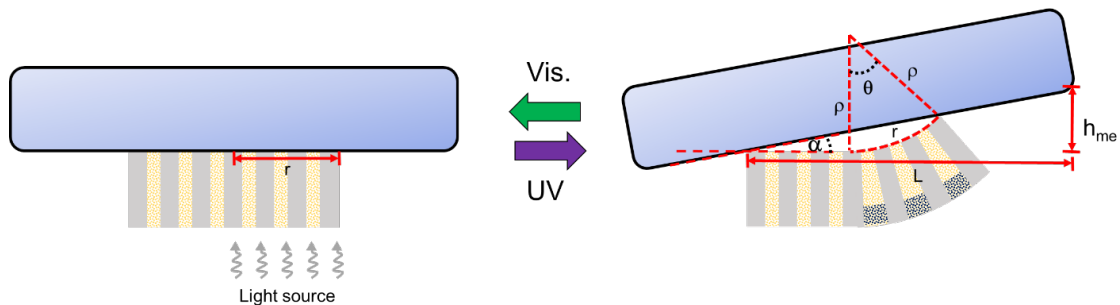
α = mirror tilting angle
θ = bending angle of the arc of the template $\approx 2\alpha$
ρ = radius of curvature
r = radius of template = neutral surface of bending = $\theta\rho$
κ = curvature of the template = $1/\theta \approx \frac{1}{2\alpha}$
L = length of mirror that has been lifted
h_{me} = vertical displacement of the mirror edge = $L\tan\alpha = L\tan(\frac{1}{2\kappa})$

Figure S5.2: Scheme of beam displacement set up with calculations relating mirror displacement, template curvature and mirror tilting angle.

thickness (mm)	channel volume (mm^3)	theoretical maximum DAE loading (mg)	measured DAE loading (mg)
0.05	3.93	5.70	1.37
0.1	7.85	11.41	3.07
0.2	15.70	22.81	4.98

Table S5.1: Theoretical maximum DAE loading and measured DAE loading of DAE-glass templates with different thicknesses. Estimated open area ratio is 51%.
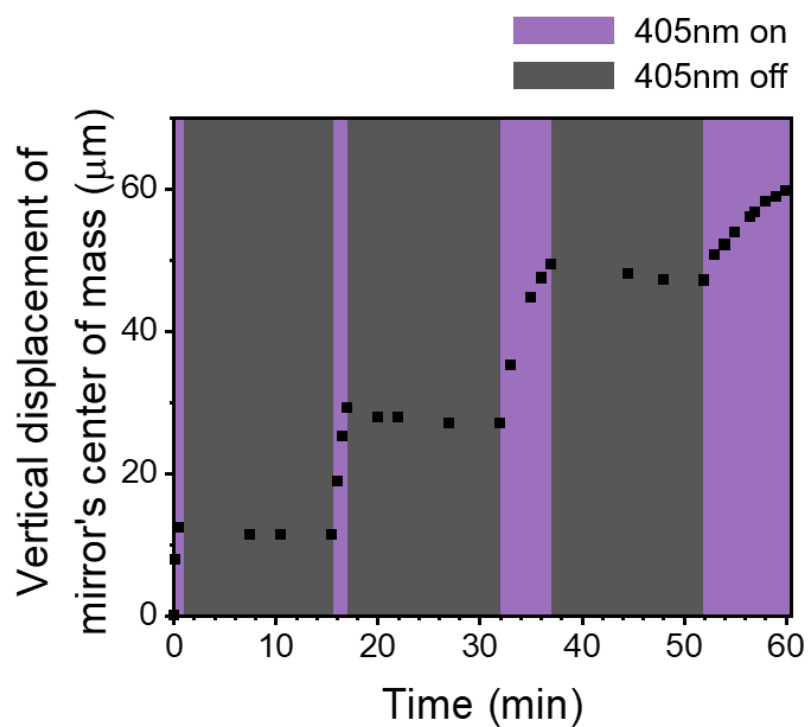
Figure S5.3: Settling experiment of a 0.06 mm thick DAE-AAO template. Vertical displacement of mirror's center of mass dropped 8%, 8% and 5% during three times of 405nm off period respectively.
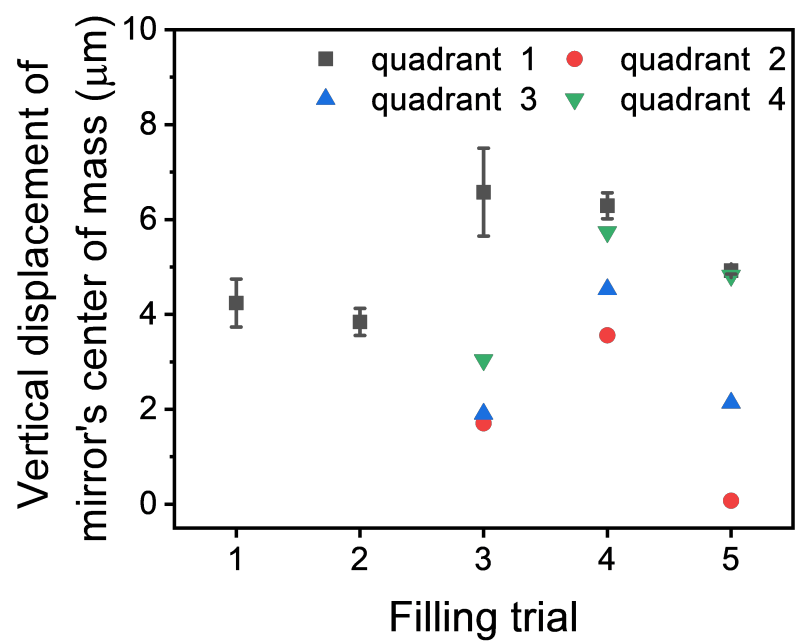
Figure S5.4: A 0.2 mm thick DAE-glass template was rotated in 90 degree increments to irradiate four different semicircles in five filling trials. Different vertical displacements of mirror's center of mass were observed when different quadrants were irradiated. The orientations with grey squares and error bars gave the largest displacements and were chosen for further experiments.

Chapter 6

Photomechanical Optical Fibers

In this chapter, we include some of the work not published. They are presented here as data instead of a complete story.

The initial purpose of this project was to make a photon powered bending actuator with optical fibers. The idea is to use an optical fiber with an asymmetric channel inside. The fiber is filled with an azobenzene (AB) derivative which can increase its volume during a phase change from solid to liquid and push the fiber to bend. (Figure 6.1) [150]

Dr. Jason Myers successfully made flexible and robust scattering fibers with a 250 μm diameter. (Figure 6.2a) The porous silica inner cladding can couple light from the core and scatter to the boundary. A 18 μm diameter hole which can be used for photomechanical material filling is close to the boundary. Figure 6.2b shows the fiber illuminated by a HeNe laser from one end and scattering the light out. The observed scattering length is about 2 feet.

The solvent annealing method was used to fill the fiber with 1,2-bis(2-methyl-
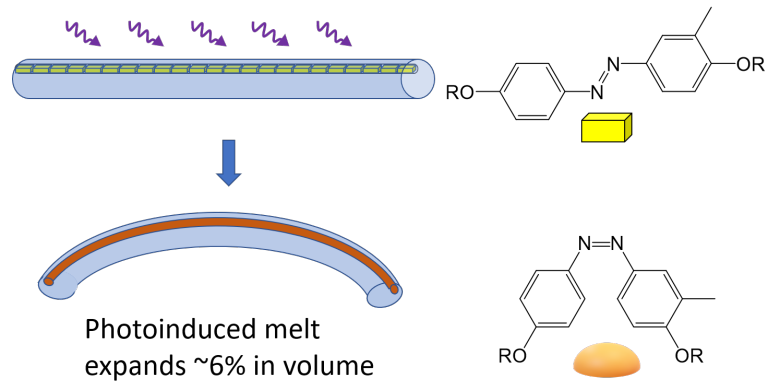
Figure 6.1: An idea of a photomechanical bending optical fibers filled with volumn-increasing photochrome upon UV. The AB photochrome expands about 6% in volume upon UV irradiation.
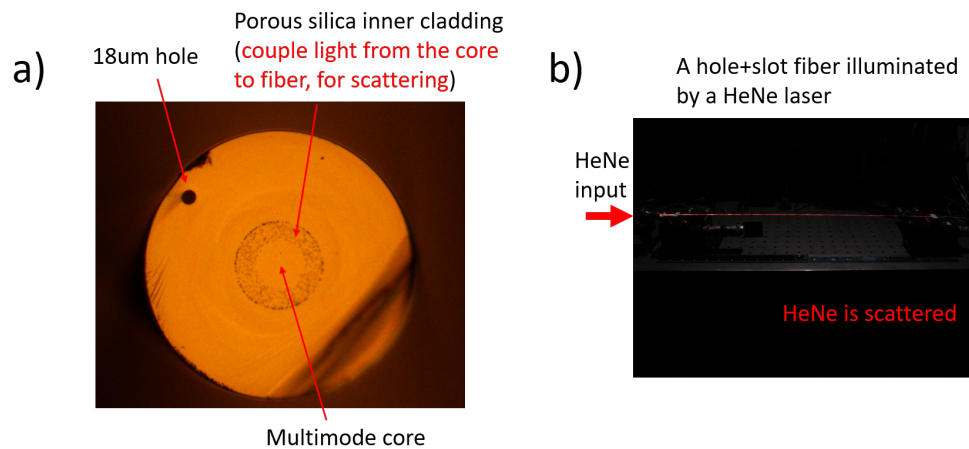
Figure 6.2: Scattering fiber with a pore. a) A microscopic image of the fiber. b) A fiber illuminated by a HeNe laser shows scattering.
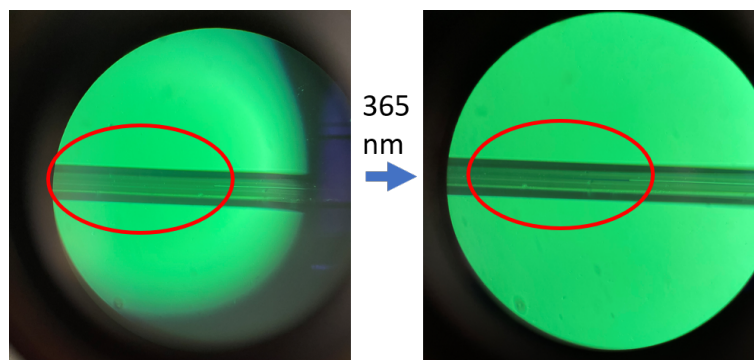
Figure 6.3: DAE solution filled fiber showed photochromic effect and turned blue.

5-phenyl-3-thienyl)perfluorocyclopentene, a DAE derivative. Experimental details can be found in Chapter 2. The DAE filled fiber showed a photochromic reaction under 365 nm irradiation. (Figure 6.3). The problem of solvent filling is the solvent is hard to evaporate out from the 18 μm diameter hole. If we wait long enough for all of the solvent to evaporate, there will be segments of solid DAE crystals left inside the channel that could not give a continuous filling.

The second filling method we tried was melt filling with AB. AB in the *trans-* form and was a yellow powder in room temperature. It isomerizes to the *cis-* form and becomes an orange liquid upon UV irradiation. *Trans*-AB yellow powder was irradiated with a 365nm flashlight (from 5 mm away) for 10 min and then turned into the *cis*-AB orange liquid. The AB orange liquid was pulled into the hole-only fiber with a micro-syringe, filling 4-5 mm of the hollow fiber. After 24 hours, the *cis* liquid returns to solid *trans* form, which no longer has an orange color. Irradiation by external 365 nm light causes *trans* to isomerize to *cis* and melt, again changing color.(Figure 6.4)
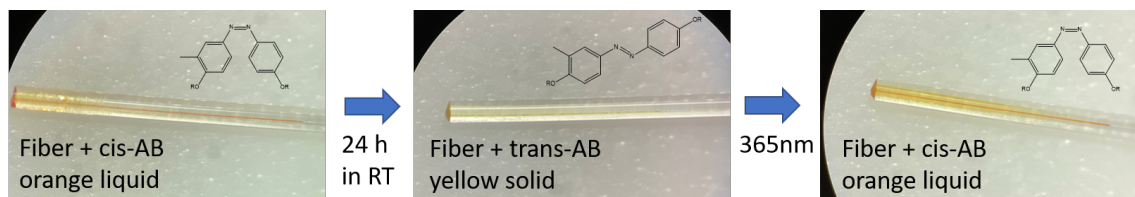
Figure 6.4: Photochromic effect of photo-induced melt filled Azobenzene derivative.
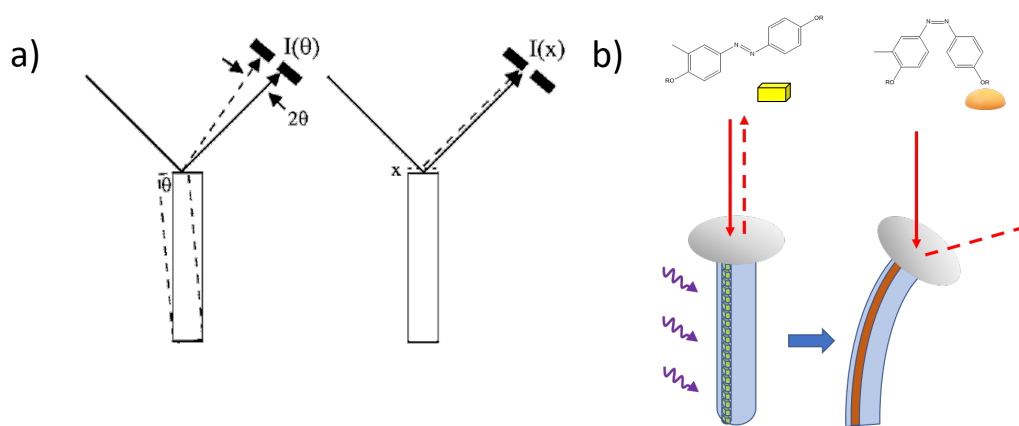
Figure 6.5: Design of photomechanical fiber measurement. a) A beam deflection method measuring fiber bending. [17] b) Our idea illustrating measurement of photomechanical bending performance.

To further investigate the photomechanical effect of the fiber, we used a mirror displacement method (Figure 6.5a) which is putting a mirror on the top of a fiber to be tested and measured the fiber bending by beam deflection as the mirror tilted (Figure 6.5b). [17]

The fiber with a reflective mirror attached to the top was mounted to a substrate. (Figure 6.6) A laser beam was aligned to hit on the reflected mirror. The fiber was then irradiated with a 365 nm flashlight for 10 min.(Figure 6.7) Unfortunately, no beam deflection was observed.

110
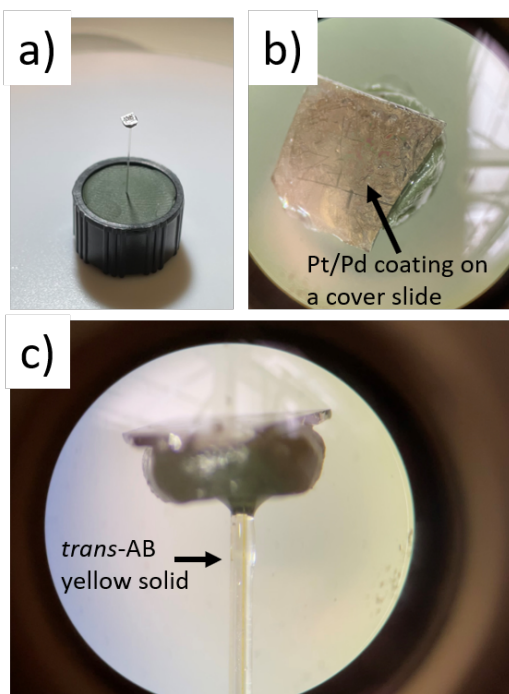
Figure 6.6: a) A DAE filled fiber with a reflective mirror on it. A two-part epoxy (F120 - Epoxy for Fiber Optic Connectors from Thorlabs) was used to attach the mirror to the end of the fiber. b) Top view of fiber actuator. The mirror was made by sputter coating Pd/Pd on a cover slide. c) Side view of fiber actuator. *Trans*-AB yellow solid was filled in the fiber
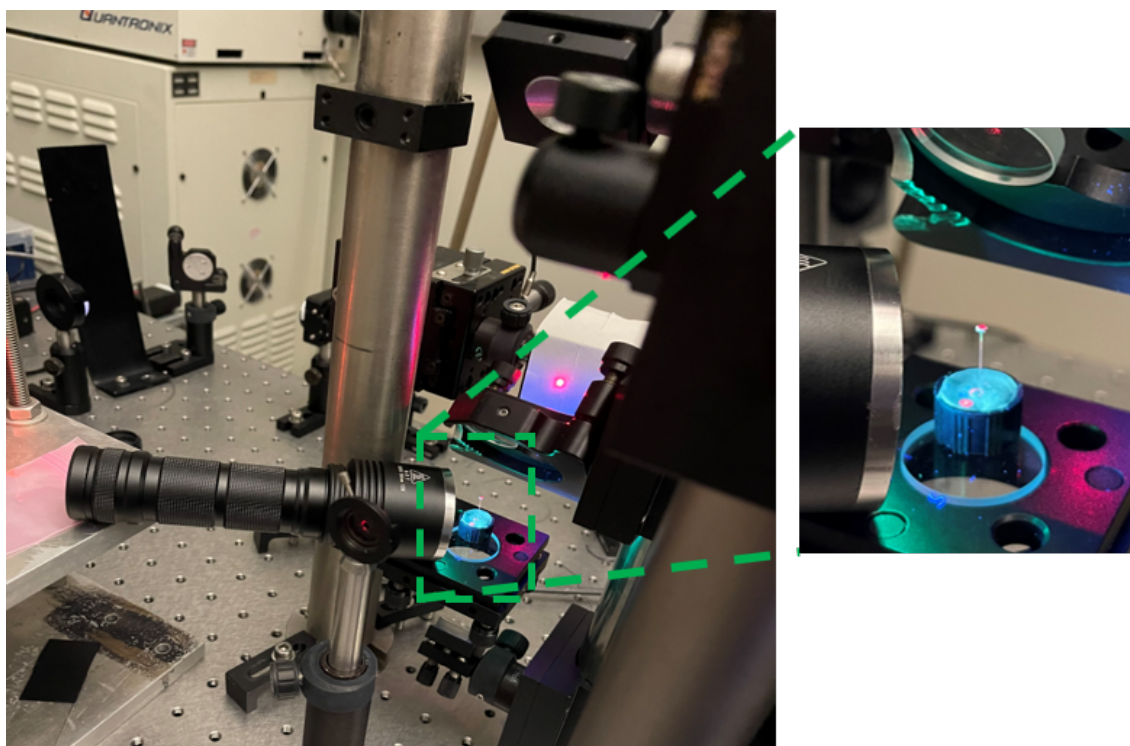
Figure 6.7: A DAE filled fiber was irradiated by a 365 nm flashlight for 10 min.

R_{fib} : radius of the fiber
R_x : radius of the cavity
D : distance between centers of the fiber and the cavity
E_{fib}: elastic modulus of the fiber
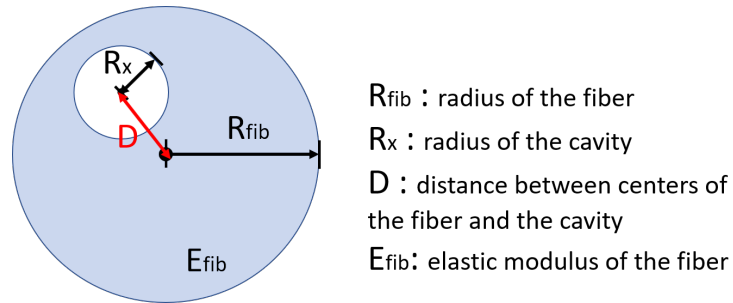
Figure 6.8: Possible parameters of the fiber geometry that affects photomechanical performance.

To study the feasibility of this design, theoretical calculation should be done on the effects of fibers geometry on the photomechancial performance. Possible parameters include the radius of the fiber, the radius of the cavity, the distance between centers of the fiber and the cavity and elastic modulus of the fiber. (Figure 6.8)

Chapter 7

Conclusions and Outlook

This thesis studies a novel photomechanical system with a hybrid organic-inorganic structure. By ordering photoresponsive diarylethene crystals at the micro-level in a porous AAO template, a hybrid actuator is capable of moving macroscopic objects which are 10^5 times heavier than itself without physical connection to an energy source. It combines the advantages from two worlds: high processability of polymers because it is not restricted by the difficulty of large crystal growth, and high performance of crystals thanks to a higher elastic modulus. By expanding well-ordered and densely packed single crystals inside porous templates upon UV irradiation, the hybrid template actuator is able to generate enough force to push up a heavy load and hold its position for a long time at room temperature. The crystal orientation inside AAO templates has been studied to prove our hypothesis of the mechanism. A beam-steering set up has been used to precisely quantify the light-to-work conversion. The hybrid actuator is flexible and can be steered in different directions based on the irradiating area. It worked well both in air and water, and the performance

was not decreased after 5 cycles. The (incident photon)-to-work efficiency was 6.15×10^{-7} and the (absorbed photon)-to-work efficiency was calculated to be 1.15×10^{-5}. This was the first time of quantitative estimate of the light-to-work conversion efficiency for a molecular crystal photomechanical actuator, which provides a starting point for future optimization such as lowering the template elastic modulus and varying the organic photochrome.

A continued study showed how both the organic and inorganic components could affect the photomechancial response. Two templates (AAO and TOP) with different morphologies and elastic moduli (16 GPa versus 68 GPa) were compared. The template with a lower average elastic modulus generated about one order of magnitude more photomechanical work. The light-generated curvature and mechanical work were evaluated using two different methods and the results agreed with each other. Two diarylethene derivatives with different crystal deformation directions were studied to determine the dependence of photomechanical response by chemical and crystal structure. Both inorganic and organic components play important roles in the photomechanical response.

To study the possible extension of the hybrid approach to other materials, porous templates made of SiO_2 instead of Al_2O_3, with thicknesses ranging from 0.05 mm to 1 mm and much larger channels (5 μm diameter instead of 0.2 μm), were used. The photon-induced bending can be repeated for 150 cycles without much loss of performance which suggests good fatigue resistance. Thinner templates give larger displacements. The glass capillary templates made it possible for us to re-use templates across different DAE filling cycles, revealing that the DAE filling step is crucial to determine performance. This work demonstrates that the hybrid method for making photomechanical actuators on macroscopic

scales can be extended to other host materials and template geometries without sacrificing performance.

We have estimated a light-to-work conversion efficiency based on the hybrid material. However it is a small number and has a big room to improve. The ultimate goal that was inspired by this work is to study the fundamental restrictions of a molecule. In other words, it is to find out intrinsic efficiency of photochemistry that transfer photon to mechanical work. The biggest challenge of this work is to optimize the hybrid material and increase the energy conversion efficiency. For future work, firstly, we can design and make a new template with channel directions the same with crystal expansion directions, or control the crystal growth to make the most expanded axis according with templates expansion direction. Secondly, improve pore filling with a different crystal growth method by changing solvent amount and annealing duration and temperature. Thirdly, diarylethens suffer from low penetration since the ring-closed isomers absorb UV light. NIR light can be used to firstly penetrate through all over the template, upconverting nanoparticles can be coated inside template channels which will convert NIR light to UV light to irradiate all of the diarylethene ring-open isomers.

Bibliography

[1] H. Nakai and K. Isobe, "Photochromism of organometallic compounds with structural rearrangement," *Coordination Chemistry Reviews*, vol. 254, no. 21-22, pp. 2652–2662, 2010.

[2] Y. Funasako, H. Miyazaki, T. Sasaki, K. Goshima, and M. Inokuchi, "Synthesis, photochromic properties, and crystal structures of salts containing a pyridinium-fused spiropyran: Positive and negative photochromism in the solution and solid state," *The Journal of Physical Chemistry B*, vol. 124, no. 33, pp. 7251–7257, 2020.

[3] M. Irie, "Discovery and development of photochromic diarylethenes," *Pure and Applied Chemistry*, vol. 87, no. 7, pp. 617–626, 2015.

[4] M. Irie, "Photochromism of diarylethene single molecules and single crystals," *Photochemical & Photobiological Sciences*, vol. 9, no. 12, pp. 1535–1542, 2010.

[5] D. Kitagawa, K. Sasaki, and S. Kobatake, "Correlation between steric substituent constants and thermal cycloreversion reactivity of diarylethene closed-ring isomers," *Bulletin of the Chemical Society of Japan*, vol. 84, no. 2, pp. 141–147, 2011.

[6] C. Huang, J.-a. Lv, X. Tian, Y. Wang, Y. Yu, and J. Liu, "Miniaturized swimming soft robot with complex movement actuated and controlled by remote light signals," *Scientific reports*, vol. 5, no. 1, pp. 1–8, 2015.

[7] Y. Yu, M. Nakano, and T. Ikeda, "Directed bending of a polymer film by light," *Nature*, vol. 425, no. 6954, pp. 145–145, 2003.

[8] M. Yamada, M. Kondo, J.-i. Mamiya, Y. Yu, M. Kinoshita, C. J. Barrett, and T. Ikeda, "Photomobile polymer materials: towards light-driven plastic motors," *Angewandte Chemie*, vol. 120, no. 27, pp. 5064–5066, 2008.

[9] M. Yamada, M. Kondo, R. Miyasato, Y. Naka, J.-i. Mamiya, M. Kinoshita, A. Shishido, Y. Yu, C. J. Barrett, and T. Ikeda, "Photomobile polymer materials—various three-dimensional movements," *Journal of Materials Chemistry*, vol. 19, no. 1, pp. 60–62, 2009.

[10] M. Irie, S. Kobatake, and M. Horichi, "Reversible Surface Morphology Changes of a Photochromic Diarylethene Single Crystal by Photoirradiation," *Science*, vol. 291, pp. 1769–1772, Mar. 2001.

[11] S. Kobatake, S. Takami, H. Muto, T. Ishikawa, and M. Irie, "Rapid and reversible shape changes of molecular crystals on photoirradiation," *Nature*, vol. 446, pp. 778–781, 2007.

[12] R. O. Al-Kaysi, A. M. Müller, and C. J. Bardeen, "Photochemically driven shape changes of crystalline organic nanorods," *Journal of the American Chemical Society*, vol. 128, no. 50, pp. 15938–15939, 2006.

[13] L. Zhu, R. O. Al-Kaysi, and C. J. Bardeen, "Reversible photoinduced twisting of molecular crystal microribbons," *Journal of the American Chemical Society*, vol. 133, no. 32, pp. 12569–12575, 2011.

[14] D. Kitagawa, H. Tsujioka, F. Tong, X. Dong, C. J. Bardeen, and S. Kobatake, "Control of photomechanical crystal twisting by illumination direction," *Journal of the American Chemical Society*, vol. 140, no. 12, pp. 4208–4212, 2018.

[15] D. Kitagawa and S. Kobatake, "Crystal thickness dependence of photoinduced crystal bending of 1, 2-bis (2-methyl-5-(4-(1-naphthoyloxymethyl) phenyl)-3-thienyl) perfluorocyclopentene," *The Journal of Physical Chemistry C*, vol. 117, no. 40, pp. 20887–20892, 2013.

[16] F. Tong, W. Xu, M. Al-Haidar, D. Kitagawa, R. O. Al-Kaysi, and C. J. Bardeen, "Photomechanically induced magnetic field response by controlling molecular orientation in 9-methylanthracene microcrystals," *Angewandte Chemie International Edition*, vol. 57, no. 24, pp. 7080–7084, 2018.

[17] S. Bian, D. Robinson, and M. G. Kuzyk, "Optically activated cantilever using photomechanical effects in dye-doped polymer fibers," *JOSA B*, vol. 23, no. 4, pp. 697–708, 2006.

[18] M. Irie, T. Lifka, S. Kobatake, and N. Kato, "Photochromism of 1,2-Bis(2-methyl-5-phenyl-3-thienyl)perfluorocyclopentene in a Single-Crystalline Phase," *Journal of the American Chemical Society*, vol. 122, pp. 4871–4876, May 2000.

[19] M. Irie, K. Sakemura, M. Okinaka, and K. Uchida, "Photochromism of dithienylethenes with electron-donating substituents," *The Journal of Organic Chemistry*, vol. 60, no. 25, pp. 8305–8309, 1995.

[20] K. Shibata, K. Muto, S. Kobatake, and M. Irie, "Photocyclization/cycloreversion quantum yields of diarylethenes in single crystals," *The Journal of Physical Chemistry A*, vol. 106, no. 1, pp. 209–214, 2002.

[21] M. Irie, T. Fukaminato, K. Matsuda, and S. Kobatake, "Photochromism of Diarylethene Molecules and Crystals: Memories, Switches, and Actuators," *Chem. Rev*, vol. 114, pp. 12174–12277, 2014.

[22] J.-P. Sauvage, "From chemical topology to molecular machines (Nobel lecture)," *Angewandte Chemie International Edition*, vol. 56, no. 37, pp. 11080–11093, 2017. Publisher: Wiley Online Library.

[23] J. F. Stoddart, "Mechanically interlocked molecules (mims)—molecular shuttles, switches, and machines (nobel lecture)," *Angewandte Chemie International Edition*, vol. 56, no. 37, pp. 11094–11125, 2017.

[24] B. L. Feringa, "The art of building small: from molecular switches to motors (nobel lecture)," in *Angew*, 56: 11060–11078, 2017.

[25] J. Zhuang, B. Han, W. Liu, J. Zhou, K. Liu, D. Yang, and D. Tang, "Liposome-amplified photoelectrochemical immunoassay for highly sensitive monitoring of disease biomarkers based on a split-type strategy," *Biosensors and Bioelectronics*, vol. 99, pp. 230–236, 2018.

[26] T. Julie, O. Hugo, S. Olivier, and L. Sebastien, "Magnetic responsive polymer composite materials," *Chem*, vol. 7099, 2013.

[27] A. Mourran, H. Zhang, R. Vinokur, and M. Möller, "Soft microrobots employing nonequilibrium actuation via plasmonic heating," *Adv. Mater*, vol. 29, no. 16048, p. 25, 2017.

[28] Z. Chen, P.-C. Hsu, J. Lopez, Y. Li, J. W. To, N. Liu, C. Wang, S. C. Andrews, J. Liu, Y. Cui, *et al.*, "Fast and reversible thermoresponsive polymer switching materials for safer batteries," *Nature Energy*, vol. 1, no. 1, pp. 1–2, 2016.

[29] G. Kocak, C. Tuncer, and V. Bütün, "pH-Responsive polymers," *Polym. Chem*, vol. 8, p. 144, 2017.

[30] S. Zhang, A. M. Bellinger, D. L. Glettig, R. Barman, Y.-A. L. Lee, J. Zhu, C. Cleveland, V. A. Montgomery, L. Gu, L. D. Nash, *et al.*, "A ph-responsive supramolecular polymer gel as an enteric elastomer for use in gastric devices," *Nature materials*, vol. 14, no. 10, pp. 1065–1071, 2015.

[31] Y. Liu, B. Xu, S. Sun, J. Wei, L. Wu, and Y. Yu, "Humidity-and photo-induced mechanical actuation of cross-linked liquid crystal polymers," *Advanced Materials*, vol. 29, no. 9, p. 1604792, 2017.

[32] T. Ikeda, M. Nakano, Y. Yu, O. Tsutsumi, and A. Kanazawa, "Anisotropic bending and unbending behavior of azobenzene liquid-crystalline gels by light exposure," *Advanced Materials*, vol. 15, no. 3, pp. 201–205, 2003.

[33] T. Kim, L. Zhu, R. O. Al-Kaysi, and C. J. Bardeen, "Organic photomechanical materials," *ChemPhysChem*, vol. 15, no. 3, pp. 400–414, 2014.

[34] Y. Norikane, E. Uchida, S. Tanaka, K. Fujiwara, E. Koyama, R. Azumi, H. Akiyama, H. Kihara, and M. Yoshida, "Photoinduced crystal-to-liquid phase transitions of azobenzene derivatives and their application in photolithography processes through a solid–liquid patterning," *Organic letters*, vol. 16, no. 19, pp. 5012–5015, 2014.

[35] T. Ikeda and O. Tsutsumi, "Optical switching and image storage by means of azobenzene liquid-crystal films," *Science*, vol. 268, p. 1873, 1995.

[36] E. Havens, E. A. Snyder, and T. H. Tong, ""Light-activated shape memory polymers and associated applications," in " *Proc. SPIE 5762*, 5762–5768, 2005.

[37] H.-K. Kim, W. Shin, and T.-J. Ahn, "UV sensor based on photomechanically functional polymer-coated FBG," *IEEE Photonics Technology Letters*, vol. 22, no. 19, pp. 1404–1406, 2010.

[38] J. Lee, S. Oh, J. Pyo, J.-M. Kim, and J. H. Je, "A light-driven supramolecular nanowire actuator," *Nanoscale*, vol. 7, no. 15, pp. 6457–6461, 2015.

[39] R. O. Al-Kaysi, F. Tong, M. Al-Haidar, L. Zhu, and C. J. Bardeen, "Highly branched photomechanical crystals," *Chemical Communications*, vol. 53, no. 17, pp. 2622–2625, 2017.

[40] D. Kitagawa and S. Kobatake, "Photoreversible current ON/OFF switching by the photoinduced bending of gold-coated diarylethene crystals," *Chemical Communications*, vol. 51, no. 21, pp. 4421–4424, 2015.

[41] J. Blass, B. L. Bozna, M. Albrecht, J. A. Krings, B. J. Ravoo, G. Wenz, and R. S. A. a. Bennewitz, "and Friction by Light Using Photosensitive Guest-Host Interactions," *Chem*, vol. 2015, p. 51, 1833.

[42] S. H. Mostafavi, F. Tong, T. W. Dugger, D. Kisailus, and C. J. Bardeen, "Noncovalent photochromic polymer adhesion," *Macromolecules*, vol. 51, no. 6, pp. 2388–2394, 2018.

[43] S. H. Mostafavi, W. Li, K. D. Clark, F. Stricker, J. R. d. Alaniz, and C. J. Bardeen, "Photoinduced deadhesion of a polymer film using a photochromic donor–acceptor stenhouse adduct," *Macromolecules*, vol. 52, no. 16, pp. 6311–6317, 2019.

[44] T. J. Gately, W. Li, S. H. Mostafavi, and C. J. Bardeen, "Reversible adhesion switching using spiropyran photoisomerization in a high glass transition temperature polymer," *Macromolecules*, 2021.

[45] F. Tong, M. Liu, R. O. Al-Kaysi, and C. J. Bardeen, "Surfactant-enhanced photoisomerization and photomechanical response in molecular crystal nanowires," *Langmuir*, vol. 34, no. 4, pp. 1627–1634, 2018.

[46] E. Uchida, R. Azumi, and Y. Norikane, "Nat," *Commun*, vol. 6, p. 7310, 2015.

[47] H. Wang, P. Chen, Z. Wu, J. Zhao, J. Sun, and R. Lu, "Bending, curling, rolling, and salient behavior of molecular crystals driven by [2+ 2] cycloaddition of a styryl-benzoxazole derivative," *Angewandte Chemie International Edition*, vol. 56, no. 32, pp. 9463–9467, 2017.

[48] N. K. Nath, T. Runcevski, C.-Y. Lai, M. Chiesa, R. E. Dinnebier, and P. Naumov, "Surface and bulk effects in photochemical reactions and photomechanical effects in

dynamic molecular crystals," *Journal of the American Chemical Society*, vol. 137, no. 43, pp. 13866–13875, 2015.

[49] F. Tong, M. Al-Haidar, L. Zhu, R. O. Al-kaysi, and B. CJ, "Photoinducedpeeling of molecular crystals," *Chem Commun*, vol. 55, p. 3709, 2019.

[50] E. Hatano, M. Morimoto, T. Imai, K. Hyodo, A. Fujimoto, R. Nishimura, A. Sekine, N. Yasuda, S. Yokojima, S. Nakamura, *et al.*, "Photosalient phenomena that mimic impatiens are observed in hollow crystals of diarylethene with a perfluorocyclohexene ring," *Angewandte Chemie International Edition*, vol. 56, no. 41, pp. 12576–12580, 2017.

[51] J. Fritzsche, "Bull Acad Imper Sci Petersbrg 1866;9:406e19," *Z Chem*, vol. 9, p. 139, 1866.

[52] S. Kobatake, "Photochromism," in *Progress in the Science of Functional Dyes*, pp. 263–281, Springer, 2021.

[53] Y. Shiraishi, T. Inoue, S. Sumiya, and T. Hirai, "Entropy-Driven Thermal Isomerization of Spiropyran in Viscous Media," *J. Phys*, vol. 115, pp. 9083–9090, 2011.

[54] M. Tanaka, M. Nakamura, M. A. A. Salhin, T. Ikeda, K. Kamada, H. Ando, Y. Shibutani, and K. S. a. Kimura, "and Photochromism of Spirobenzopyran Derivatives Bearing an Oxymethylcrown Ether Moiety: Metal Ion-Induced Switching between Positive and Negative Photochromisms," *J. Org. Chem*, vol. 66, pp. 1533–1537, 2001.

[55] F. Tong, W. Xu, T. Guo, B. F. Lui, R. C. Hayward, P. Palffy-Muhoray, R. O. Al-Kaysi, and C. J. Bardeen, "Photomechanical molecular crystals and nanowire assemblies based on the [2+ 2] photodimerization of a phenylbutadiene derivative," *Journal of Materials Chemistry C*, vol. 8, no. 15, pp. 5036–5044, 2020.

[56] T. Kim, L. Zhu, L. J. Mueller, and C. J. Bardeen, "Mechanism of photoinduced bending and twisting in crystalline microneedles and microribbons composed of 9-methylanthracene," *Journal of the American Chemical Society*, vol. 136, no. 18, pp. 6617–6625, 2014.

[57] S. Helmy, F. A. Leibfarth, S. Oh, J. E. Poelma, C. J. Hawker, and J. Read de Alaniz, "Photoswitching using visible light: a new class of organic photochromic molecules," *Journal of the American Chemical Society*, vol. 136, no. 23, pp. 8169–8172, 2014.

[58] J. R. Hemmer, S. O. Poelma, N. Treat, Z. A. Page, N. D. Dolinski, Y. J. Diaz, W. Tomlinson, K. D. Clark, J. P. Hooper, C. Hawker, *et al.*, "Tunable visible and near infrared photoswitches," *Journal of the American Chemical Society*, vol. 138, no. 42, pp. 13960–13966, 2016.

[59] T. Nakagawa, T. Ubukata, and Y. Yokoyama, "Chirality and stereoselectivity in photochromic reactions," *Journal of Photochemistry and Photobiology C: Photochemistry Reviews*, vol. 34, pp. 152–191, 2018.

[60] K. Nakatani, J. Piard, P. Yu, and R. Métivier, "Introduction: organic photochromic molecules," *Photochromic materials: preparation, properties and applications*, pp. 1–45, 2016.

[61] L. Vetráková, V. Ladányi, J. Al Anshori, P. Dvořák, J. Wirz, and D. Heger, "The absorption spectrum of cis-azobenzene," *Photochemical & Photobiological Sciences*, vol. 16, no. 12, pp. 1749–1756, 2017.

[62] K. Masutani, M.-a. Morikawa, and N. Kimizuka, "A liquid azobenzene derivative as a solvent-free solar thermal fuel," *Chemical Communications*, vol. 50, no. 99, pp. 15803–15806, 2014.

[63] S. Nakamura and M. Irie, "Thermally irreversible photochromic systems. a theoretical study," *The Journal of Organic Chemistry*, vol. 53, no. 26, pp. 6136–6138, 1988.

[64] M. Irie, "Diarylethenes for memories and switches," *Chemical Reviews*, vol. 100, no. 5, pp. 1685–1716, 2000.

[65] W. Li, C. Jiao, X. Li, Y. Xie, K. Nakatani, H. Tian, and W. Zhu, "Separation of photoactive conformers based on hindered diarylethenes: efficient modulation in photocyclization quantum yields," *Angewandte Chemie*, vol. 126, no. 18, pp. 4691–4695, 2014.

[66] T. Hugel, N. B. Holland, A. Cattani, L. Moroder, M. Seitz, and H. E. Gaub, "Single-molecule optomechanical cycle," *Science*, vol. 296, no. 5570, pp. 1103–1106, 2002.

[67] Y. Kishimoto and J. Abe, "A fast photochromic molecule that colors only under uv light," *Journal of the American Chemical Society*, vol. 131, no. 12, pp. 4227–4229, 2009.

[68] K. Inaba, R. Iwai, M. Morimoto, and M. Irie, "Thermally reversible photochromism of dipyrrolylethenes," *Photochemical & Photobiological Sciences*, vol. 18, no. 9, pp. 2136–2141, 2019.

[69] M. Irie, T. Fukaminato, K. Matsuda, and S. Kobatake, "Photochromism of diarylethene molecules and crystals: memories, switches, and actuators," *Chemical Reviews*, vol. 114, no. 24, pp. 12174–12277, 2014.

[70] E. Merian, "Steric factors influencing the dyeing of hydrophobic. Fibers," *Textile Research Journal*, vol. 36, no. 7, pp. 612–618, 1966.

[71] N. Hosono, M. Yoshikawa, H. Furukawa, K. Totani, K. Yamada, T. Watanabe, and K. Horie, "Photoinduced deformation of rigid azobenzene-containing polymer networks," *Macromolecules*, vol. 46, no. 3, pp. 1017–1026, 2013.

[72] Y. Takashima, S. Hatanaka, M. Otsubo, M. Nakahata, T. Kakuta, A. Hashidzume, H. Yamaguchi, and A. Harada, "Expansion–contraction of photoresponsive artificial muscle regulated by host–guest interactions," *Nature communications*, vol. 3, no. 1, pp. 1–8, 2012.

[73] C. D. Eisenbach, "Isomerization of aromatic azo chromophores in poly(ethyl acrylate) networks and photomechanical effect," *Polymer*, vol. 21, p. 1175, 1980.

[74] E. Zimmermann and J. Stille, "Photoresponsive polyquinolines," *Macromolecules*, vol. 18, p. 321, 1985.

[75] d. G. PG, "Reflexions sur un type de polymeres nematiques," *C R Seances Acad Sci Ser B*, vol. 281, p. 101, 1975.

[76] J. Küpfer and H. Finkelmann, "Nematic liquid single-crystal elastomers," *Makromol Chem Rapid Commun*, vol. 12, p. 717, 1991.

[77] P. Naumov, S. Chizhik, M. K. Panda, N. K. Nath, and E. Boldyreva, "Mechanically responsive molecular crystals," *Chemical reviews*, vol. 115, no. 22, pp. 12440–12490, 2015.

[78] M. Kondo, "Photomechanical materials driven by photoisomerization or photodimerization," *Polymer Journal*, vol. 52, no. 9, pp. 1027–1034, 2020.

[79] G. Abakumov and V. Nevodchikov, "Thermomechanical and photomechanical effects observed on crystals of a free-radical complex," *Doklady Akademii Nauk Sssr*, vol. 266, no. 6, pp. 1407–1410, 1982.

[80] D. Kitagawa, R. Tanaka, and S. Kobatake, "Dependence of photoinduced bending behavior of diarylethene crystals on irradiation wavelength of ultraviolet light," *Physical Chemistry Chemical Physics*, vol. 17, no. 41, pp. 27300–27305, 2015.

[81] A. Hirano, T. Hashimoto, D. Kitagawa, K. Kono, and S. Kobatake, "Dependence of photoinduced bending behavior of diarylethene crystals on ultraviolet irradiation power," *Crystal Growth & Design*, vol. 17, no. 9, pp. 4819–4825, 2017.

[82] A. Hirano, D. Kitagawa, and S. Kobatake, "Photomechanical bending behavior of photochromic diarylethene crystals induced under polarized light," *CrystEngComm*, vol. 21, no. 15, pp. 2495–2501, 2019.

[83] D.-D. Han, Y.-L. Zhang, J.-N. Ma, Y.-Q. Liu, B. Han, and H.-B. Sun, "Light-Mediated Manufacture and Manipulation of Actuators," *Adv. Mater*, vol. 28, pp. 8328–8343, 2016.

[84] T. White, *Photomechanical Materials, Composites, and Systems*. Hoboken, New Jersey: Wiley, 1 ed., 2017.

[85] T. Ikeda, J. Mamiya, and Y. Yu, "Photomechanics of liquid-crystalline elastomers and other polymers," *Angew. Chem. Int. Ed*, vol. 46, pp. 506–528, 2007.

[86] S. Iamsaard, S. Abhoff, B. Matt, T. Kudernac, J. Cornelissen, S. Fletcher, and N. Katsonis, "Conversion of Light into Macroscopic Helical Motion," *Nat. Chem*, vol. 6, pp. 229–235, 2014.

[87] N. Nath, L. Pejov, S. Nichols, C. Hu, N. Saleh, B. Kahr, and P. Naumov, "Model for photoinduced bending of slender molecular crystals," *J. Am. Chem. Soc*, vol. 136, pp. 2757–2766, 2014.

[88] E. Boldyreva, A. Sinelnikov, A. Chupakhin, N. Lyakhov, and V. Boldyrev, "Deformation and mechanical destruction of [Co(NH3)5NO2]X2 crystals (X = chloride, bromide, nitrate) during photostimulated linkage isomerization," *Doklady Akad. Nauk USSR*, vol. 277, pp. 893–896, 1984.

[89] P. Naumov, J. Kowalik, K. Solntsev, A. Baldridge, J.-S. Moon, C. Kranz, and L. Tolbert, "Topochemistry and photomechanical effects in crystals of green fluorescent protein-like chromophores: effects of hydrogen bonding and crystal packing," *J. Am. Chem. Soc*, vol. 132, pp. 5845–5857, 2010.

[90] H. Koshima, N. Ojima, and H. Uchimoto, "Mechanical motion of azobenzene crystals upon photoirradiation," *J. Am. Chem. Soc*, vol. 131, pp. 6890–6891, 2009.

[91] H. Koshima, K. Takechi, H. Uchimoto, M. Shiro, and D. Hashizume, "Photomechanical bending of salicylideneaniline crystals," *Chem. Commun*, vol. 47, pp. 11423–11425, 2011.

[92] R. Al-Kaysi and C. Bardeen, "Reversible photoinduced shape changes of crystalline organic nanorods," *Adv. Mater*, vol. 19, pp. 1276–1280, 2007.

[93] O. Bushuyev, T. Singleton, and C. Barrett, "Reversible, and General Photomechanical Motion in Single Crystals of Various Azo Compounds Using Visible Light," *Adv. Mater*, vol. 25, pp. 1796–1800, 2013.

[94] O. Bushuyev, A. Tomberg, T. Friscic, and C. Barrett, "Shaping Crystals with Light: Crystal-to-Crystal Isomerization and Photomechanical Effect in Fluorinated Azobenzenes," *J. Am. Chem. Soc*, vol. 135, pp. 12556–12559, 2013.

[95] M. Garcia-Garibay, "Molecular crystals on the move: From single-crystal-to-single-crystal photoreactions to molecular machinery," *Angew. Chem. Int. Ed*, vol. 46, pp. 2–5, 2007.

[96] H. Koshima, M. Matsudomi, Y. Uemura, F. Kimura, and T. Kimura, "Light-driven bending of polymer films in which salicylidenephenylethylamine crystals are aligned magnetically," *Chemistry Letters*, vol. 42, no. 12, pp. 1517–1519, 2013.

[97] T. Lan and W. Chen, "Hybrid nanoscale organic molecular crystals assembly as a photon-controlled actuator," *Angewandte Chemie*, vol. 125, no. 25, pp. 6624–6628, 2013.

[98] S. C. Sahoo, N. K. Nath, L. Zhang, M. H. Semreen, T. H. Al-Tel, and P. Naumov, "Actuation based on thermo/photosalient effect: a biogenic smart hybrid driven by light and heat," *RSC advances*, vol. 4, no. 15, pp. 7640–7647, 2014.

[99] Q. Yu, X. Yang, Y. Chen, K. Yu, J. Gao, Z. Liu, P. Cheng, Z. Zhang, B. Aguila, and S. Ma, "Fabrication of light-triggered soft artificial muscles via a mixed-matrix membrane strategy," *Angewandte Chemie International Edition*, vol. 57, no. 32, pp. 10192–10196, 2018.

[100] H. Colfen and S. Mann, "Higher-Order Organization by Mesoscale Self-Assembly and Transformation of Hybrid Nanostructures," *Angew. Chem. Int. Ed*, vol. 42, pp. 2350–2365, 2003.

[101] M. O'Brien, M. Jones, and C. Mirkin, "The Nature and Implications of Uniformity in the Hierarchical Organization of Nanomaterials," *Proc. Nat. Acad. Sci*, vol. 113, pp. 11717–11725, 2016.

[102] F. Terao, M. Morimoto, and M. Irie, "Light-driven molecular-crystal actuators: rapid and reversible bending of rodlike mixed crystals of diarylethene derivatives," *Angew. Chem. Int. Ed*, vol. 51, pp. 901–904, 2012.

[103] M. Morimoto and M. Irie, "A diarylethene cocrystal that converts light into mechanical work," *J. Am. Chem. Soc*, vol. 132, pp. 14172–14178, 2010.

[104] L. Kuroki, S. Takami, K. Yoza, M. Morimoto, and M. Irie, "Photoinduced shape changes of diarylethene single crystals: correlation between shape changes and molecular packing," *Photochem. Photobio. Sci*, vol. 9, pp. 221–225, 2010.

[105] S. Ohshima, M. Morimoto, and M. Irie, "Light-Driven Bending of Diarylethene Mixed Crystals," *Chem. Sci*, vol. 6, pp. 5746–5752, 2015.

[106] D. Kitagawa, R. Tanaka, and S. Kobatake, "Photoinduced Stepwise Bending Behavior of Photochromic Diarylethene Crystals," *CrystEngComm*, vol. 18, pp. 7236–7240, 2016.

[107] W. Lee and S.-J. Park, "Porous anodic aluminum oxide: anodization and templated synthesis of functional nanostructures," *Chemical reviews*, vol. 114, no. 15, pp. 7487–7556, 2014.

[108] R. Al-Kaysi and C. Bardeen, "General method for the synthesis of crystalline organic nanorods using porous alumina templates," *Chem. Comm*, pp. 1224–1226, 2006.

[109] T. Yamada, K. Muto, S. Kobatake, and M. Irie, "Crystal structure- reactivity correlation in single-crystalline photochromism of 1, 2-bis (2-methyl-5-phenyl-3-thienyl) perfluorocyclopentene," *The Journal of organic chemistry*, vol. 66, no. 18, pp. 6164–6168, 2001.

[110] M. Herder, B. M. Schmidt, L. Grubert, M. Pätzel, J. Schwarz, and S. Hecht, "Improving the Fatigue Resistance of Diarylethene Switches," *Journal of the American Chemical Society*, vol. 137, pp. 2738–2747, Feb. 2015.

[111] L. Cheng, Y. Torres, K. Lee, A. McClung, J. Baur, T. White, and W. Oates, "Photomechanical Bending Mechanics of Polydomain Azobenzene Liquid Crystal Polymer Network Films," *J. Appl. Phys*, vol. 112, pp. 013513 1–17, 2012.

[112] L. Zhang, S. Chizhik, Y. Wen, and P. Naumov, "Directed Motility of Hygroresponsive Biomimetic Actuators," *Adv. Funct. Mater*, vol. 26, pp. 1040–1053, 2016.

[113] S. Chizhik, A. Sidelnikov, B. Zakharov, P. Naumov, and E. Boldyreva, "Quantification of Photoinduced Bending of Dynamic Molecular Crystals: from Macroscopic Strain to Kinetic Constants and Activation Energies," *Chem. Sci*, vol. 9, pp. 2319–2335, 2018.

[114] L. Liu, M.-H. Liu, L.-L. Deng, B.-P. Lin, and H. Yang, "Near-Infrared Chromophore Functionalized Soft Actuator with Ultrafast Photoresponsive Speed and Superior Mechanical Property," *J. Am. Chem. Soc*, vol. 139, p. 11333 11336, 2017.

[115] J. Loomis and B. Panchapakesan, "Dimensional Dependence of Photomechanical Response in Carbon Nanostructure Composites: a Case for Carbon-Based Mixed-Dimensional Systems," *Nanotechnology*, vol. 23, pp. 215501 1–12, 2012.

[116] J. Loomis, X. Fan, F. Khosravi, P. Xu, M. Fletcher, R. Cohn, and B. Panchapakesan, "Graphene/Elastomer Composite-Based Photo-Thermal Nanopositioners," *Sci. Rep*, vol. 3, pp. 1900 1–10, 2013.

[117] S. Serak, N. Tabiryan, R. Vergara, T. White, R. Vaia, and T. Bunning, "Liquid Crystalline Polymer Cantilever Oscillators Fueled by Light," *Soft Matter*, vol. 6, pp. 779–783, 2010.

[118] "Piezo Physik Instrumente Models. PL112-PL140 PICMA bender." `https://www.physikinstrumente.com/en/products/piezoelectric-transducers-actuators/pl112-pl140-picma-bender-103000/#specification`. Accessed: 2019-01-02.

[119] "Piezo physik instrumente models. PD410 Round PICMA multilayer bender actuators." `https://www.physikinstrumente.com/en/products/piezoelectric-transducers-actuators/bender-actuators/pd410-round-picma-multilayer-bender-actuators-103050/#specification`. Accessed: 2019-01-02.

[120] "Thorlabs. piezoelectric benders. PB4NB2W." `https://www.thorlabs.com/newgrouppage9.cfm\?objectgroup_id=10958`. Accessed: 2019-01-02.

[121] F. Tong, D. Kitagawa, X. Dong, S. Kobatake, and C. Bardeen, "Photomechanical motion of diarylethene molecular crystal nanowires," *Nanoscale*, vol. 10, pp. 3393–3398, 2018.

[122] L. Zhu, F. Tong, C. Salinas, M. Al-Muhanna, F. Tham, D. Kisailus, R. Al-Kaysi, and C. Bardeen, "Improved Solid-State Photomechanical Materials by Fluorine Substitution of 9-Anthracene Carboxylic Acid," *Chem. Mater*, vol. 26, pp. 6007–6015, 2014.

[123] S. Liu, S. C. Mannsfeld, W. M. Wang, Y.-S. Sun, R. M. Stoltenberg, and Z. Bao, "Patterning of α-sexithiophene single crystals with precisely controlled sizes and shapes," *Chemistry of Materials*, vol. 21, no. 1, pp. 15–17, 2009.

[124] H. Minemawari, T. Yamada, H. Matsui, J. Tsutsumi, S. Haas, R. Chiba, R. Kumai, and T. Hasegawa, "Inkjet printing of single-crystal films," *Nature*, vol. 475, no. 7356, pp. 364–367, 2011.

[125] A. Keating and M. Garcia-Garibay, "Organic and inorganic photochemistry," *Organic and inorganic photochemistry. Marcel Dekker, New York*, pp. 195–248, 1998.

[126] D.-K. Bucar and L. R. MacGillivray, "Preparation and reactivity of nanocrystalline cocrystals formed via sonocrystallization," *Journal of the American Chemical Society*, vol. 129, no. 1, pp. 32–33, 2007.

[127] S. Takahashi, H. Miura, H. Kasai, S. Okada, H. Oikawa, and H. Nakanishi, "Single-crystal-to-single-crystal transformation of diolefin derivatives in nanocrystals," *Journal of the American Chemical Society*, vol. 124, no. 37, pp. 10944–10945, 2002.

[128] X. Dong, F. Tong, K. M. Hanson, R. O. Al-Kaysi, D. Kitagawa, S. Kobatake, and C. J. Bardeen, "Hybrid organic–inorganic photon-powered actuators based on aligned diarylethene nanocrystals," *Chemistry of Materials*, vol. 31, no. 3, pp. 1016–1022, 2019.

[129] M. Warner and L. Mahadevan, "Photoinduced deformations of beams, plates, and films," *Physical Review Letters*, vol. 92, no. 13, p. 134302, 2004.

[130] M. Hoffmann and R. Birringer, "Quantitative measurements of young's modulus using the miniaturized disk-bend test," *Materials Science and Engineering: A*, vol. 202, no. 1-2, pp. 18–25, 1995.

[131] M. Asmani, C. Kermel, A. Leriche, and M. Ourak, "Influence of porosity on young's modulus and poisson's ratio in alumina ceramics," *Journal of the European ceramic society*, vol. 21, no. 8, pp. 1081–1086, 2001.

[132] D. R. Askeland, P. P. Phulé, W. J. Wright, and D. Bhattacharya, "The science and engineering of materials," 2003.

[133] J. J. Rasmussen, G. B. Stringfellow, I. B. Cutler, and S. D. Brown, "Effect of impurities on the strength of polycrystalline magnesia and alumina," *Journal of the American Ceramic Society*, vol. 48, no. 3, pp. 146–150, 1965.

[134] T. Ostrowski and J. Rödel, "Evolution of mechanical properties of porous alumina during free sintering and hot pressing," *Journal of the American Ceramic Society*, vol. 82, no. 11, pp. 3080–3086, 1999.

[135] A. F. Bower, *Applied mechanics of solids*. CRC press, 2009.

[136] B. D. Hamilton, I. Weissbuch, M. Lahav, M. A. Hillmyer, and M. D. Ward, "Manipulating crystal orientation in nanoscale cylindrical pores by stereochemical inhibition," *Journal of the American Chemical Society*, vol. 131, no. 7, pp. 2588–2596, 2009.

[137] Q. Jiang, C. Hu, and M. D. Ward, "Stereochemical control of polymorph transitions in nanoscale reactors," *Journal of the American Chemical Society*, vol. 135, no. 6, pp. 2144–2147, 2013.

[138] S. Kobatake, H. Hasegawa, and K. Miyamura, "High-convertible photochromism of a diarylethene single crystal accompanying the crystal shape deformation," *Crystal Growth & Design*, vol. 11, no. 4, pp. 1223–1229, 2011.

[139] J. Li, R. Zhang, L. Mou, M. Jung de Andrade, X. Hu, K. Yu, J. Sun, T. Jia, Y. Dou, H. Chen, *et al.*, "Photothermal bimorph actuators with in-built cooler for light mills, frequency switches, and soft robots," *Advanced Functional Materials*, vol. 29, no. 27, p. 1808995, 2019.

[140] Y. Zhou, L. You, S. Wang, Z. Ku, H. Fan, D. Schmidt, A. Rusydi, L. Chang, L. Wang, P. Ren, *et al.*, "Giant photostriction in organic–inorganic lead halide perovskites," *Nature communications*, vol. 7, no. 1, pp. 1–8, 2016.

[141] L. Zhu, R. O. Al-Kaysi, and C. J. Bardeen, "Reversible photoinduced twisting of molecular crystal microribbons," *Journal of the American Chemical Society*, vol. 133, no. 32, pp. 12569–12575, 2011.

[142] L. Zhu, R. O. Al-Kaysi, and C. J. Bardeen, "Photoinduced ratchet-like rotational motion of branched molecular crystals," *Angewandte Chemie International Edition*, vol. 55, no. 25, pp. 7073–7076, 2016.

[143] C. J. Easley, F. Tong, X. Dong, R. O. Al-Kaysi, and C. J. Bardeen, "Using light intensity to control reaction kinetics and reversibility in photomechanical crystals," *Chemical science*, vol. 11, no. 36, pp. 9852–9862, 2020.

[144] K. R. Chalek, X. Dong, F. Tong, R. A. Kudla, L. Zhu, A. D. Gill, W. Xu, C. Yang, J. D. Hartman, A. Magalhães, *et al.*, "Bridging photochemistry and photomechanics with nmr crystallography: the molecular basis for the macroscopic expansion of an anthracene ester nanorod," *Chemical Science*, vol. 12, no. 1, pp. 453–463, 2021.

[145] T. Kim, L. Zhu, R. Al-Kaysi, and C. Bardeen, "Organic photomechanical materials," *ChemPhysChem*, vol. 15, pp. 400–414, 2014.

[146] F. Tong, D. Kitagawa, I. Bushnak, R. O. Al-Kaysi, and C. J. Bardeen, "Light-powered autonomous flagella-like motion of molecular crystal microwires," *Angewandte Chemie International Edition*, vol. 60, no. 5, pp. 2414–2423, 2021.

[147] B. B. Rath and J. J. Vittal, "Single-crystal-to-single-crystal [2+ 2] photocycloaddition reaction in a photosalient one-dimensional coordination polymer of pb (ii)," *Journal of the American Chemical Society*, vol. 142, no. 47, pp. 20117–20123, 2020.

[148] X. Dong, T. Guo, D. Kitagawa, S. Kobatake, P. Palffy-Muhoray, and C. J. Bardeen, "Effects of Template and Molecular Nanostructure on the Performance of Organic–Inorganic Photomechanical Actuator Membranes," *Advanced Functional Materials*, vol. 30, no. 2, p. 1902396, 2020.

[149] X. Dong, F. Tong, K. M. Hanson, R. O. Al-Kaysi, D. Kitagawa, S. Kobatake, and C. J. Bardeen, "Hybrid Organic–Inorganic Photon-Powered Actuators Based on Aligned Diarylethene Nanocrystals," *Chemistry of Materials*, vol. 31, pp. 1016–1022, Feb. 2019.

[150] Y. Norikane, E. Uchida, S. Tanaka, K. Fujiwara, H. Nagai, and H. Akiyama, "Photoinduced phase transitions in rod-shaped azobenzene with different alkyl chain length," *Journal of Photopolymer Science and Technology*, vol. 29, no. 1, pp. 149–157, 2016.
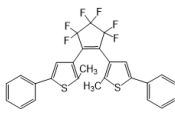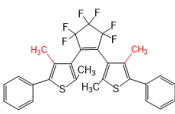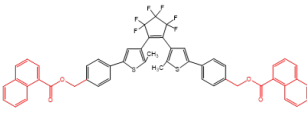
Chemical structure					
Chemistry name			1,2-Bis(2-methyl-5-phenyl-3-thienyl)perfluorocyclopentene	1,2-bis(2,4-dimethyl-5-phenyl-3-thienyl)perfluorocyclopentene	1,2-bis(2-methyl-5-(4-(1-naphthoyloxymethyl)-phenyl)-3-thienyl)perfluorocyclopentene
Nick name			reference	commercially available	DE-biNaph
In solution	quantum yield	cyclization	0.59 (at 280 nm in Hexane at room T)	0.46 (at 313 nm)	Not measured, almost same as 'reference'
		cycloreversion	0.013 (at 492 nm in Hexane at room T)	0.015 (at 618 nm)	
	forward conversion at photostationary state (%)		97		
	Absorption maximum (nm)	open-ring	280	268	Similar with other DAEs.
		coefficient	35600	28400	
		close-ring	306, 380, **575**	562	
		coefficient	15,600	10900	
In crystal	Absorption maximum (nm)	close-ring			600.5
	quantum yield	cyclization	1	0.96 (at 370 nm)	Not measured, almost same as 'reference'
		cycloreversion	0.017	0.027 (618 nm)	
	crystal system		monoclinic	monoclinic	triclinic

Table A1: Important properties of three DAE derivatives used in the lab. [18–21]